REVIEW

AI-Driven Inverse Design of Materials: Past, Present, and Future

AI-Driven Inverse Design of Materials: Past, Present, and Future

Xiao-Qi Han(韩小琪)[1], Xin-De Wang(王馨德)[1], Meng-Yuan Xu(徐孟圆)[2], Zhen Feng(冯祯)[1], Bo-Wen Yao(姚博文)[1], Peng-Jie Guo(郭朋杰)[1], Ze-Feng Gao(高泽峰)[1*], and Zhong-Yi Lu(卢仲毅)[1*]

[1]*School of Physics, Renmin University of China, Beijing 100872, China*
[2]*School of Physics and Information, Shaanxi Normal University, Xi'an 710119, China*

(Received 10 December 2024; accepted manuscript online 31 January 2025)

The discovery of advanced materials is a cornerstone of human technological development and progress. The structures of materials and their corresponding properties are essentially the result of a complex interplay of multiple degrees of freedom such as lattice, charge, spin, symmetry, and topology. This poses significant challenges for the inverse design methods of materials. Humans have long explored new materials through numerous experiments and proposed corresponding theoretical systems to predict new material properties and structures. With the improvement of computational power, researchers have gradually developed various electronic-structure calculation methods, such as the density functional theory and high-throughput computational methods. Recently, the rapid development of artificial intelligence (AI) technology in computer science has enabled the effective characterization of the implicit association between material properties and structures, thus forming an efficient paradigm for the inverse design of functional materials. Significant progress has been achieved in the inverse design of materials based on generative and discriminative models, attracting widespread interest from researchers. Considering this rapid technological progress, in this survey, we examine the latest advancements in AI-driven inverse design of materials by introducing the background, key findings, and mainstream technological development routes. In addition, we summarize the remaining challenges for future directions. This survey provides the latest overview of AI-driven inverse design of materials, which can serve as a useful resource for researchers.

DOI: 10.1088/0256-307X/42/2/027403 CSTR: 32039.14.0256-307X.42.2.027403

1. Introduction. Advanced materials form a cornerstone of our modern information society as they function as key catalysts for technological progress and industrial expansion, and they have been advancing at an unprecedented rate.[1–6] Their utilization extends across diverse industries such as aerospace, biomedical engineering, energy storage, and information technology, which will all benefit significantly from the integration of innovative materials that can overcome existing constraints.[7] Undoubtedly, the evolution of novel materials is crucial for fostering technological breakthroughs, invigorating economic prosperity, and elevating the standard of living.

Generally, *materials science* is a major scientific discipline dedicated to studying advanced functional materials. The search for advanced materials through inverse design is an important research field within materials science. The inverse design of materials essentially involves creating an optimization space based on the desired performance attributes of materials. This process strives to establish a high-dimensional nonlinear mapping from material properties to structural configurations while adhering to physical constraints. The development of the inverse design of materials has attracted widespread interest in academic research and can be categorized into four major paradigms:

- *Experiment-Driven Paradigm.* The experimental-driven paradigm is the original method of material discovery. Methods under this paradigm have significantly advanced the field of materials science. For example, Madame Curie used experiments to discover the new elements radium and polonium, Onnes discovered the superconductivity phenomenon in mercury,[8] and Nagamatsu *et al.* discovered the high-temperature superconducting material MgB_2.[9] However, this experimental-driven paradigm relies heavily on trial-and-error experimentation, individual expertise, and phenomenological scientific theories. Moreover, these methods are characterized by iterative cycles of experiments and observations to determine the properties and behaviors of materials, which is not only time-consuming and resource-intensive but also results in extended research cycles and increased costs. In materials research, a heavy dependence on personal experience is also common. Although experienced researchers can guide experimental design with their intuition and prior knowledge, this method is limited in terms of reproducibility and scalability. The quantification and transfer of personal experience are often challenging, hindering the process of knowledge accumulation and dissemination.[10] Additionally, personal biases and misunderstandings may occur owing to individual backgrounds and cognitive limitations.[2]
- *Theory-Driven Paradigm.* The theory-driven paradigm emphasizes the key role of theoretical insights

*Corresponding author. Email: zfgao@ruc.edu.cn; zlu@ruc.edu.cn

and computational models in materials science. This paradigm is characterized by the widespread use of molecular dynamics (MD) simulations and thermodynamic models to understand and predict material behavior. These developments have, to a certain extent, simplified material research and enhanced the efficiency of investigations into new materials. Some very famous materials and states of matter were first predicted through theory and then verified experimentally, and these discoveries have extremely high scientific significance, even winning Nobel Prizes. In 1930, British physicist Paul Dirac derived the existence of "antimatter" from his quantum mechanical equations, suggesting that for every particle a corresponding antiparticle exists.[11] Dirac's equations first predicted the existence of the positron, the antiparticle of the electron. In 1932, Carl Anderson discovered the positron in cosmic rays, confirming Dirac's prediction.[12] Anderson was awarded the Nobel Prize in Physics in 1936 for this discovery, and Dirac also received the Nobel Prize in Physics in 1933 for his contributions to quantum mechanics, including the theoretical prediction of antimatter. John Bardeen, Leon Cooper, and John Schrieffer proposed the BCS theory, which explained the cause of superconductivity—the pairing of electrons to form Cooper pairs resulting in zero electrical resistance.[13–15] Although the BCS theory itself did not directly predict new materials, it became the foundation for research into low-temperature superconductivity. Bardeen, Cooper, and Schrieffer were awarded the Nobel Prize in Physics in 1972 for their work. In 2005, Charles Kane and Eugene Mele predicted the existence of the quantum spin Hall effect through topological quantum theory, a phenomenon in which edge state conduction occurs without an external magnetic field. This concept laid the foundation for topological insulators. In 2007, scientists first achieved the quantum spin Hall effect in HgTe quantum wells, verifying the accuracy of the theory. These classic predictions demonstrate the powerful predictive ability of theoretical physics in the exploration of new materials and phenomena and promote the development of experimental physics. Many such theoretical breakthroughs ultimately won the Nobel Prize for experimental verification, marking significant advances in physics. Nevertheless, these theoretical frameworks often require complex mathematical models that are demanding in terms of computational resources and expertise. Their applicability may be limited, particularly for material systems that exhibit multi-scale phenomena and complex interactions.

• *Computation-Driven Paradigm.* Established on the foundation of theoretical progress, the computation-driven paradigm has progressed alongside the surge in computational power and data accessibility. This paradigm leverages computational models to simulate material behaviors and inform the design process. The application of density functional theory (DFT)[16–18] and computational chemistry tools such as Hartree–Fock theory has revolutionized our ability to predict and optimize material properties. The DFT has played a crucial role in the investigation of the electronic structure of graphene. The DFT revealed the zero-bandgap structure of graphene, a characteristic that is essential for its electronic properties and holds significant potential for its application in electronic devices.[19] Furthermore, the Hartree–Fock method has been extensively applied in calculating molecular orbitals, such as in studies on water molecules, thus offering vital insights into their geometric and electronic characteristics.[20] The potency of these methods is clear in their capacity to manage complex systems that were once difficult to understand. However, reliance on computational models introduces challenges, as the accuracy of predictions heavily relies on model quality and available computational resources. Additionally, high-throughput screening (HTP) and combinatorial screening have become significant methodologies for exploring new materials and systems. This approach significantly expedites the discovery and development of novel materials, particularly in drug discovery, catalyst design, and energy storage material development, where it enables the parallel assessment of vast compound libraries to identify potential new materials.[3] Despite the achievements of HTP in materials science, challenges remain, including substantial resource requirements for physical or computational experiments, constraints by existing material libraries, and insufficient consideration of intricate relationships between material properties.[21]

• *Artificial Intelligence (AI)-Driven Paradigm.* With the advent of the big data era, materials science has transitioned into an AI-driven paradigm. AI is a significant shift within the engineering field, heralding an era defined by enhanced intelligence and automation. Both the widely utilized auto-regressive models based on the transformer architecture[22] and the robust diffusion models[23,24] have contributed significantly to the advancement of inverse design of materials.[25–28] The capacity of AI to discern patterns and formulate predictions from data has enabled notable transformations in materials science. By examining vast experimental data and computational simulation outcomes, AI models reveal intricate correlations between material properties and their underlying crystal structures.[29,30] Furthermore, a recent survey[25] has integrated inverse design methodologies with machine learning (ML) models to forecast the mechanical properties of materials, including elastic modulus and yield strength, thus expediting the discovery and development of innovative materials. These data-driven strategies not only bolster the precision of predictions but also considerably shorten material development cycles. Consequently, "ML materials discovery" is attracting much research interest [see Fig. 1(a)]. In parallel, the exponential growth of the total known materials over time highlights the accelerated pace of material discovery processes, with significant contributions from Google's GNoME[31] and Meta's OMat24.[32]

As discussed earlier, AI-driven methods are not a new technical concept for inverse design of functional materials, but they have evolved with the advance of AI over the decades. The experiment-driven and theory-driven paradigms primarily aim to discover new functional ma-

terials based on heavily trial-and-error experiments or theoretical models, whereas the latest AI-driven methods concentrate on constructing the hidden mappings between material functions and crystal structures. The progress from conventional experiment methods to data-driven methods is an important leap in the use of modern advanced computational methods to design target functional materials. In Fig. 2, we delineate the evolution of materials science discoveries over time and with technological advancements. Initially, the confirmation of new materials was primarily achieved through experimentation (such as Madame Curie's discovery of new elements), which entailed significant costs and numerous trials. Subsequently, theoretical paradigms were introduced, predicting physical properties that were later experimentally verified (for instance, the prediction and validation of semiconductors). With the advancement of computer technology and the enhancement of computational ability, high-throughput computational methods have become a significant avenue for the discovery of new materials. Ultimately, as the latest generation of technology, AI methods can efficiently generate and screen new functional materials by elucidating the hidden correlations between crystal structures and properties, thereby accelerating the discovery of new materials. In summary, throughout this evolutionary process, technological progress has enabled us to employ more sophisticated methods to expedite the discovery of new functional materials.

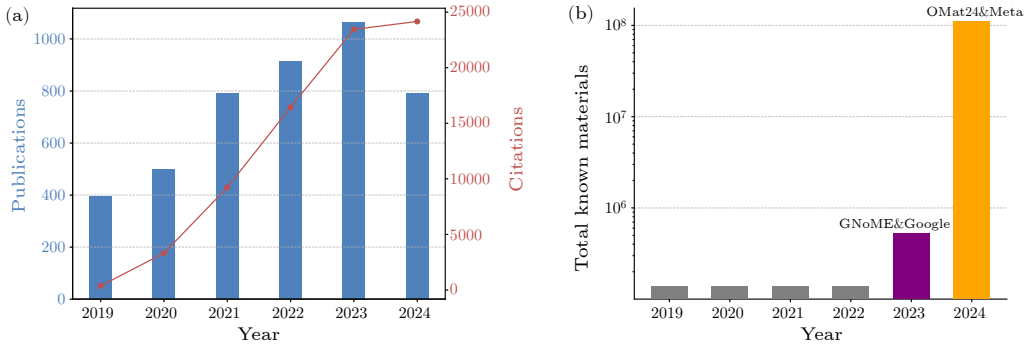

Fig. 1. Trends in publications and citations in the field of "machine learning materials discovery" from 2019 to 2024. The left panel (a) shows the increase in the number of publications (represented by blue bars) alongside the total citations (depicted by the red line with markers), reflecting a significant increase in both metrics over the past few years. The right panel (b) presents the variation in the total known materials over time on a logarithmic scale, highlighting the acceleration of material discovery processes facilitated by GNoME [31] of Google and OMat24 [32] of Meta. This figure underscores the rapid development within the field of ML materials discovery.

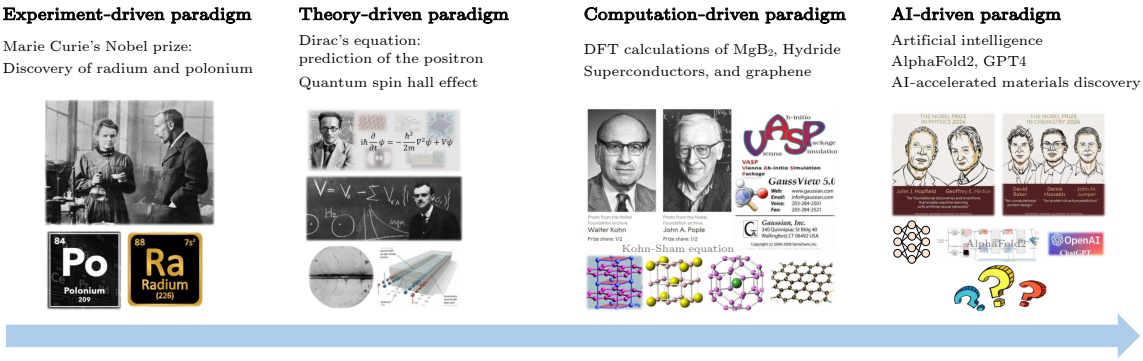

Fig. 2. Materials science research paradigms. This figure depicts the evolution of research paradigms in materials science, emphasizing key milestones across various approaches. It highlights the increasing role of AI in driving future materials discovery, with AI becoming the dominant force in shaping the field. The experiment-driven paradigm is exemplified by Marie Curie's Nobel Prize-winning discovery of radium and polonium. The theory-driven paradigm is represented by Dirac's equation, which predicted the existence of the positron and the quantum spin Hall effect. The computation-driven paradigm is demonstrated through DFT calculations applied to materials such as MgB_2, hydride superconductors, and graphene. Finally, the AI-driven paradigm showcases recent breakthroughs in AI, including AlphaFold2, GPT-4, and AI-accelerated materials discovery, signaling the frontier of research in the field.

With the development of technology, a research field has emerged in materials science known as the inverse design of materials. Unlike traditional trial-and-error methods, it utilizes complex computational techniques to design materials with specific properties systematically. The process involves several key steps: defining the target properties or functionalities; selecting an appropriate design space; using modeling and simulation tools (such as DFT and finite element analysis) to simulate material properties; optimizing the material structure through algorithms to minimize the difference between simulated properties and target goals; finally, validating the design through

experimental verification, followed by iterative refinement based on experimental results. This approach is widely applied in areas such as optics, electronics, energy storage, catalysis, and composite materials, and it significantly accelerates the development of new materials. However, inverse design also faces challenges such as computational cost, data quality, and experimental validation. With the advancement of computational power and optimization algorithms, materials inverse design is expected to play an increasingly important role in the future development of materials science.

In the existing literature, the inverse design of materials has been extensively discussed and surveyed.[2–6] However, current surveys often focus on specific ML algorithms or particular types of materials, resulting in a lack of systematic integration of diverse methodologies and a broad range of material systems. Many existing surveys predominantly focus on specific categories of materials or application scenarios, such as topological insulators or high-entropy alloys,[33,34] thereby failing to provide a comprehensive examination of AI-driven inverse design of materials. Specifically, comparative and analytical studies across different researches about AI-driven inverse design of materials are lacking, which hinders a holistic understanding of the advantages, disadvantages, and applicable contexts of various methodologies. These limitations pose challenges for readers attempting to fully grasp the overarching landscape of AI-driven inverse design of materials, particularly with respect to the dynamic evolution of new methods and their applications.

Owing to both opportunities and challenges, more attention is required on the research and development of AI-driven inverse design of materials. To provide a basic understanding of this research field, this survey aims to address the gaps in the current body of research by comprehensively examining previous studies from two perspectives: the discovery of functional materials based on AI methods and the development of AI methods in materials science. We systematically analyze the latest advancements in AI technologies within the domain of inverse design of materials. We conduct an exhaustive survey of the literature to synthesize the pivotal discoveries, AI methods, and procedural methods in the inverse design of functional materials. We are also aware of several relative survey articles on inverse design of materials.[35,36] Ref. [36] provided an overview of the importance and utilization of graph neural networks (GNNs) within chemistry and materials science. GNNs can directly process the graphical representations of molecules and materials, thereby capturing the essential information required to characterize these materials. The review further outlined the fundamental principles of GNNs, including commonly used datasets and architectures, and emphasized their critical role throughout the materials development. Another Ref. [35] systematically explored the research advancements of geometric GNNs in the applications of materials and drug discovery. It emphasized the significance of geometric graphs in scientific fields, particularly their ability to capture geometric features such as the three-dimensional (3D) coordinates of nodes. The survey further defined geometric graphs and compared them with traditional graphs, elucidating their distinct characteristics. Additionally, it summarized existing models, including invariant and equivariant GNNs. Our survey presents the latest advancements in functional materials accelerated by ML techniques, with particular emphasis on the robust representational capabilities of geometric GNNs. Furthermore, we provide a comprehensive overview of advanced generative models and large language models (LLMs), highlighting their pivotal roles in driving materials discovery. Finally, we have gathered standard datasets and benchmarks that are crucial for material discovery to advance the methods of AI-driven inverse design of materials.

"*All significant achievements take time.*" The inverse design of materials has undergone a long development to achieve the latest successes. Our aim is to discuss the historical progression of material directional design, with a particular focus on the innovative approaches to material discovery that have occurred in the era of AI. This survey will elucidate the critical challenges inherent in inverse design of materials. Subsequently, we discuss the specific classes of materials that are currently at the forefront of materials science (including superconducting materials and magnetic materials), and detail the AI technologies. We have also compiled a comprehensive overview of the evolution of AI technologies within the materials domain. We expect that the contributions presented in this paper will propel the field of AI-driven inverse design of materials to new heights of advancement. In the following, we introduce the recent applications of AI-driven method in expediting the inverse design of functional materials in Section 2. We then elaborate on the development history of AI technology in the field of materials science in Section 3. Finally, we briefly discuss a series of open problems and promising directions for the future in Section 4 and conclude in Section 5.

2. Discovery of Functional Materials Based on AI Methods. The AI-accelerated discovery of functional materials has emerged as a dominant trend in materials science. As the demand for novel materials continues to increase, traditional material discovery methods often become too slow and labor-intensive to match the pace of technological innovation. Consequently, AI–particularly ML and deep learning (DL)–has demonstrated significant potential in advancing material discovery. AI facilitates the efficient identification of patterns in data, the prediction of material properties, and the optimization of complex material compositions, thus offering tools for materials science that were previously unimaginable. This chapter comprehensively reviews AI applications across several key categories of functional materials, including superconducting materials, magnetic materials, thermoelectric materials, carbon-based nanomaterials, two-dimensional (2D) materials, photovoltaic materials, catalytic materials, high-entropy alloys, and porous materials. These materials are crucial to the development of advanced technologies in areas such as energy storage, electronics, and environmental sustainability.

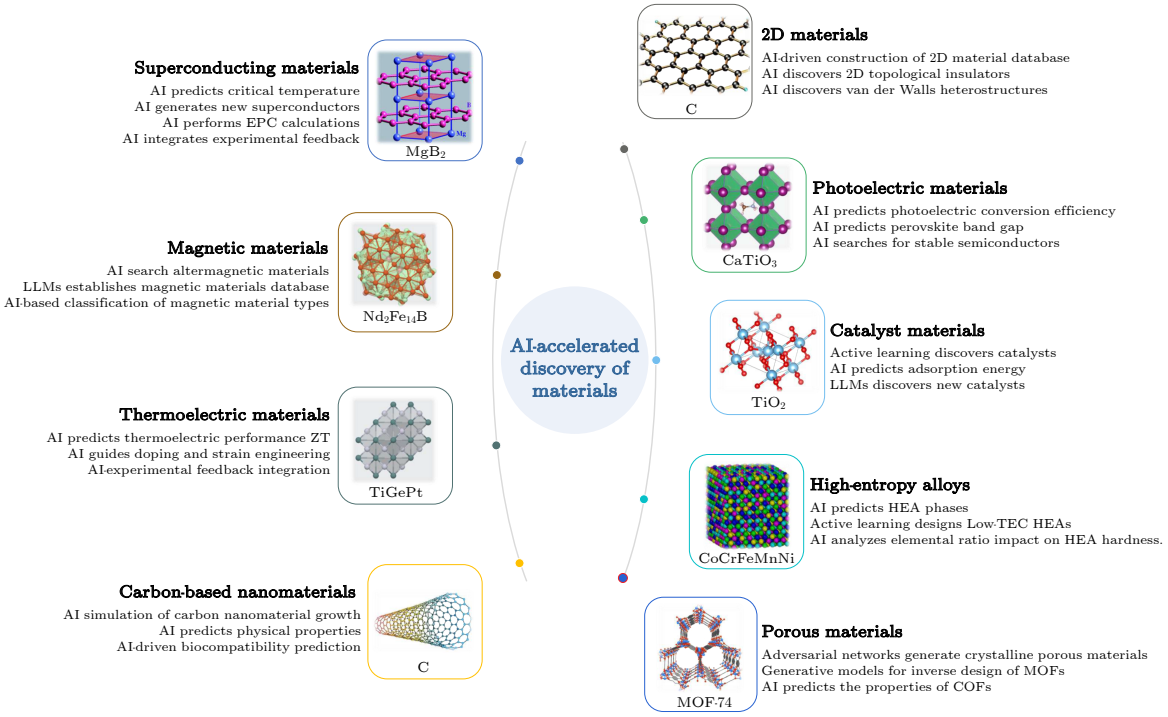

Fig. 3. AI-driven discovery of materials. This figure shows the role of AI in accelerating the discovery of various types of materials. The examples presented highlight how the AI-driven approaches are employed to optimize the identification, design, and property prediction of materials across diverse categories, including superconducting materials, magnetic materials, thermoelectric materials, carbon-based nanomaterials, 2D materials, photovoltaic materials, catalyst materials, high-entropy alloys, and porous materials. By leveraging large datasets and advanced computational techniques, AI methods facilitate more efficient screening and prediction, thereby significantly advancing the pace of material discovery. These examples represent only a subset of the broad potential of AI in transforming materials research. Further discussion is provided in the main text.

2.1. Superconducting Materials. Superconducting materials exhibit zero electrical resistance and complete expulsion of magnetic fields below a critical temperature (T_c). These materials have wide applications owing to their outstanding physical properties, such as in magnetic resonance imaging[37] and nuclear fusion technology.[38] Superconductor-based devices are used in quantum information processors, advanced sensors, and communication systems.[39–41] Superconducting materials were discovered in 1911 when mercury exhibited zero resistance at 4.2 K.[42] In 1933, the Meissner effect,[43] where superconductors expel magnetic fields entirely, was observed. Significant milestones include the 1973 discovery of niobium-germanium alloy[44] with a T_c of 23.2 K, the 1986 breakthrough in copper oxide superconductors[45] reaching 35 K, and yttrium-barium-copper-oxide materials[46] surpassing 77 K in 1987. In 2008, iron-based compounds exceeded 55 K.[47] In recent years, high-T_c superconductors have advanced, with scandium setting a record for elemental superconductors at 36 K[48] and pressed nickelate bilayers reaching liquid-nitrogen temperatures.[49] Hydride superconductors, such as H_3S, have also been confirmed under high pressure.[50]

The search for new high-T_c superconductors is a significant task in condensed matter physics. With the advancement of AI technologies, extensive exploration has been conducted in the field of AI-accelerated superconducting material discovery. The study in Ref. [51] utilized data extracted from the SuperCon database,[52] comprising approximately 16,400 compounds (without crystal structures). They employed a random forest (RF) algorithm to build ML models for predicting the T_c of superconducting materials. Separate regression models were developed for different superconducting families, such as cuprates, iron-based superconductors, and low-T_c superconductors. Ablation studies demonstrated that these regression models cannot be generalized across different superconducting families, likely owing to their distinct superconducting mechanisms. Considering the crucial role of band theory in explaining superconducting mechanisms, a recent study[53] employed electronic band structure data and applied a transformer-based model with attention mechanisms to predict the superconducting T_c of materials. Zhang *et al.* released the SuperBand dataset, comprising electronic band structures suitable for ML training, generated through high-throughput DFT calculations.[54]

Traditional ML algorithms struggle to effectively model complex crystal structures, whereas GNNs[55–60] have a natural advantage in representing such structures. Choudhary *et al.*[61] leveraged the atomistic line graph neural network (ALIGNN)[62] to accelerate the discovery of superconductors. They employed ALIGNN to predict key physical properties such as Debye temperature, electronic density of states (DOS) at the Fermi level, and the

T_c of superconducting materials. By screening materials with high Debye temperatures and high electronic densities of states at the Fermi level, they conducted electron-phonon coupling (EPC) calculations on 1,058 materials, constructing a systematic BCS superconductivity performance database. Using the McMillan-Allen-Dynes formula, they identified 105 dynamically stable materials with a T_c exceeding 5 K. Recent reserch [63–66] has demonstrated that ALIGNN can also be used to predict the superconducting T_c of hydride superconductors under varying pressures, resulting in the discovery of 122 dynamically stable structures with a T_c higher than that of MgB_2 (39 K). With the advancement of algorithms, superconducting datasets containing crystal structures, such as 3DSC [67] and SuperCon3D, have been successively released.

The method of searching for high-T_c superconductors based on existing databases has explored only a small region of chemical space. In recent years, generative models [68–70] have attracted significant interest because they can produce highly realistic images, and such algorithms have been widely applied in areas such as molecular docking [71] and material generation. [23,24] In principle, generative models can explore an infinite chemical space. Han *et al.* [72] developed an AI workflow for discovering high-T_c superconductors. This workflow first generates new candidate superconducting crystal structures using a diffusion-based generative model. Thereafter, a superconductivity classification model [73,74] assesses the likelihood of the material being a superconductor, followed by a formation energy prediction model [75,76] that evaluates the material's stability. Subsequently, a DPA-2 model [77] optimizes the structure, and finally, ALIGNN is used to predict the T_c of materials. The results have been validated through first-principles electronic-structure calculations, which identified 74 dynamically stable superconducting candidates with T_c values higher than 15 K, none of which are found in existing datasets. A series of similar studies [78] have also employed generative models to explore superconducting materials.

When validating the stability of candidate superconducting materials, the DFT requires expensive phonon spectrum calculations. Recent studies [79] introduced the virtual node graph neural network (VGNN), which can directly predict Γ-point phonon spectra and full dispersion relations across the entire Brillouin zone using only atomic coordinates as input. A Γ-point phonon database containing over 146,000 materials was also developed. Further validation of superconducting materials requires the calculation of EPC, and Zhong *et al.* [80] provided an ML approach to accelerate the computation of EPC matrices.

Most of the above-mentioned AI models are primarily combined with high-throughput DFT calculations to discover new high-T_c superconductors, where the superconducting mechanisms are well-understood within the framework of BCS theory. However, the superconducting mechanisms for most high-T_c superconductors remain unclear, and these materials are considered unconventional superconductors. Additionally, empirical rules [81–84] that describe correlations between T_c and structural features exist, but these rules are limited to cuprates and iron-based superconductors and cannot be generalized to other materials. Because chemical bonding and electronic interactions in the lattice are crucial factors for superconductivity, Liang *et al.* [85] developed a bond sensitive GNN (BSGNN) to predict the upper limit of T_c (T_{cmax}) in different materials. This model integrates three modules: nearest neighbor graph representation (NGR), communication message passing (CMP), and graph attention (GAT). It reveals a close relationship between T_{cmax} and chemical bonding, showing that shorter bond lengths favor higher T_{cmax}, consistent with existing domain knowledge. However, this model can only predict T_c and cannot determine whether a material is superconducting. Additionally, expert input is required for further screening to eliminate particularly unreasonable materials, such as insulators.

The above-mentioned AI methods are primarily combined with theoretical calculations. In contrast, the research in Ref. [86] introduces a closed-loop ML approach, which integrates ML with experimental feedback to accelerate the discovery of superconducting materials. Using an active learning strategy, this method iteratively selects and experimentally validates materials predicted by an ML model; subsequently, it feeds the experimental results back into the model to continually improve its predictions. Through this approach, the research team discovered a previously unreported superconductor in the Zr-In-Ni system and rediscovered five known superconductors that were not part of the training dataset, significantly enhancing the success rate of superconductor discovery. This closed-loop method highlights the potential of combining ML with experimental feedback to accelerate new material discoveries and demonstrates the critical role of experimental validation in refining ML predictions.

2.2. Magnetic Materials. Magnetic materials are substances that can generate magnetization when subjected to a magnetic field and exhibit attraction to ferromagnetic elements such as iron. Dating back approximately 2,500 years, humanity had discovered that certain materials possess the ability to attract iron. For centuries, the creation of artificial magnets was confined to a singular method: friction with a natural magnet or an existing artificial magnet, the latter having been initially produced through contact with a natural source. A pivotal moment occurred in 1820 when Hans Christian Oersted uncovered the magnetic effects induced by electric currents. This discovery laid the foundation for the invention of the electromagnet in 1825, a breakthrough that introduced a novel means of generating significantly stronger artificial magnetic fields. Consequently, this period marked the commencement of extensive scientific inquiry into the properties and applications of magnetic materials. [87]

Based on their properties, magnetic materials can be categorized into three types: ferromagnetic, [88] antiferromagnetic, [89] and altermagnetic. [90–98] The difference between ferromagnetic and antiferromagnetic mate-

rials lies in the arrangement of the magnetic moments and the resulting magnetic behavior. Ferromagnetic materials exhibit a wide range of magnetic domains,[99] where the magnetic moments within each domain are aligned in the same direction. However, the magnetic moments in different domains may have different orientations. Under the influence of an external magnetic field, ferromagnetic materials can be strongly magnetized, and they have a high coercivity, meaning that a strong reverse magnetic field is required to change the direction of magnetization. After the removal of the external magnetic field, ferromagnetic materials maintain a certain level of remanence and exhibit high permeability. The altermagnetic materials, despite exhibiting antiferromagnetic compensated magnetic order, show macroscopic time-reversal symmetry-breaking phenomena and spin polarization similar to ferromagnets. This seemingly contradictory behavior has caused scientists to reclassify them based on spin-symmetry principles, thereby defining altermagnetism as a new magnetic phase. As research on altermagnetic materials deepens, more material candidates have been discovered with these properties, including insulators, semiconductors, metals, and high-temperature superconductors.[91]

Moreover, altermagnetic materials have attracted significant interest owing to their novel physical effects, such as giant magnetoresistance (GMR),[100] unconventional superconductivity,[101,102] tunneling magnetoresistance (TMR),[100] piezomagnetic effects,[103] spin-splitting torque,[104–106] time-reversal odd anomalous effects,[94,107–112] quantum anomalous Hall effects,[113] higher-order topological states,[114] altermagnetic ferroelectricity,[115] and strong spin-orbit coupling effects in light-element altermagnetic materials.[116] Recent studies[117] have demonstrated the theoretical feasibility of achieving bipolarized Weyl semimetals and the quantum crystal valley Hall effect in 2D altermagnetic materials.

With the development of science and technology, the discovery of new magnetic materials with a greater operating temperature range and better performance is essential. Recently, a comprehensive experiment-based database of magnetic materials based on LLMs, named the northeast materials database (NEMAD), has been created.[118] Itani *et al.* indicated that several ML models can classify magnetic materials and predict their magnetic properties, but the lack of a comprehensive database of magnetic materials results in poor generalization of the models, that is, the accuracy of the models in predicting different classes of new magnetic materials is low. Based on this, they created an application, GPTArticleExtractor,[119] to automatically extract data from scientific articles to build a comprehensive database of material properties. Similarly, an AI search engine named MatAltMag[74] was proposed to accelerate the discovery of altermagnetic materials. The engine first undergoes pre-training using crystal graph convolutional neural networks (CGCNNs)[73] and the Materials Project database[120] to learn the intrinsic features of material crystal structures. It then fine-tunes the classifier using a limited number of positive samples to accurately predict intercalated magnetism. This engine has successfully discovered 50 new altermagnetic materials, including metals, semiconductors, and insulators, significantly expanding the known range of altermagnetic materials. The altermagnetism of these materials has been validated through DFT calculations, revealing novel physical effects such as the anomalous Hall effect, anomalous Kerr effect, and topological properties. Furthermore, the discovery of four i-wave altermagnetic materials is a breakthrough in the study of altermagnetic phases. The AI-driven method demonstrates significant potential in accelerating the discovery of altermagnetic materials.

Owing to the relatively recent emergence of altermagnetic materials, only few researchers have employed ML algorithms in this field, and the potential of AI has yet to be fully tapped. We anticipate that future research will utilize generative models to explore a broader chemical space in the search for novel altermagnetic materials while leveraging AI algorithms to accelerate the DFT validation process.

2.3. Thermoelectric Materials. Thermoelectric materials represent a class of functional materials that can directly convert heat into electricity, and vice versa, through the Seebeck effect, which generates an electric current in response to a temperature gradient.[121] These materials hold significant promise for applications in waste heat recovery and solid-state cooling technologies. Currently, approximately two-thirds of global energy consumption is considered to be lost as waste heat, and thermoelectric materials provide a potential pathway to reclaim this wasted energy, thereby improving overall energy efficiency.[122] Furthermore, thermoelectric devices, which require neither mechanical components nor harmful working fluids, present an environmentally friendly and sustainable solution for various applications, including space power systems, automotive and industrial waste heat recovery, and thermal management in microelectronics.[123]

The performance of thermoelectric materials is generally evaluated using the dimensionless figure of merit, ZT, defined as $\mathrm{ZT} = \dfrac{\alpha^2 \sigma T}{\kappa}$, where α is the Seebeck coefficient, σ is the electrical conductivity, T is the absolute temperature, and κ is the thermal conductivity.[124] The term $\alpha\sigma$, known as the power factor, is a function of both carrier concentration (n) and carrier mobility (μ).[125] Achieving a high ZT value requires materials that exhibit both a high electrical conductivity and high Seebeck coefficient while maintaining a low thermal conductivity. However, optimizing ZT is challenging owing to the interdependence of these parameters; for example, increasing electrical conductivity often results in a concomitant increase in thermal conductivity, which can diminish the desired improvement in ZT.[126] This trade-off remains one of the central challenges in thermoelectric material research.

Recent advancements in computational methods, particularly through the integration of ML and high-throughput screening techniques, have created new avenues for addressing this challenge. By leveraging large

datasets and advanced algorithms, researchers can now identify promising thermoelectric materials more efficiently and accurately than with traditional trial-and-error approaches or first-principles calculations alone. Studies have demonstrated the potential of ML models, such as the RF model combined with Bayesian optimization, to predict new M2X3-type thermoelectric materials with rhombohedral structures from large datasets, successfully identifying candidates with high thermoelectric performance.[127] Similarly, unsupervised learning techniques, including K-means and Gaussian mixture models, have been applied to cluster half-Heusler compounds, effectively identifying materials with favorable thermoelectric properties.[128] These approaches underscore the utility of ML in uncovering complex structure-property relationships relevant to thermoelectric performance.

For doped materials, the DopNet neural network architecture has been introduced to capture the effects of dopants accurately, enabling the prediction of the thermoelectric properties of doped materials based on extensive datasets.[129] This model has successfully predicted the impact of various dopants on crucial properties such as the Seebeck coefficient and electrical conductivity. In addition, artificial neural networks (ANNs) combined with techniques such as combinatorial gradient thermal annealing have optimized the internal strain of bismuth telluride films, resulting in significant improvements to their Seebeck coefficient.[130] Such studies illustrate the importance of doping and strain engineering in enhancing thermoelectric performance and reveal how ML can assist in identifying critical relationships.

In the realm of high-throughput computing and screening, frameworks have been established to analyze compounds such as diamond-like ABX2, thus identifying materials with high ZT values and highlighting key conductive mechanisms contributing to thermoelectric efficiency.[131] Similarly, approaches that combine high-throughput ab initio calculations with deep neural networks have predicted the thermoelectric properties of IV-V-VI layered semiconductors, revealing high-performance candidates, such as n-type $Pb_2Sb_2S_5$, with ZT values surpassing 1.0.[132] These integrated approaches expedite the discovery of new thermoelectric materials by leveraging ML and high-throughput screening. Additionally, the ToBaCCo 3.0* code has been employed for large-scale screening of metal–organic frameworks (MOFs). MD simulations on 10,194 hypothetical MOFs were conducted to investigate the structural characteristics affecting thermal conductivity, revealing that parameters such as density, pore size, porosity, and surface area significantly influence thermal transport properties.[133] Although ML models were not utilized in this study, the computational screening provided valuable insights into the structure-performance relationships governing MOF thermal conductivity.

High-throughput screening techniques have also been instrumental in identifying materials with excellent Peltier cooling performances among Heusler compounds, revealing their potential for sustainable cooling applications.[134] The identification of compounds with desirable electronic structures and thermoelectric transport properties demonstrates the utility of high-throughput approaches for applications in efficient cooling technologies.

Finally, the integration of ML with experimental feedback has been proposed as a promising approach for accelerating material discovery. By iteratively refining ML models with experimental data, methods such as error correction learning (ECL) have successfully predicted high-performance thermoelectric materials with improved power factors, minimizing experimental trials and enhancing predictive accuracy.[135]

Looking ahead, the convergence of ML and high-throughput computational methods is expected to be pivotal in advancing the inverse design of thermoelectric materials. As computational capabilities expand and larger and more diverse datasets become available, these technologies will continue to drive breakthroughs in addressing the challenges associated with optimizing thermoelectric properties. ML models–such as RFs, neural networks, and clustering algorithms–have already demonstrated their ability to uncover intricate structure-property relationships across various material classes, including M2X3 compounds, half-Heuslers, and doped systems. Coupled with high-throughput screening, which facilitates the exploration of extensive material libraries, such as MOFs and Heusler compounds, researchers can swiftly identify high-ZT candidates and deepen their understanding of key factors affecting thermoelectric performance, such as thermal conductivity and electronic transport. Moreover, the integration of experimental feedback with ML models, as exemplified by the error correction learning (ECL) approach, holds significant promise for accelerating material discovery by continuously improving predictive accuracy. As these techniques become more refined and collaborations between computational and experimental domains intensify, they are expected to revolutionize the design and discovery of next-generation thermoelectric materials. Ultimately, these advancements will contribute to the development of highly efficient environmentally sustainable energy systems for applications such as waste heat recovery, energy harvesting, and sustainable cooling technologies.

2.4. Carbon-Based Nanomaterials. Carbon-based nanomaterials are structures composed of carbon atoms arranged in a hexagonal honeycomb lattice, including carbon nanotubes (CNTs) and graphene. Because of their distinct physical and chemical properties, these materials have attracted significant interest in materials science since their discovery.[136,137] CNTs are classified into single-walled and multi-walled CNTs. The former consist of a single layer of rolled graphene, and the latter comprise multiple concentric graphene layers.[138] These two forms exhibit notable differences in mechanical, electrical, and thermal properties. Graphene, a 2D carbon-based nanomaterial, is formed by a single layer of carbon atoms in a hexagonal lattice, offering exceptional carrier mobility and

*https://github.com/tobacco-mofs/tobacco_3.0

mechanical strength.[19]

Owing to their outstanding electrical conductivities, mechanical strengths, and thermal conductivities, carbon-based nanomaterials are widely applied in various advanced technology sectors. For example, CNTs and graphene are used in the electronics industry to manufacture miniaturized circuits and efficient semiconductor components and may potentially surpass the limitations of Moore's law.[139] In the mechanical field, carbon-based nanomaterials are ideal for reinforcing composites owing to their lightweight and high-strength characteristics, making them integral in high-performance structural materials for aerospace, automotive, and other industries.[140] In the energy sector, the superior conductivity and energy storage capabilities of CNTs and graphene have significant promise for improving the energy density of batteries and supercapacitors.[141] However, the synthesis and design of carbon-based nanomaterials involve complex multivariable optimization challenges. Traditional experimental approaches struggle to address these challenges effectively, prompting the integration of AI technologies as a promising solution for the inverse design and performance optimization of carbon-based nanomaterials.

Some researchers have proposed an active learning model to elucidate the growth mechanisms of carbon-based nanomaterials on metallic substrates.[142] This study combined MD with the time-stamped force-bias Monte Carlo method, enhanced by the Gaussian approximation potential model for sampling. By simulating graphene growth on a copper substrate (Cu(111)), the researchers analyzed carbon monomer and dimer diffusion, the formation of carbon chains and rings, and the copper-assisted edge growth mechanism. The model dynamically generates ML potentials during the simulations, thus offering key insights into the growth processes of carbon materials on various metal substrates. Similarly, ML-enhanced molecular simulations have investigated the high-temperature growth dynamics of CNTs, using the DeepCNT-22 ML force field to model interfacial behaviors, defect formation, and defect healing mechanisms during CNT growth.[143] By utilizing machine learning force fields (MLFFs) trained on first-principles calculations, this study extended simulation time scales while maintaining computational accuracy, revealing atomic-level processes from CNT nucleation to growth. Additionally, combining ML with automation enhances the synthesis efficiency of carbon-based nanomaterials, as demonstrated by the AI-driven platform carbon copilot. This platform integrates transformer-based language models (Carbon-GPT and Carbon-BERT), a robotic chemical vapor deposition (CVD) system, and data-driven ML models to optimize synthesis processes, significantly improving controllability and yield in the growth of CNTs and graphene, particularly for horizontally aligned CNT arrays.[144]

Beyond synthesis optimization, ML is pivotal in predicting the physical properties of carbon-based nanomaterials, particularly for key attributes such as thermal and electrical conductivity. Compared with traditional methods, ML techniques provide more efficient and accurate solutions. For example, ML-based multi-scale modeling predicts the thermal conductivity of CNT-reinforced polymer composites, effectively capturing the impact of structural uncertainties on thermal conductivity by combining MD simulations with finite element analysis, regression tree models (RFs and gradient boosting machines), and deep neural networks.[145] Similarly, an interpretable ML framework predicts the electrical conductivity of CNT/polymer composites using stochastic multi-scale numerical models. This approach employs AI techniques, RFs, and extreme gradient boosting (XGBoost) models along with Shapley Additive exPlanations (SHAP) analysis to elucidate the influence of CNT structural parameters on conductivity, offering a robust theoretical framework for material design optimization.[146] Another study applied ANN models to accurately predict the electrical conductivity of CNT-reinforced polymer composites, reducing computational costs while maintaining predictive accuracy across various conductive network structures.[147]

Modeling the structure-property relationship is critical for understanding the behavior of carbon-based nanomaterials. ML is particularly adept at capturing the nonlinear relationships between complex structures and their properties, facilitating the design and optimization of new materials. For instance, a DL model called CNTNeXt, based on multi-layer synthesized images, predicts the mechanical properties of vertically aligned CNT (VACNT) forests. By utilizing a ResNeXt feature extractor paired with an RF regression model, the model improves prediction accuracy by generating 2.5D morphological images that simulate real VACNT structures, enhancing understanding of CNT self-assembly processes.[148] Additionally, a neural network-based surrogate model (NN-EBE) efficiently predicts higher-order phenomena such as buckling and nonlinear deformation for CNTs, providing computational advantages over traditional micromechanical models, particularly for large-scale simulations in composite material design.[149] For electronic property predictions, ML predicts the electronic properties of graphene nanosheets based on geometric features. Using the density functional tight binding (DFTB) method to generate data, this approach applies linear regression, multilayer perceptrons (MLPs), and support vector machines (SVMs) to efficiently identify graphene structures with desirable electronic properties, aiding high-throughput material screening in electronic applications.[150]

In terms of interface design and load transfer in composites, ML models have proven to be effective in optimizing chemical linkages and the mechanical behavior of CNTs within composites. Alred *et al.* employed ML models to predict the electron density and mechanical properties of sulfur cross-linked CNTs.[151] By generating training data from DFT and MD simulations, the study utilized MLP neural networks and RF models for accurate predictions, significantly reducing computational costs. This research highlighted the importance of ML in interface design for CNT composites.

ML techniques can also be applied to optimize the biocompatibility of carbon-based nanomaterials, particularly in predicting their biocompatibility and toxicity. Singh *et al.* explored the use of AI and ML to address the limitations of traditional experimental methods, which are often time-consuming and costly. By combining extensive experimental validation data with CNT physical properties (e.g., length, diameter, surface functionalization) and the chemical composition of polymers, they developed predictive models for biocompatibility and toxicity. Using ANN, RF, and XGBoost models, with ANN excelling in capturing the complex interactions between CNTs and biological systems, the study utilized K-fold cross-validation and regularization techniques to improve generalization, whereas SHAP analysis was used to further enhance model interpretability.[152] The results demonstrated the efficiency of the ANN in predicting toxicity responses, significantly reducing experimental time and cost while revealing critical relationships between the CNT structure and biocompatibility. This research was the first application of AI and ML in predicting nanomaterial biocompatibility, offering a novel tool for efficient toxicity assessment in future material design.

In the future, the continued advancement of ML and DL technologies will further automate and enhance the inverse design of carbon-based nanomaterials. Automated experimental platforms, combined with intelligent experimental planning, will accelerate the synthesis and screening of materials, particularly in complex multi-variable systems. Future active learning algorithms will dynamically update models with real-time feedback, improving design efficiency. In multi-scale modeling, future approaches will better integrate micro- and macro-scale features through the combination of first-principles calculations, MD simulations, and experimental data, establishing comprehensive multi-scale prediction frameworks. Additionally, the interpretability of ML models will become increasingly important, particularly in high-risk fields such as biomedicine and environmental safety, ensuring transparency and accountability in decision-making processes. Interdisciplinary collaboration will be pivotal in advancing carbon-based nanomaterial design, with the convergence of computational science, materials science, and biomedicine driving further innovations. In conclusion, future ML technologies will significantly improve the efficiency of carbon-based nanomaterial design, accelerating the transition from laboratory research to industrial applications and creating new avenues for the discovery and development of novel materials.

2.5. Two-Dimensional Materials. 2D materials consist of only one to a few atomic layers in the direction of thickness, and they have the potential to extend indefinitely in the plane. These materials are characterized by their unique physical and chemical properties, which differ significantly from their bulk counterparts. Different layers of materials can be adhered together by van der Waals forces. Materials that rely solely on these interlayer van der Waals interactions, without any covalent bonds between the layers, are referred to as van der Waals heterostructures. These heterostructures combine the unique properties of individual 2D layers to create materials with tailored functionalities, making them promising for a wide range of applications in electronics, photonics, and nanotechnology.[153]

Because of the extremely small thickness, the movement of electrons in 2D materials is highly constrained, resulting in the quantum confinement effect. This effect often results in novel physical properties, making 2D materials of significant interest in fields such as electronics,[154–156] spintronics,[157] valleytronics,[158] optoelectronics,[159] twistronics,[160] and slidetronics.[161] Common examples of 2D materials include graphene, which consists of a single layer of carbon atoms arranged in a honeycomb lattice.[162] Another important class of 2D materials is transition metal dichalcogenides, typically composed of one layer of transition metal atoms (such as Mo or W) sandwiched between two layers of chalcogenide atoms (such as S, Se or Te).[163] For van der Waals heterostructures, interlayer coupling can be performed by regulating the interaction between different 2D material layers.[164] By changing the number of layers and the stacking order, the properties of the van der Waals heterostructures can be fine-tuned, and 2D materials can be converted into topological insulators through specific layering structures.[165]

Currently, experimental methods for obtaining single- or multi-layer 2D materials include exfoliating them from 3D bulk materials or directly growing them on substrates using CVD. Exfoliation techniques involve peeling off individual layers from bulk materials, whereas CVD enables the controlled growth of 2D materials on various substrates.[166,167] However, discovering new 2D materials through experimental methods can be resource-intensive and time-consuming, requiring significant investment in both materials and research efforts. ML can learn to capture material features from a large number of crystals, thus guiding the synthesis of new 2D materials.[168,169]

Topological insulators are a typical category of 2D materials; they behave as insulators in the body but exhibit electrical conductivity at the surface or edge. This unique property results from the topological properties of the material, i.e., the electron band structure of the material has a special topological invariant mathematically. In 2D topological insulators, the spin and momentum of electrons are locked together to form edge states. This phenomenon is called the quantum spin Hall effect.[170,171] Topological insulators have a wide range of applications, including field-effect transistors in electronics, efficient optoelectronic devices in optics, topological qubits in quantum computing to enhance the stability of quantum systems, and magnetic topological insulators in magnetism. However, owing to the lack of sufficient candidate materials, the research on topological insulators is limited. In traditional methods, materials are evaluated individually through a trial-and-error process, making the search of the material space resource-intensive and time-consuming. Thus,

a pipeline for determining new 2D topological insulators was developed.[172] With this method, 56 topological materials were identified, of which 17 are quantum spin Hall insulators, nine have not been reported in the literature, and three exhibit large energy gaps suitable for room-temperature applications.

Van der Waals heterostructures are another category of materials that have attracted interest; they consist of 2D materials that are combined. However, computational screenings have suggested that the number of possible 2D materials could be in the thousands, resulting in potentially millions of distinct heterointerface combinations.[173,174] Subsequently, a computational database, web applications, and ML models have been developed to accelerate the design and discovery of 2D heterostructures.[175] Based on 674 non-metallic 2D materials, they generate 226,779 heterostructures classified into three types, of which type-II was observed to be the most common and type-III the least common. Other researchers can also use their network applications and ML model to generate 2D heterostructures and predict physical properties of the new 2D heterostructures.

AI-Driven Experiments. With AI-assisted experimental procedures, 2D thin film materials can be synthesized through automatic control.[176] Specifically, the growth conditions are selected by the experimenter to initialize the algorithm, which then autonomously grows 125 samples. The process is about ten times faster than the traditional one. In addition to supervised learning styles, with the existing positive samples and a large number of unlabeled samples, an ML model can be trained using semi-supervised or unsupervised learning.[177] A large number of potential 2D materials with known properties can be screened through high-throughput clustering. This approach can aid in the design of new 2D materials.[178] Additionally, the query strategy of AI can be optimized based on reinforcement learning, and the classification performance of the model through rewards can be improved. Moreover, through the framework of active learning, only a limited number of labels can be iteratively obtained and updated more positive sample labels.[179]

The research described above used ML models to directly design crystal structures, which can aid researchers identify 2D materials of interest. Additionally, experimenters can be indirectly assisted in synthesizing new 2D and quasi-1D materials by training an ML model to control the parameters of CVD through the integration of AI in the experimental process.[180,181] They can also predict the probability of synthesizing new materials based on the parameters of a given CVD and recommend the most favorable parameters.[182]

2D Materials Datasets. Currently, the number of known 2D materials is still relatively limited, far fewer than the number of 3D bulk materials. Therefore, the construction of a comprehensive 2D material database is a crucial task in condensed matter physics. The Computational 2D Materials Database (C2DB) is a database for 2D material discovery that is aided by ML.[183,184] C2DB first generates new crystals by replacing experimentally known crystal structures with reasonable atoms. Subsequently, stable materials are selected through a series of steps, including structural relaxation, deduplication, and stability calculation using DFT. Finally, stable materials are screened to build a 2D material database. 2DMatPedia selects 3D materials with layered structures from the Materials Project database through high-throughput topological analysis. It generates new materials by performing atomic replacements after stripping the layers. Stable materials are then identified through DFT calculations and added to its database.[185]

Moreover, AI can also be used to replace the DFT calculation part in the construction of 2D material databases. With discriminative AI models, the properties of 2D materials can be directly predicted and classified.[186,187] A 2D perovskite database can predict band gaps and atomic charges using ML models.[188] This demonstrates that ML can assist in the design of new 2D mixed perovskite materials through material classification.

Furthermore, new 2D materials can be generated and their properties can be predicted directly using AI, without requiring traditional computational methods such as DFT. The fabrication of solid-state devices with tailored optoelectronic, quantum emission, and resistive properties requires the design of 2D materials with point defects. Owing to the strong correlation effect of electrons and the exponential growth of the defect site search space, traditional methods cannot determine these 2D materials on a large scale. Through deep transfer learning, an ML model is first pre-trained on 3D materials and then used to predict 2D materials that are likely to produce effective point defects. Based on these predicted 2D materials, another ML model is trained to map these materials from the initial graph structure to calculated defect properties.[189] In addition, manual data extraction from publications is the mainstream method for collecting 2D materials. However, through natural language processing and text mining technologies in the field of AI, crystals with interesting properties can be automatically extracted from publications.[190,191]

2.6. Photovoltaic Materials. Photovoltaic conversion is one of the most important energy conversion methods mastered by humanity, enabling us to "store light." The search for high-performance photovoltaic materials has long been a crucial pursuit. Not only do they provide support for lighting and display but they also contribute to reducing dependence on fossil fuels, thereby having a profound impact on addressing global climate change. The essence of "storing light" lies in capturing excitons generated by photons. Enhancing photovoltaic conversion efficiency (PCE) generally involves two main strategies: improving photon-to-exciton conversion efficiency and designing effective junctions to capture excitons. Photovoltaic conversion works operated in both directions, and these improvements have the potential to inspire new applications in fields such as solar cells, light-emitting diodes (LEDs), laser diodes, photodetectors, and

photocatalysis.

Currently, monocrystalline silicon is the most mainstream photovoltaic material. It is widely used in ground-based photovoltaic power generation owing to its relatively high power generation efficiency (27.3%[192]) and long service life. However, it suffers from several limitations. In classical studies, the ideal bandgap for single-junction solar cells is approximately 1.34 eV, which can theoretically achieve a maximum efficiency of 33.7%.[193] However, the bandgap of monocrystalline silicon is approximately 1.1 eV and cannot be adjusted.[194] To address these limitations, Wang *et al.*[195] successfully identified 22 silicon crystal structures with direct bandgaps through high-throughput calculations and ML methods, overcoming the limitations of traditional diamond-like silicon materials. They utilized the Carbon-24 dataset to construct initial silicon structures and optimized them using ML potentials, such as the GPUMD neural evolutionary potential, resulting in 2,637 stable silicon crystals. Subsequently, the electronic structures were predicted using an ML Hamiltonian model (HamGNN),[196] and structures with direct bandgaps were selected. These structures were then validated through DFT calculations for their bandgaps, transition dipole moments, and other properties. Ultimately, the researchers confirmed 22 stable direct bandgap silicon structures, several of which exhibit higher bandgaps and potential for photovoltaic applications, providing a new theoretical foundation for the design of silicon-based optoelectronic devices. The second is indirect bandgap. It requires phonons as a medium for light absorption, resulting in lower absorption efficiency and making it difficult to reduce the material thickness.[194] The final one is the high sensitivity to impurities. Although the silicon industry is mature, producing high-purity monocrystalline silicon remains costly.[197]

III-V compounds represent another important class of photovoltaic materials as they offer significant advantages over silicon in certain applications. These compounds have direct bandgaps that can be precisely tuned through doping, enabling their use across a broad spectrum of optoelectronic devices.[198] For instance, gallium nitride (GaN), with a bandgap of approximately 3.4 eV, is widely utilized in blue and ultraviolet LEDs,[199,200] whereas gallium arsenide (GaAs), with a bandgap of about 1.42 eV, is commonly applied in red LEDs.[200] III-V compounds exhibit superior thermal stability, high defect tolerance, and exceptional efficiency, making them particularly suitable for applications in extreme environments, such as space-based photovoltaics.[201] Despite these advantages, III-V compounds also pose challenges, including high production costs, the inclusion of toxic elements, and moderate chemical stability, which may limit their widespread adoption.[198,202] In the exploration of next-generation photovoltaic materials, perovskites and organic solar cells (OSCs) stand out as two prominent directions.

Perovskite Materials. Perovskite materials have been some of the most important subjects of study in materials science owing to their outstanding optoelectronic properties and complex crystal structures.[203,204] The term "perovskite" refers to the materials that share the crystal structure of calcium titanate ($CaTiO_3$), an inorganic perovskite, characterized by a general chemical formula of ABX_3, where A and B are cations, and X is an anion that bonds with both cations.[205] These materials typically adopt a cubic structure, but various distortions can result in alternative configurations.[205] Such structural flexibility enables the incorporation of a wide range of elements, making the perovskite family remarkably diverse, with potentially tens of thousands of possible compositions. Moreover, when considering element substitution and doping, the number of potential perovskite variants could exceed millions.[206]

The surge of interest in perovskites began with early demonstrations of their potential in solar cells, and the power conversion efficiency (PCE) of perovskite solar cells (PSCs) has increased dramatically over the past decade, reaching certified values above 25%.[207] This exceptional performance is largely owing to the unique properties of perovskites, such as their high light absorption coefficients, direct and tunable bandgaps, high charge-carrier mobilities, and long carrier diffusion lengths. However, the prototypical organic–inorganic hybrid lead halide perovskites are highly sensitive to environmental factors, including moisture, oxygen, and temperature, and their performance depends on the presence of toxic lead. Consequently, current research is increasingly focused on identifying stable, non-toxic alternatives to traditional lead halide perovskites. Addressing these challenges will be crucial for transitioning perovskites from the laboratory to practical optoelectronic applications.

ML has demonstrated significant potential in accelerating the discovery of high-performance perovskite materials, particularly in terms of predicting photovoltaic efficiency and identifying stable synthesizable structures. Various ML models have been successfully deployed to predict key properties of PSCs, including the PCE, short-circuit current density, open-circuit voltage, fill factor, and external quantum efficiency.[208] In a recent study, several models were compared for PCE prediction, and XGBoost was identified as the most accurate.[209] Furthermore, XGBoost has also been utilized to predict recombination losses in PSCs, revealing insights into dominant recombination mechanisms.[210]

Beyond performance prediction, ML is essential in assessing structural stability and guiding the synthesis of promising candidates. ML interatomic potential (MLIP) models have been developed to predict the crystal structures of hybrid organic–inorganic perovskites (HOIPs), enabling researchers to evaluate the stability of these compounds accurately.[211] Additionally, MLIP has been applied to explore the dynamic behaviors of metal halide perovskites, shedding light on their structural characteristics under different conditions.[212] Through a combination of ML and MD simulations, researchers have also investigated the stability of HOIPs.[213] Moreover, ML methods are actively used to identify synthesizable

PSCs, which is crucial for material validation in practical applications.[214] Additionally, ML aids in the search for non-toxic perovskite materials as well. Active learning has been applied to identify lead-free white-light LEDs by training models on oxide perovskites and datasets selected from six halide perovskites using active learning methods.[215] This study successfully predicted photoluminescence quantum yield (PLQY), observing a significant correlation between ionic radii and PLQY. A simpler ML model has also been applied to identify non-toxic PSCs,[216] focusing on the importance of the d_{10} orbital in double perovskite doping. Improving interpretability and identifying chemical patterns is another key area of development in perovskite-related ML research. Genetic algorithms (GAs) have been used as a pre-screening tool to aid graph convolutional networks (GCNs) in bandgap prediction, facilitating the identification of relevant chemical trends.[217] Moreover, decision tree models have been enhanced to improve interpretability in applications to solid-state chemistry, enabling researchers to identify significant descriptors across diverse materials, including perovskites, spinels, and rare-earth intermetallics.[218]

Organic Solar Cells. OSCs represent another prominent class of next-generation photovoltaic materials. While inorganic materials are known for their efficiency and durability, their production can be costly. In contrast, OSCs offer distinct advantages, such as lightweight and flexible structures that can be easily fabricated into various shapes and sizes, along with the potential for low-cost and scalable production. However, OSCs generally have lower efficiency and shorter lifetimes, presenting a significant challenge for widespread adoption.[219] The primary device architecture is bulk-heterojunction, which features an active layer composed of interpenetrating networks of donor and acceptor materials, which facilitates efficient charge separation and transport.[220] The initial breakthrough in acceptor materials occurred with the use of fullerene derivatives, such as C_{60},[221] which exhibited promising efficiency and laid the groundwork for further advancements in OSCs. Soluble fullerene-based acceptors such as $PC_{61}BM$ and $PC_{71}BM$ have since been developed and attracted significant interest. However, the inherent limitations of fullerene acceptors, such as weak absorption in the solar spectrum, difficulty in tuning energy levels, and the propensity for aggregation and crystallization–have hindered their further development and highlighted the need for alternative materials.[222]

Recently, the focus has shifted toward non-fullerene acceptors (NFAs), which have demonstrated significant promise owing to their tunable energy levels, improved absorption properties, straightforward synthesis, and better morphological stability. A major milestone was reached in 2019 with the introduction of Y6,[223] a new benchmark NFA that achieved a PCE of 18%,[224] attracting widespread interest for its high performance. Since its introduction, Y6 and related NFAs have become a central topic in the field, with research efforts dedicated to further improving performance, understanding the underlying mechanisms responsible for the high efficiency, and exploring new applications. The next phase of development in OSCs will likely involve optimizing Y6 derivatives to further enhance performance and stability, as well as the continued search for novel NFAs with unique properties. These efforts aim to push the limits of efficiency while addressing the remaining challenges related to the lifetime of organic solar cells, laying the foundation for more practical and commercially viable OSC technologies. In materials science, decision tree algorithms have been widely utilized to accelerate the discovery of new materials, particularly for predicting optical and electronic properties of molecules and materials. The general workflow typically includes collecting molecular datasets, mapping molecular structures to descriptor spaces, and then employing ML models to learn and predict key properties such as PCE. This approach has been applied extensively in various studies. RF has been used to predict the PCE for NFAs,[225] aiding in the development of new acceptor materials for MP6 donors. In Ref. [226], RF was applied to predict the short-circuit current density (JSC), assisting in the creation of new donor molecules compatible with NFAs. Additionally, XGBoost is leveraged for high-throughput screening to predict PCE for DA pairs.[227]

Comparative studies have also been conducted on various decision tree models, with RF often emerging as advantageous in PCE prediction. RF is used to screen and predict performance for NFA and broader DA pairs.[228,229] Meanwhile, other studies have observed that gradient boosting models exhibit superiority in predicting JSC and open-circuit voltage (VOC), as noted in Ref. [231]. To further enhance model performance, some studies have explored algorithmic improvements. In a recent study,[232] an RF's PCE predictions for NFAs were observed to be enhanced by the introduction of artificial failure data. Another approach integrates geometric GNNs, automatically extracting features from molecular structures, and then uses decision tree models (such as LightGBM) as a backend for analysis, as described in Ref. [233]. Additionally, owing to the lag in available datasets, leveraging LLMs to retrieve literature can expand material libraries and accelerate the discovery of novel materials, which is shown in Ref. [230].

2.7. Catalyst Materials. Catalyst materials are substances that can alter the rate of a chemical reaction. Note that catalysts are not themselves involved in the final product of the reaction; however, they accelerate or decelerate the rate of the reaction by modifying the path of the reaction and reducing the activation energy required for the reaction to occur. A catalyst retains its chemical nature and quality both before and after a reaction; therefore, it can be reused on numerous occasions.

The history of the application of catalysts can be traced back several hundred years. Over time, catalyst technology has developed in a direction that is increasingly efficient, environmentally friendly, and sustainable. It has contributed significantly to various fields, including the chemical industry, energy, environmental protection,

life science, and medicine. Recently, the field of material synthesis has undergone accelerated development, largely owing to the advent of advanced AI technologies. The synthesis of catalyst materials has been no exception to this trend. Owing to the extensive scope of catalyst materials and the diverse applications of corresponding ML technology, selecting a representative sample of work for presentation is deemed prudent, considering the limitations of author's knowledge in this field.

Descriptors are important in improving the accuracy of ML models. While ML techniques can improve the accuracy of predictions, descriptors often determine the upper limit of the prediction.[234] Some researchers focus on searching for additives in the electrochemical deposition of copper catalysts for the reduction of CO_2 (CO2RR).[235] Selecting an appropriate combination of additives for the preparation of the catalyst is a challenging process. To solve this problem, scholars have devised a strategy comprising three rounds of learning, integrating experimental outcomes and ML and subsequently applied it to an additive library. The process enabled researchers to identify crucial chemical components and to synthesize the requisite molecules. This research represents a significant contribution to the field of experiment-based descriptors.

Furthermore, the descriptors for product selectivity in the oxidative coupling of methane (OCM) reaction were analyzed using ML and physical quantities derived from the periodic table.[236] One of the principal objectives of this study was to investigate the selectivity of C_2H_4/C_2H_6 (C_2s). The process employs the use of hierarchical clustering, RF classifier, and support vector classifier. Eventually, three previously unreported catalysts with high C_2s were identified as potential candidates, i.e., Ti-V-Ce-BaO, Y-Y-Eu-TiO_2, and La-Pr-Hf-BaO, and their performance was verified through experimental analysis. The authors additionally examined five additional related descriptors. They additionally examined five related descriptors and concluded that high C_2s values are associated with low first ionization energies, electron affinities, and electronegativities, as well as high second ionization energies and densities.

In addition to experiment-based descriptors, some studies have utilized theory-guided descriptors. The sure independence screening and sparsifying operator (SISSO) descriptors are expressed as nonlinear functions of intrinsic properties of the clean catalyst surface.[237] The authors demonstrated that their method was more general and accurate in predicting the adsorption energy of alloys on mixed metal surfaces, even when based on training data that included only pure metals. If a considerable number of features are available, the compressive sensing method SISSO represents an appropriate solution.[238] This approach has also been applied to study other materials, including perovskite oxides and halides[239] and doped transition metal oxides.[240] However, this method still has some limitations, such as the presence of nearly degenerate models, stability challenges under data perturbations, and unclear physical interpretations.[241] Extensive research has been conducted on theory-guided descriptors from other perspectives, such as intrinsic atomic properties,[242] electronic and structural properties,[243–245] and others.[246–248] Similarly, efforts have been made to identify descriptors that integrate theoretical and experimental data.[249–252]

Additionally, research has been conducted from alternative perspectives on the subject of catalysts. For example, the utilization of active learning in conjunction with DFT calculations to develop an efficient copper-aluminum electrocatalyst for the conversion of CO_2 to ethylene is remarkable.[253] This approach has resulted in the highest reported Faradaic efficiency to date. In their study, the researchers employed probabilistic models with Gaussian processes, trained with *ab initio* data and a set of multifidelity features, to identify high-performance ABO_3-type cubic perovskites that can catalyze the oxygen evolution reaction (OER).[244] The method has successfully identified several known perovskites, which demonstrate superior performance to the benchmark $LaCoO_3$. A series of perovskites with favorable properties have also been obtained, including $KRbCo_2O_6$, $BaSrCo_2O_6$, and $KBaCo_2O_6$.

The discovery of single-atom alloy catalysts (SAACs) represents a significant area of focus within the scientific community.[254] In this particular study, they combined first-principles calculations with compressed-sensing data-analytics methodology. With this approach, they finalized more than 200 unreported candidate SAACs, some of which exhibit greater stability than previously observed. Concurrently, their investigation highlighted the significance of data analysis in avoiding bias in catalytic design.

A recent publication presented an active learning workflow for the generation of fuel cell catalysts.[255] The authors focused on ternary alloys in the form of Pt_2CoM (in the practical application of proton exchange membrane fuel cells, PtCo is the most promising alloy catalyst, whereas M represents another base metal element). Guided by theoretical calculations, the researchers ultimately prepared the Pt_2CoCu and Pt_2CoNi compounds through experimental synthesis. These materials exhibited a large electrochemically active surface area of approximately $90\,m^2/g_{Pt}$ and a high specific activity of approximately $3.5\,mA/cm^2$.

Chen *et al.* leveraged local ML capabilities to rapidly and accurately identify structure descriptors by integrating fundamental physical attributes with graph convolutional neural networks (CGNNs).[256] They successfully identified 43 high-performance alloys as electrocatalysts for the hydrogen evolution reaction, with some candidates already validated. To further validate the method's precision, they conducted a comprehensive study of AgPd through ab initio calculations in a realistic electrocatalytic environment.

An intriguing prospect emerged from the utilization of language models in catalyst discovery.[257] The discovery of catalyst materials was presented with the aid of an LLM, designated CatGPT. The focus is on the two-electron oxy-

gen reduction reaction (2e-ORR), with the model being applied to identify the catalyst for this process. Ultimately, several materials that were not present in the database were identified, including RhSe, CdAg, and SnAu.

The field of technology catalysts is vast, encompassing a multitude of applications for ML technology and its associated techniques. The aforementioned examples represent a selection of the most influential or recently developed outcomes, and a comprehensive account of all relevant findings is beyond the scope of this discussion.

2.8. High-Entropy Alloys. High-entropy alloys (HEAs) are a class of innovative materials fabricated from five or more elements in nearly equal proportions. The traditional concept of creating alloys is to add reinforcing elements to a metal, which has been used extensively throughout human history. In 2004, the discovery of HEAs offered a distinctive alloying strategy.[258,259] These new materials are referred to as HEAs owing to their increased configurational entropy, which was considered to be the key factor in their stabilization. Although configurational entropy was later identified to not be as important as first assumed.[260,261] HEAs have many excellent mechanical properties and a large component space, which provides a suitable platform for material research.

However, for the design of HEAs, conventional methods encounter significant challenges. Considering only the usual elements of the periodic table, this encompasses a significantly large composition space, which cannot be managed using conventional material design approaches, such as the calculation of phase diagrams and DFT.[262]

ML has developed rapidly over the past decades, which suggests that it is likely to make a difference in the area of material design for HEAs.[34] Some researchers utilized several ML models including some simple deep neural networks and selected a conditional random search as the inverse predictor to design the new HEAs.[263] They successfully observed two HEAs with better ultimate tensile strength and total elongation than the input datasets. An SVM was also utilized to solve problems of HEAs.[264] In their approach, the authors emphasized the framework of hyperparameter tuning and the use of weighted values. Through experiments, they discovered that their architecture performed very well and even exceeded the results of an ANN. Some studies have compared the effectiveness of different methods. Huang *et al.* tested three different ML algorithms, namely K-nearest neighbors (KNNs), SVM, and two ANNs, i.e. unsupervised self-organizing maps and supervised multi-layer feed-forward neural network (MLFFNN).[265] They concluded that MLFFNN performed better. Krishna *et al.* tested logistic regression, decision tree, SVM, RF, gradient boosting classifier, and ANN. They claimed that the ANN exhibited the highest accuracy.[266]

All of the above-mentioned studies attempted to employ ML techniques but did not fully incorporate the characteristics of HEAs. The dataset for HEAs is not sufficiently large; therefore, architectures that can be trained from small samples to produce sufficiently adaptive structures are required. Some recent studies have considered this problem to some degree.

The first aspect to mention is active learning. A typical example demonstrated the successful implementation of an iterative approach for the synthesis of new HEAs.[262] Their workflow was a closed loop in which ML techniques, DFT, thermodynamic calculations, and experiments were used in the process. Their research focused on the design of high-entropy Invar alloys with low thermal expansion coefficients (TECs), and they investigated FeNiCoCr and FeNiCoCrCu HEAs. Their data showed that the HEAs have lower TECs and higher configurational entropy than past materials. In addition to the ability of discovering new HEAs, one of the greatest strengths of this workflow is its efficiency: the entire process of their work took only a few months, whereas in the past, the corresponding discoveries could have taken several years and more experiments. Note that other efforts have proposed frameworks with a similar structure.[267]

Some researchers employed a deep network architecture with residual connections to predict the phase formation in HEAs.[268] Compared with traditional neural networks, the overall accuracy of this framework could reach 81.9%. This research provided a new approach for predicting the phase formation of HEAs and is also significant for designing new HEAs.

Wang *et al.* devised a novel type of neural network called the elemental convolution neural network (ECNet), which can attain global element-wise representations.[269] The authors investigated FeNiCoCrMn/Pd systems using ECNet and the data obtained using DFT calculations. The authors also used transfer learning to enhance the performance of the network. With this framework, the concentration-dependent formation energies, magnetic moments, and local displacements in various sub-ternary and binary systems could be obtained.

The application of ML to the analysis of materials microstructure provides a basis for the reverse engineering of alloys, which is then integrated with the accumulated knowledge of human experience. As a result of employing their own methodologies, Pei *et al.* identified a novel alloy, provisionally named 9% Cr steel.[270] The authors posited that the success of the approach can be attributed to the optimization of neural network structures and the fine-tuning of associated parameters.

Some of the studies described above effectively mitigated the problem of small size of datasets. However, the quality of the datasets and the selection of appropriate ML techniques remain problematic.

2.9. Porous Materials. Porous materials are a class of materials with a pore structure filled with holes or voids of varying sizes. The size, shape, and distribution of the pores determine the properties of the material. Porous materials typically have a high specific surface area, low density, and good adsorption capacity, which enables them to have a wide range of applications in various fields, such as the chemical, energy, environment, and biomedicine industries. Zeolites are a representative class of porous mate-

rials. Newly emerging porous materials, including MOFs, covalent organic framework materials (COFs), and carbon-based porous materials, have expanded the range of applications of porous materials.[271,272]

In recent years, significant developments have been achieved in the field of AI, with notable advances in the area of porous material synthesis. Because zeolites were synthesized earlier and are more widely used than other porous materials, it is unsurprising that research has been conducted into the AI-assisted synthesis of zeolites. In their study, Kim *et al.* employed a generative adversarial network, designated ZeoGAN, to generate 121 crystalline porous materials.[10] The neural network receives inputs in the form of energy and material dimensions. The results demonstrated that zeolites with a desired range of 4 kJ/mol methane heat of adsorption can be produced reliably. Four years later, a study employing diffusion modeling in the context of porous materials was conducted,[273] and the corresponding architecture is known as ZeoDiff. The authors asserted that the diffusion model outperforms the ZeoGAN with respect to structural validity, exhibiting an improvement in performance of over 2000-fold. Furthermore, the authors implemented conditional generation, namely the generation of structures with user-desired properties, with ZeoDiff. To achieve conditional generation, they had to perform adjustments to the network, such as integrating an additional channel that was closely relevant to the property of interest.

The synthesis of MOFs is a more complex and challenging process than that of zeolites. Over 100 known species of atoms can form MOFs, with an average number of atoms per unit cell that is significantly higher than that of zeolites. The variation autoencoder (VAE) has been successfully applied for generative modeling of MOFs.[274] A VAE framework, designated SMVAE, was employed to generate MOFs. The structural validity of SMVAE was demonstrated to be 61.5%. By focusing on the adsorption capacity of CO_2 in their model, the authors demonstrated its ability to modulate the CO_2 adsorption capacity and selectivity. The top-performing MOF they discovered has a CO_2 capacity of 7.55 mol/kg and a selectivity over CH_4 of 16. A generative AI framework called GHP-MOFassemble was proposed in the study.[275] The GHP-MOFassemble method was employed to synthesize MOF linkers, which were then utilized with one of three preselected metal nodes (Cu paddlewheel, Zn paddlewheel, Zn tetramer) to form MOFs with a primitive cubic topology. The linker molecules were generated through the utilization of DiffLinker.[276] Molecular fragments with high expression levels were extracted from an existing database. The aforementioned molecular fragments were employed to obtain linkers, which in turn facilitated the generation of MOFs. Subsequently, the MOFs were evaluated using a predictive model, resulting in the identification of six MOFs with a CO_2 capacity exceeding 2 mmol/g, indicative of high performance. Researchers developed a coarse-grained (CG) diffusion model, designated MOFDiff, which can generate CG MOF structures through a denoising diffusion process.[277] The authors proposed that template-based methodologies can constrain the search space and preclude the inclusion of viable materials. Consequently, they devised a process for generating MOFs that entails the direct identification of coarse-grained building blocks within 3D coordinates. As a subsequent processing stage, an additional MOF assembly procedure is necessary to orientate the components and ascertain the interconnectivity between them. The utilization of MOFDiff has enabled the identification of potential candidates for high CO_2 working capacities, with nine of the current top ten being generated by this framework. A recent study used signed distance functions (SDFs).[278] They introduced a latent diffusion model, MOFFUSION, which utilizes SDFs as the input representation of MOFs. The model demonstrated a high structural validity of 81.7%. Additionally, the authors revealed its capacity for conditional generation across a range of data modalities, including numeric, categorical, text data, and their combinations.

In addition to zeolites and MOFs, research has been conducted into the use of AI in the inverse design of other porous materials. For example, a methodology employing ML approaches for the identification of highly porous carbon materials was devised.[279] A methodology employing quantitative structure–property relationships in conjunction with ML techniques to forecast the properties of COFs was developed. This methodology utilizes the structural characteristics of the solvents and COF building blocks.[280] Furthermore, the integration of ML with porous media has facilitated several advancements across diverse research domains.[281,282] The application of ML technology in the synthesis of porous materials is now widely acknowledged. Further attempts are currently underway.

3. Development of AI Methods in Materials Science. In this chapter, we present a comprehensive review of the advancements in AI technologies within the field of materials science. Drawing upon recent trends and the growing significance of AI, we explore traditional ML methods, geometric GNNs, discriminative AI, generative AI, and LLMs. As depicted in Fig. 4, GNNs are classified into invariant and equivariant models. Invariant GNNs are extensively applied in discriminative AI to predict material properties, thereby enabling high-throughput screening. In contrast, equivariant GNNs are predominantly employed in generative AI to facilitate structural predictions of materials. Next, we provide a detailed overview of the development of these algorithms and their applications in materials discovery.

3.1. Traditional Machine Learning Methods. We categorize techniques such as RFs, convolutional neural networks (CNNs), SVMs, and MLPs as traditional ML methods. These algorithms are among the most commonly applied in materials discovery, with each offering distinct advantages in addressing different design challenges. RF, as an ensemble method, combines the predictions of multiple

decision trees to reduce the risk of overfitting from individual trees. Its formula is given by

$$\hat{y} = \frac{1}{N}\sum_{i=1}^{N} h_i(x), \tag{1}$$

where $\hat{y}$ represents the final prediction, N denotes the number of trees in the ensemble, and $h_i(x)$ refers to the prediction made by the i-th tree.[283] The decision tree, renowned for its interpretability, performs classification by recursively splitting the data. While decision trees are prone to overfitting, this risk can be mitigated by controlling the depth of the tree. Common splitting criteria include the Gini coefficient and entropy, with entropy defined as

$$\text{Entropy}(D) = -\sum_{i=1}^{n} p_i \log(p_i), \tag{2}$$

where D is the dataset, and p_i is the probability of class i in the dataset.[284] The SVM determines an optimal hyperplane that maximizes the margin between classes; for nonlinear data, it uses kernel functions to map data to a higher-dimensional space, optimizing $\min_{w,\,b} \frac{1}{2}|w|^2$ to determine the hyperplane, where w is the weight vector and b is the bias term.[285] The MLP is an NN with at least one hidden layer, which minimizes the mean squared error (MSE) via backpropagation to learn from complex data. Its MSE formula is

$$\text{MSE} = \frac{1}{n}\sum_{i=1}^{n}(y_i - \hat{y}_i)^2, \tag{3}$$

where n denotes the number of samples, y_i is the true value, and $\hat{y}_i$ is the predicted value.[286,287] Furthermore, the MLP utilizes nonlinear activation functions, such as ReLU, to capture complex data features. Together, these algorithms exhibit strong capabilities in addressing the high-dimensional nonlinear challenges inherent in materials science and design.

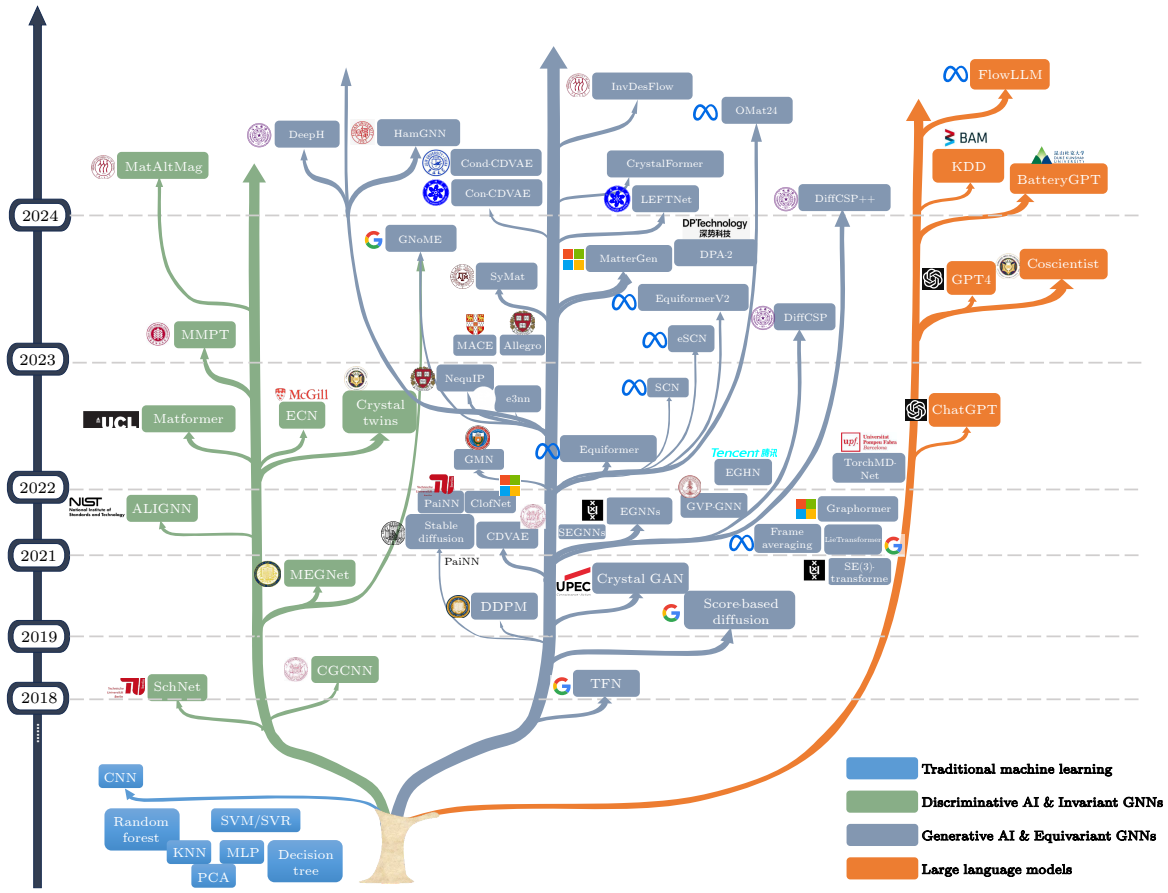

Fig. 4. Rapid advancement of AI technologies accelerating materials discovery in various ways. Blue indicates traditional ML; green represents the development of invariant GNNs and their application in discriminative AI for predicting material properties; deep blue denotes the progress of equivariant GNNs, generative AI techniques, and their integration for structural predictions; orange signifies the role of LLMs in expediting materials discovery.

In the design of nonlinear responses for mechanical metamaterials, neural networks, when combined with evolutionary strategies within an optimization framework, enable the precise engineering of metamaterials with specified stress–strain behaviors.[288] PCA generates a stress–strain dataset consisting of 7,500 elements, effectively reducing data dimensionality to facilitate neural network training. With precise stress–strain behavior design, the

relative error in the test set is as low as 4.8%, supporting personalized material design for applications such as soft robotics and energy absorption systems. This method introduces innovation by controlling the nonlinear response of metamaterials through geometric parameter optimization, thereby enhancing the efficiency of nonlinear mechanical metamaterial design and expanding their potential in smart device applications.

In alloy optimization, multiple regression algorithms are employed to predict the hardening curves of boron steels, thereby improving alloy design. Using experimental hardening curve data from 62 boron steels, with input variables including chemical composition, Jominy bar distance, and material hardness as the output, a 10-fold cross-validation was applied to evaluate various regression algorithms.[289] The RF model had the highest correlation coefficient and lowest error, facilitating the design of boron steel alloys with enhanced hardening performance. This model exhibited considerable potential for commercial application in software such as JMatPro[†], underscoring the significant role of ML in optimizing material performance.

In the field of optical metasurface solar absorber design, decision tree and RF regressors are employed to optimize geometric parameters for spectral absorption.[290] Using data from full-wave electromagnetic simulations, PCA reduces dimensionality, enhancing computational efficiency. The RF model achieves high prediction precision for spectral absorption, with an R^2 value of 0.99, improving the design efficiency of solar absorbers for green energy applications and paving new pathways in optical material design. To accelerate the development of polymeric biomaterials, various ML models, including DL, RF, and Gaussian process models, process the physical properties of polymers encoded by SMILES notation and molecular descriptors.[291] These ML models significantly enhance the design of novel polymer materials, optimizing physical, electrical, and rheological properties under data-scarce conditions, thereby accelerating progress in polymer biomaterials within the medical field.

In real-time topology optimization, support vector regression (SVR) and KNN models generate optimized material distributions.[292] Through feature extraction and PCA for dimensionality reduction, simplified design variable vectors from direct optimization serve as training inputs. The model adapts structures rapidly to different external loads, supporting applications in short-beam structure optimization and illustrating the potential of ML in real-time structural optimization for complex industrial structures.

CNNs[293] represent a powerful class of DL algorithms that are particularly suited for processing images and sequential data owing to their capability to efficiently extract complex features. Widely applied in computer vision and related scientific fields, CNNs perform a series of convolution operations across multiple layers, progressively abstracting high-dimensional input data into lower-dimensional representations. This hierarchical feature extraction enhances their effectiveness in tasks such as pattern recognition and predictive modeling. Mathematically, the convolution operation in each layer l with filter k is expressed as follows:

$$\boldsymbol{f}_{ij}^{k} = \sum_{m=0}^{M-1} \sum_{n=0}^{N-1} \boldsymbol{W}_{mn}^{k} \cdot \boldsymbol{X}_{(i+m)(j+n)} + \boldsymbol{b}^{k}, \tag{4}$$

where $\boldsymbol{f}_{ij}^{k}$ denotes the output feature map for filter k at spatial position, $\boldsymbol{W}_{mn}^{k}$ represents the weights in the convolutional kernel k of size, $\boldsymbol{X}_{(i+m)(j+n)}$ is the input feature map from the previous layer, and $\boldsymbol{b}^{k}$ is the bias term associated with filter k. Unlike traditional neural networks, CNNs use a combination of convolutional, pooling, and fully connected layers, enabling them to detect spatial and positional relationships within structured data effectively. In materials science, CNNs have become increasingly instrumental in optimizing material properties and structural design, yielding notable advancements in the topology optimization and inverse design of complex materials.

A CNN architecture based on ResNet[294] was proposed for the topology optimization of nonlinear structures, specifically targeting large-deformation hyperelastic materials such as neo-Hookean materials.[295] The study generated an extensive dataset, consisting of 15,000 data pairs for linear elastic materials, 18,000 pairs for hyperelastic materials, and 20,000 pairs for linear stress materials, all aimed at optimizing material distribution to achieve maximal structural performance. By integrating the residual learning capabilities of ResNet with the U-net architecture, the model attains a Dice similarity coefficient of 0.964 in nonlinear material topology optimization, significantly improving both predictive accuracy and optimization efficiency. This method offers a robust tool for structural optimization of hyperelastic materials and highlights the potential of ML in addressing complex nonlinear topology optimization challenges in materials science.

A transfer learning framework integrating CNN with simplified ML (SML) techniques was used to design a novel steel alloy with superior rotating bending fatigue resistance.[296] Utilizing a database of 411 samples, the study extracted static mechanical performance features and employed a transfer learning model to predict fatigue strength, resulting in the design of Alloy R–an innovative alloy with fatigue strength that significantly surpasses that of existing alloys. This novel application of transfer learning effectively reduces data requirements, providing a practical solution for high-cost property predictions such as fatigue strength. Moreover, it establishes a theoretical foundation for exploring the relationship between fatigue performance and alloy design, offering valuable insights for material engineers. Additionally, a CNN-based approach was developed to predict the toughness and strength of composite materials under crack conditions, with finite element models generating data that treat composite materials as 8×8-pixel images with binary values representing

[†]https://jmatpro.cn/

different material properties (e.g., soft or hard).[297] The CNN model achieved a prediction accuracy exceeding 98%, enabling high-performance composite design even under data-scarce conditions. This research highlighted the potential of ML to facilitate accurate design with minimal data, providing a foundational method for reverse engineering in composite materials, and demonstrating the effectiveness of ML in enhancing material design efficiency and predictive accuracy.

In this section, we review the development and application of traditional ML algorithms in the inverse design of materials. These algorithms have provided significant impetus for material discovery. Although they emerged early, this does not imply that they are outdated; different problems and scenarios require the selection of appropriate algorithms.

3.2. Geometric Graph Neural Networks. The prediction of properties and structures of crystalline materials has long been a crucial task in materials science. Owing to the necessity to account for complex symmetry constraints, crystal data are challenging to model using conventional networks such as CNNs. Geometric GNNs are models designed to process graph data with geometric information (e.g., spatial coordinates and angles) and are well-suited for studying spatial structures such as molecules, proteins, and materials. Based on scientific requirements, geometric GNNs are categorized into two types. The first type, invariant GNNs, maintain invariant outputs under Euclidean transformations, making them ideal for predicting properties such as band gaps, formation energies, and T_c, which are independent of the absolute position and orientation of the material structure. The second type, equivariant GNNs, update both invariant and equivariant features such that outputs change in similarly to the inputs under geometric transformations, making them particularly effective for capturing directional relationships in applications such as material structure prediction and generation.

Table 1. Basic notations. Following Han's[35] notation conventions, we present the commonly used symbols.

Notation	Description
$\mathcal{G} := (\boldsymbol{A}, \boldsymbol{H})$	Graph with N nodes, characterized by its adjacency matrix $\boldsymbol{A}$ and node feature matrix $\boldsymbol{H}$.
$\vec{\mathcal{G}} := (\boldsymbol{A}, \boldsymbol{H}, \vec{\boldsymbol{X}})$	Geometric graph incorporating a 3D coordinate matrix $\vec{\boldsymbol{X}}$ in addition to $\boldsymbol{A}$ and $\boldsymbol{H}$.
$\mathcal{N}_i$	Set of nodes neighboring node i.
$\boldsymbol{h}_i \in \mathbb{R}^{C_h}$	Feature of node i containing C_h attributes.
$\boldsymbol{u}$	Global state vector.
$\bigoplus$	Aggregation of neighboring node features, such as sum, mean, or max.
$\vec{\boldsymbol{x}}_i \in \mathbb{R}^3$	3D spatial coordinates of node i.
$\vec{\boldsymbol{V}}_i \in \mathbb{R}^{3\times C}$	Multi-channel 3D vector representing node i.
$\vec{\boldsymbol{V}}_i^{(l)} \in \mathbb{R}^{(2l+1)\times C_l}$	Type-l irreducible vector associated with node i.
$\boldsymbol{e}_{ij} \in \mathbb{R}^{C_e}$	Edge feature vector from node j to node i.
G, g	Group G and its element g, relevant to transformations in the graph.
$\times$, $\otimes$	Operators for vector operations: cross product $\times$ and Kronecker product $\otimes$.
$\otimes_{\text{cg}}$	Clebsch–Gordan tensor products.
$Y^{(l)}(\vec{\boldsymbol{x}}) \in \mathbb{R}^{2l+1}$	Type-l spherical harmonic vector evaluated at point $\vec{\boldsymbol{x}}$.
$\boldsymbol{D}^{(l)}(g)$	l-th degree Wigner-D matrix for rotation $g \in \text{SO}(3)$.
ϕ, ψ, φ, σ	Functions achieved through MLP.
$\mathcal{L}$	Loss function.
$\boldsymbol{W}$	Weight matrix.

Graph Neural Networks. GNNs differ from traditional neural networks in that they operate on graph-structured data rather than tensor-structured data. A graph $\mathcal{G} := (\boldsymbol{A}, \boldsymbol{H})$ represents a graph with N nodes, characterized by its adjacency matrix $\boldsymbol{A}$ and node feature matrix $\boldsymbol{H}$. The core concept of GNNs is message passing, where, as the graph propagates forward, the features stored at node i, denoted as $\boldsymbol{h}_i$, are updated based on information from its neighborhood:

$$\boldsymbol{h}_i' = \sigma_{upd}\left(\boldsymbol{h}_i, \bigoplus_{j\in\mathcal{N}_i} \boldsymbol{h}_j\right). \tag{5}$$

The equation illustrates how the feature $\boldsymbol{h}_i'$ of node i is updated through a message-passing mechanism. In this framework, the function σ_{upd}, which is typically a nonlinear activation function, takes as inputs both the original feature $\boldsymbol{h}_i$ and an aggregated summary of the features $\boldsymbol{h}_j$ from neighboring nodes j within the set $\mathcal{N}_i$. The aggregation operator $\bigoplus$ can encompass operations such as summation, averaging, or obtaining the maximum. This methodology enables node i to effectively incorporate information from its local neighborhood, thereby enriching its updated feature representation. This mirrors the behavior of physical systems, where long-range correlations are governed by local interactions. Specifically, when features include spatial information–typically represented as 3D vectors–the networks are categorized as geometric GNNs, denoted as $\vec{\mathcal{G}} := (\boldsymbol{A}, \boldsymbol{H}, \vec{\boldsymbol{X}})$, where a geometric graph incorporates a 3D coordinate matrix $\vec{\boldsymbol{X}}$ in addition to $\boldsymbol{A}$ and $\boldsymbol{H}$.

To establish a framework for categorizing various types of geometric GNNs, we first present the message-passing neural network (MPNN).[298] In this framework, features h_i are associated with nodes and are iteratively updated at each hidden layer,

$$\boldsymbol{h}_i' = \sigma_{upd}\left(\boldsymbol{h}_i, \bigoplus_{j\in\mathcal{N}_i} \boldsymbol{m}_{ij}\right), \tag{6}$$

whereas messages m_{ij} are stored on the edges, serving as update buffers for the connected nodes.

$$\boldsymbol{m}'_{ij} = \sigma_{msg}\left(\boldsymbol{h}_i,\ \boldsymbol{h}_j,\ \bigoplus_{(kl)\in\mathcal{N}_{(ij)}} \boldsymbol{m}_{kl}\right). \tag{7}$$

Messages guide the feature updates and propagate along the edges, thereby reinforcing the locality principle in GNNs.

Invariant Geometric GNNs. Invariant geometric GNNs can be classified according to the scalar geometric quantities they utilize for message passing, such as pairwise distances, triplet-wise angles, and quadruplet-wise torsion angles. In the following, we introduce one model from each category as an example.

SchNet[299] is one of the earliest invariant GNN models, developed as a variant of the deep tensor neural network[300] for modeling atomic structures. In SchNet, continuous filters are employed to capture interaction terms based on the pairwise distances between atoms:

$$\boldsymbol{h}'_i = \boldsymbol{h}_i + \sum_{j\in\mathcal{N}_i} \boldsymbol{m}'_{ij}\ \boldsymbol{h}_j, \tag{8}$$

$$\boldsymbol{m}'_{ij} = \boldsymbol{W}(\|\vec{\boldsymbol{x}}_i - \vec{\boldsymbol{x}}_j\|), \tag{9}$$

where $\boldsymbol{W}$ denotes the learnable filter. The filter employs Gaussians as radial basis functions in its first layer to encode pairwise distances.

$$e_k(\|\vec{\boldsymbol{x}}_i - \vec{\boldsymbol{x}}_j\|) = \exp(-\gamma(\|\vec{\boldsymbol{x}}_i - \vec{\boldsymbol{x}}_j\| - \mu_k)^2). \tag{10}$$

Notably, later studies[301] have shown that spherical Bessel functions serve as more effective bases. Other distance-based models include CGCNN[302] and PhysNet.[303] While simple and effective, these models are limited in that they cannot distinguish between molecular structures that have identical pairwise distances but differ in bond angles.

DimeNet[304] utilizes triplet information by introducing directional message passing:

$$\boldsymbol{m}'_{ji} = \sigma_{msg}\left(\boldsymbol{m}_{ji},\ \bigoplus_{j\in\mathcal{N}_j\setminus\{i\}} \boldsymbol{m}_{kj}\right), \tag{11}$$

where $\boldsymbol{m}_{ji}$ denotes a directional message passed from node j to node i, which is updated by iterating over all messages directed toward node j, excluding those from node i. The angle information $\angle ijk$ can be computed, enabling the differentiation of structures with varying bond angles. While DimeNet represents an advancement over SchNet by capturing angular information, it still cannot resolve torsions or distinguish chiral structures.

SphereNet[305] also applies a directional message-passing approach but with further refinement. It introduces "spherical message passing" using a local spherical coordinate system. The messages encode not only polar angles, such as $\angle ijk$ and $\angle ijk'$, but also the azimuthal angle between $\vec{\boldsymbol{x}}_k - \vec{\boldsymbol{x}}_j$ and $\vec{\boldsymbol{x}}_{k'} - \vec{\boldsymbol{x}}_j$. This enables SphereNet to capture complete geometric information around node j, including quadruplet torsional angles. Consequently, SphereNet can distinguish chiral structures, achieving SE(3)-invariance, whereas prior models were limited to E(3)-invariance. Although failure cases exist in which SphereNet cannot distinguish certain configurations, such scenarios are theoretically possible but highly improbable in natural settings. Later research[306] proposed quaternion message passing, which encodes these geometric features more efficiently. Other models in this category include GemNet[307] and ComENet.[308]

Equivariant Geometric GNNs. Geometric GNNs achieve equivariance in two main ways: one approach achieves scalarization-based models through inner product operators, whereas the other utilizes group representation theory, spherical harmonics, and tensor product methods. Finally, we introduce several studies that integrated attention mechanisms into geometric GNNs models, significantly enhancing their expressive power.

To achieve equivariance, some studies[309–311] implemented a scalarization-based models approach, with equivariant GNNs[309] being the most prominent. This model does not require costly higher-order representations; instead, it first converts the 3D coordinates into invariant scalars, specifically squared distances $\|\vec{\boldsymbol{x}}_i - \vec{\boldsymbol{x}}_j\|^2$, and then uses this invariant information, node representations, and edge attributes to perform edge message passing:

$$\boldsymbol{m}_{ij} = \sigma_1(\boldsymbol{h}_i, \boldsymbol{h}_j, \|\vec{\boldsymbol{x}}_i - \vec{\boldsymbol{x}}_j\|^2, \boldsymbol{e}_{ij}), \tag{12}$$

where $\boldsymbol{e}_{ij}$ represents the edge attributes between the i-th and j-th nodes, and $\boldsymbol{h}_i$ denotes the node representations of the i-th node. Geometric messages can be expressed as

$$\vec{\boldsymbol{m}}_{ij} = (\vec{\boldsymbol{x}}_i - \vec{\boldsymbol{x}}_j)\sigma_2(\boldsymbol{m}_{ij}), \tag{13}$$

where $\vec{\boldsymbol{x}}_i$ and $\vec{\boldsymbol{x}}_j$ represent the coordinates of the i-th and j-th nodes, respectively. Node features are updated by passing invariant messages:

$$\boldsymbol{h}'_i = \sigma_3\left(\boldsymbol{h}_i, \sum\nolimits_{j\in\mathcal{N}_i} \boldsymbol{m}_{ij}\right). \tag{14}$$

The position of each atom is then updated using a vector field along the radial direction; in other words, each atom's position is updated by a weighted sum of all relative vector differences:

$$\vec{\boldsymbol{x}}'_i = \vec{\boldsymbol{x}}_i + \gamma \sum\nolimits_{j\in\mathcal{N}_i} \vec{\boldsymbol{m}}_{ij}, \tag{15}$$

where σ_1, σ_2, σ_3 are MLPs, and γ is a predefined constant equal to $1/(M-1)$, where M is the number of atoms.

In addition to coordinates, a node's vector information can include attributes such as velocity and acceleration. Graph Mechanics Network[312] introduces a multi-channel vector representation $\vec{\boldsymbol{V}}_i \in \mathbb{R}^{3\times C}$ for each node to capture these attributes. Before message passing, these vectors undergo a scalarization process: $\frac{\vec{\boldsymbol{V}}_{ij}^\top \vec{\boldsymbol{V}}_{ij}}{\|\vec{\boldsymbol{V}}_{ij}^\top \vec{\boldsymbol{V}}_{ij}\|_F}$, where $\vec{\boldsymbol{V}}_{ij} = \vec{\boldsymbol{V}}_i - \vec{\boldsymbol{V}}_j$. This subtraction ensures that $\vec{\boldsymbol{V}}_{ij}$ remains translation-invariant. Many models, such as ClofNet,[313] achieve scalarization and preserve equivariance by constructing local frames. Other studies, such as those in Ref. [314,315], followed similar approaches. Specifically, the message passing is conducted as follows:

$$\boldsymbol{m}_{ij} = \sigma_1(\boldsymbol{h}_i, \boldsymbol{h}_j, \vec{\boldsymbol{V}}_{ij}^\top \vec{\boldsymbol{F}}_{ij}), \tag{16}$$

where $\vec{\boldsymbol{F}}_{ij}$ is translation-invariant.[35] Many other GNNs achieve scalarization through inner product operators while maintaining equivariance, such as GVP-GNN,[316] LEFTNet,[317] Frame Averaging,[318] and EGHN.[319]

By combining the Wigner-D matrix $\boldsymbol{D}^{(l)}(g)$,[320] spherical harmonics $Y^{(l)}(\vec{\boldsymbol{x}}) \in \mathbb{R}^{2l+1}$, and the Clebsch–Gordan tensor product $\otimes_{\text{cg}}$, e3nn[321] and TFN[320] offer a neural network approach that can handle 3D data while preserving equivariance to rotations, translations, and inversions. This integration enables the network to learn richer and more robust feature representations. The Wigner-D matrix represents the irreducible representations of the SO(3) group (the 3D rotation group) and describes the rotational behavior of angular momentum in quantum mechanics. Wigner-D matrices ensure that network layers maintain equivariance under rotation. Spherical harmonics, functions defined on the unit sphere that are equivariant under SO(3), can be extended to the entire $\mathbb{R}^3$ space and are used to construct equivariant polynomials. In e3nn, spherical harmonics are applied to build equivariant convolutional layers that can process point cloud data in 3D space. Their equivariance enables the network to learn features that are invariant to rotation. The CG tensor product combines two irreducible representations of angular momentum into a new irreducible representation that retains equivariance. The e3nn framework leverages the CG tensor product to combine outputs from different layers and construct complex equivariant operations, such as convolutions and attention mechanisms. The CG tensor product ensures that these operations remain equivariant under rotation, enabling learned patterns to be invariant to transformations in 3D space. By employing higher-order representations ($l > 1$), these networks can capture complex 3D spatial relationships, which traditional CNNs struggle to achieve.

Steerable E(3) equivariant GNNs (SEGNNs)[322] can handle geometric and physical information contained in node and edge attributes, such as position, force, velocity, or spin. SEGNNs integrate this information into the message passing and node updating functions and introduce a new class of equivariant activation functions, based on manipulable node attributes and manipulable MLPs, enabling the injection of geometric and physical information into the node updates. Neural Equivariant Interatomic Potentials (NequIP)[323] uses a similar approach to learn interatomic potentials from *ab initio* calculations. NequIP provides significant improvements in the accuracy and efficiency of MD simulations, facilitating the application of this method across a broader range of research fields. Wang *et al.*[324] enhanced the prediction accuracy and computational efficiency of material potential energy surfaces and physical properties by replacing traditional MLP with Kolmogorov–Arnold networks (KANs) in various ML frameworks.

In summary, much work remains to be accomplished on neural networks based on the integration of Wigner-D matrices, spherical harmonics, and CG tensor products, such as DimeNet,[325] SCN,[326] eSCN,[327] MACE,[328] PaiNN,[329] and Allegro.[330]

Transformers have demonstrated remarkable capabilities in the field of LLMs, primarily owing to their attention mechanism. A natural consideration is to incorporate this attention mechanism into GNNs. Meta proposed the equivariant graph attention transformer for 3D atomistic graphs (Equiformer),[331] which combines the transformer architecture with SE(3)/E(3) equivariant features based on irreducible representations, introducing an equivariant graph attention mechanism. By replacing traditional dot product attention with MLP attention and integrating nonlinear message passing, this approach enhances the attention expressiveness of the transformer. The network employs equivariant operations, such as independent linear transformations, layer normalization, and depth-wise tensor products, to handle different types of vectors while processing 3D graph structures through embedding layers and transformer blocks. Meta further introduced EquiformerV2,[332] an advancement over Equiformer, with key architectural improvements to enhance stability, computational efficiency, and model expressivity. EquiformerV2 incorporates an additional normalization layer preceding attention weight computation to stabilize the training process, and it refines the nonlinear activation function to more effectively handle representations across different orders. This approach uses specialized activation functions for each order and independently normalizes vectors to preserve their relative importance. Leveraging eSCN convolutions, EquiformerV2 simplifies the computation of SO(3) tensor products by transforming them into SO(2) linear operations, significantly reducing computational complexity. These innovations enable EquiformerV2 to achieve improved accuracy and efficiency on large-scale and complex 3D atomic graph datasets, particularly through the effective utilization of higher-order irreducible representations.

A prominent method integrating attention mechanisms with GNNs is Graphormer,[333] a GNN built on the standard transformer architecture. Graphormer excels in a range of graph representation learning tasks by proficiently encoding the structural information of graphs. It introduces several straightforward yet effective structural encodings, namely, centrality encoding, spatial encoding, and edge encoding, which enhance its ability to model graph-structured data. Theoretical analysis further underscores Graphormer's expressive power, proving that numerous popular GNNs variants can be considered as special cases within its overarching framework. Many similar approaches combine attention mechanisms with GNNs, such as SE(3)-Transformer,[334] TorchMD-Net,[335] and LieTransformer.[336]

3.3. Discriminative AI.

Introduction to Discriminative AI. A common task in inverse design of materials involves leveraging AI to predict the physico-chemical properties of materials, enabling high-throughput screening based on these properties. Discriminative models are primarily employed to directly predict the category (e.g., superconducting material, magnetic material) or label (e.g., formation energy, T_c) asso-

ciated with a given input (e.g., crystal structure, chemical composition). These models focus on learning how to map input data to the corresponding output labels. The objective of discriminative models is to infer the conditional probability distribution $P(y\,|\,x)$ of the target variable y given the input features x.

CGCNN. The CGCNN [73] is one of the earliest tools to use GNNs for predicting material properties. The CGCNN achieves comparable or slightly better accuracy than the DFT calculations in predicting properties such as formation energy, band gap, Fermi level, bulk modulus, shear modulus, and Poisson's ratio, with significantly faster computational speed. By analyzing the energy of each site in perovskite structures, the CGCNN aids in discovering new stable perovskite materials, significantly reducing the search space for high-throughput screening.

Specifically, the CGCNN uses an undirected multilateral graph to represent atoms and chemical bonds as nodes and edges, respectively. In this graph, the i-th node is represented by the feature vector $\boldsymbol{h}_i$, which corresponds to the properties of the i-th atom. Each edge $(i,\,j)_k$ is represented by the feature vector $\boldsymbol{m}_{(i,\,j)_k}$, corresponding to the k-th bond between atoms i and j. Atoms are considered to be connected if the distance between them does not exceed 6 Å. For discrete values, such as atomic numbers, a unique one-hot vector is used for direct embedding. For continuous values, such as bond lengths, the value range is divided into 10 intervals, and the value is encoded using a one-hot vector.

In the model, two types of neural networks are employed: GCN and fully connected networks (FCNs). Convolutional layers are used to aggregate information from the neighboring atoms around each atom:

$$\boldsymbol{h}_i^{(t+1)f} = \mathrm{Conv}\left(\boldsymbol{h}_i^{(t)},\,\boldsymbol{h}_j^{(t)},\,\boldsymbol{m}_{(i,\,j)_k}\right),\,(i,\,j)_k \in \mathcal{G}, \quad (17)$$

where $\boldsymbol{h}_i^{(T)}$ represents the feature vector of node i after T convolutions. The pooling layer uses normalized summation as the pooling function to generate a feature vector representing the entire graph. Finally, the target property $\hat{y}$ is predicted through two fully connected layers. A loss function $J(y,\,\hat{y})$ is defined, and the model parameters are updated by minimizing this loss function:

$$\min_{\boldsymbol{W}} J(y,\,f(\mathcal{C};\,\boldsymbol{W})), \quad (18)$$

where $\boldsymbol{W}$ represents weights of the CGCNN, and f is a function means that maps the crystal $\mathcal{C}$ to the target property $\hat{y}$. For more specific details, please refer to the original paper. [73]

MEGNet. The materials graph network (MEGNet) [75] is a general material graph network model that can accurately predict the properties of both molecules and crystals. The model outperforms previous ML models in predicting various properties. Because earlier models did not embed the entire crystal structure, MEGNet introduces global state attributes to the graph representation, including temperature, pressure, and entropy. MEGNet is trained on the QM9 [337] molecular and Materials Project (MP) crystal datasets. On the 13 properties in QM9, MEGNet outperforms previous models in predicting 11 of them. On the MP dataset, which includes 60,000 crystals, MEGNet not only outperforms earlier ML models but also achieves higher accuracy than DFT on a larger dataset.

In the model, the feature vector of the edge is updated by applying a specific update rule that incorporates information from both the node features and the edge's previous state. This process ensures that the edge representation evolves through successive layers, capturing the interactions between atoms in the crystal structure:

$$\boldsymbol{m}'_k = \phi_e(\boldsymbol{h}_i \oplus \boldsymbol{h}_j \oplus \boldsymbol{m}_{ij} \oplus \boldsymbol{u}), \quad (19)$$

where ϕ_e is the bond update function, $\oplus$ is the concatenation operator, $\boldsymbol{h}_i$ and $\boldsymbol{h}_j$ are the i-th and j-th atoms corresponding feature vector, respectively, and $\boldsymbol{u}$ is the global state vector. Next, the feature vector of each atom is updated using

$$\overline{\boldsymbol{h}}_i^e = \frac{1}{N_i^e}\sum_{k=1}^{N_i^e}\{\boldsymbol{m}'_{ij}\}, \quad (20)$$

$$\boldsymbol{h}'_i = \phi_v(\overline{\boldsymbol{h}}_i^e \oplus \boldsymbol{h}_i \oplus \boldsymbol{u}), \quad (21)$$

where N_i^e is the degree of atom i, and ϕ_v is the atom update function. Finally, the global state attribute is updated as follows:

$$\overline{\boldsymbol{u}}^e = \frac{1}{N^e}\sum_{k=1}^{N^e}\{\boldsymbol{m}'_{ij}\}, \quad (22)$$

$$\overline{\boldsymbol{u}}^v = \frac{1}{N^v}\sum_{i=1}^{N^v}\{\boldsymbol{h}'_i\}, \quad (23)$$

$$\boldsymbol{u}' = \phi_u(\overline{\boldsymbol{u}}^e \oplus \overline{u}^v \oplus \boldsymbol{u}), \quad (24)$$

where ϕ_u is the global state update function. The model combines two layers of FCN and MEGNet modules into a large MEGNet block. Multiple MEGNet blocks are then connected through a residual network, enabling the model to have deep hidden layers.

ALIGNN. The atomistic line graph neural network (ALIGNN) [338] introduces an innovative GNN architecture that alternates message passing between atomic bond and line graphs (capturing bond angles) to explicitly incorporate critical geometric information often ignored by traditional GNN models. Compared with models solely based on interatomic distances, ALIGNN significantly improves the accuracy of material property predictions. Its dual-graph message-passing mechanism, combined with edge-gated convolution, efficiently updates both node and edge representations. Tests on datasets such as JARVIS-DFT, Materials Project, and QM9 demonstrate that ALIGNN not only outperforms existing GNN models (such as CGCNN, MEGNet, and SchNet) in predicting properties such as formation energy and band gaps but also maintains high computational efficiency and robust generalization. By incorporating bond angle information into the GNN architecture, this models is an effective tool for accelerating materials design and discovery, with its open-source code and datasets further promoting advancements in materials science research.

In ALIGNN models, the node feature embedding and convolution design is similar to the that of the CGCNN, but the feature vector is updated using the edge-gate graph convolution.

$$\hat{\boldsymbol{m}}_{ij} = \frac{\sigma(\boldsymbol{m}_{ij})}{\sum_{k\in\mathcal{N}_i}\sigma(\boldsymbol{m}_{ik})+\epsilon}, \tag{25}$$

$$\boldsymbol{h}_i' = \boldsymbol{h}_i + \mathrm{SiLU}\left(\mathrm{Norm}\left(\boldsymbol{W}_s\boldsymbol{h}_i + \sum_{j\in\mathcal{N}_i}\hat{\boldsymbol{m}}_{i,j}\boldsymbol{W}_d\boldsymbol{h}_j\right)\right), \tag{26}$$

$$\boldsymbol{m}_{ij}' = \boldsymbol{m}_{ij} + \mathrm{SiLU}(\mathrm{Norm}(\boldsymbol{A}\boldsymbol{h}_i + \boldsymbol{B}\boldsymbol{h}_j + \boldsymbol{C}\boldsymbol{m}_{ij})), \tag{27}$$

where $\boldsymbol{W}_s$, $\boldsymbol{W}_d$, $\boldsymbol{A}$, $\boldsymbol{B}$, and $\boldsymbol{C}$ are learnable parameters, σ is sigmoid function, SiLU is the sigmoid linear unit, and equation (27) is equivalent to the gating term in the CGCNN.

An ALIGNN layer consists of edge-gated graph convolutions on both the bond graph (g) and its line graph ($L(g)$). To avoid confusion between the node and edge features in the atomistic graph and its line graph, we denote atoms, bonds (nodes in the line graph), and triplets (angles between bonds) as h, m, and t, respectively. The line graph convolution generates bond messages m, which are propagated to the atomistic graph and combined with atomic features h to update bond representations:

$$H', \boldsymbol{t}' = \mathrm{EdgeGatedGraphConv}(L(g), \boldsymbol{m}, \boldsymbol{t}), \tag{28}$$

$$\boldsymbol{h}', \boldsymbol{m}' = \mathrm{EdgeGatedGraphConv}(g, \boldsymbol{h}, H'). \tag{29}$$

OGCNN. The orbital graph CNN (OGCNN) is a crystal CGN that incorporates atomic orbital interaction features.[339] Beyond accounting for orbital contributions, the authors introduced a technique known as the orbital field matrix (OFM),[340] which captures orbital interactions by leveraging the electron configurations of both the central atom and its neighboring atoms. The study evaluated various properties, including formation energy, band gap, and Fermi energy. The results indicated that the model achieves improved predictive accuracy over the CGCNN, underscoring the critical role of orbital–orbital interactions. The OFM is defined as

$$\boldsymbol{X}^{\mathrm{c}} = \boldsymbol{O}^{\mathrm{cT}} + \sum_{i=1}^{M}\boldsymbol{O}^{\mathrm{cT}}\boldsymbol{O}^{i}\theta_{ci}\zeta(r_{ci}), \tag{30}$$

where $\boldsymbol{X}^{\mathrm{c}}$ represents the OFM for the central atom, $\boldsymbol{O}^{\mathrm{c}}$ and $\boldsymbol{O}^{i}$ represent the 1D binary vectors for the central and neighboring atoms, respectively, $\boldsymbol{M}$ denotes the number of neighboring atoms, θ_{ci} denotes the solid angle between center-neighbor pairs in the Voronoi cell, and $\zeta(r_{ci})$ denotes the function related to the distance between central and neighboring atoms, which can be selected as required. The total framework contains four modules: input, encoder–decoder, graph convolution, and output modules. The input module processes the atom configuration and OFM features and output vectors containing information about basic atoms and OFM. The function of the second module is to learn significant information among atoms using an MLP. The operation in the graph convolution module can be expressed as

$$\boldsymbol{V}_i' = \boldsymbol{V}_i + \sum \sigma(\boldsymbol{z}_{(i,j)_k}\boldsymbol{W}_f + \boldsymbol{b}_f) \odot g(\boldsymbol{z}_{(i,j)_k}\boldsymbol{W}_s + \boldsymbol{b}_s), \tag{31}$$

where $\boldsymbol{z}_{(i,j)} = \boldsymbol{V}_i \oplus \boldsymbol{V}_j \oplus \boldsymbol{u}_{(i,j)_k}$, $\boldsymbol{u}_{(i,j)_k}$ contains the information of kernelized distance features, σ denotes a sigmoid function, and g denotes the softplus function. The OGCNN architecture uses a total of three convolutional operations and a summation operation is performed next. Finally, in the output module, a pooling layer and FCN are implemented to map to the desired result.

ECN. The equivariant crystal network (ECN)[341] incorporates spatial group symmetries into GNNs. The ECN emphasizes that symmetry invariance is a necessary condition for practical applications. The authors experimented using the Materials Project dataset, filtering it to retain only data relevant to 3D materials. They then predicted physical properties such as formation energy, Fermi energy, band gap, and magnetic moment per atom. The authors framed their work as both regression and classification tasks. Experimental results revealed improved performance compared with previous models, supporting the authors' claim that symmetry provides a beneficial inductive bias.

In practice, using models that are equivariant to the actual symmetry of the data can be more beneficial in terms of the model's expressiveness. This is because the corresponding group is significantly smaller than the symmetric group; thus, equivariance to a smaller group may reduce parameter sharing, making the model more expressive. Moreover, the authors emphasized the importance of equivariance, noting that invariant functions can be constructed by combining equivariant layers with an output pooling layer. Additionally, equivariant functions can be used to predict local properties, such as charge distribution and magnetization.

The construction of an ECN is based on two key principles. The first challenge is the difficulty of supervised learning when a dataset encompasses a diverse range of crystal structures for a specific species. To address the discrepancies inherent in the unit cell structures, the researchers introduced the direct product of groups. The second principle in constructing the ECN is the equivariant message-passing framework. The authors defined the layer based on the update equation within this message-passing framework.

The ECN model takes as input a graph representing the crystal structure and generates a single encoded feature vector for each atom. This is followed by the integration of hidden layers and average pooling layers, culminating in a two-layer MLP for output prediction.

Matformer. Matformer[342] is specifically designed for periodic graph representation learning to predict the properties of crystalline materials. It computes various physical quantities, such as formation energy, band gap, and total energy, across multiple benchmark datasets, surpassing existing baseline methods such as ALIGNN,[338] SchNet,[310]

and CGCNN,[73] and demonstrating notable performance improvements. The model achieves periodic invariance through a specialized graph construction method, ensuring that the learned representations remain invariant to translations of the unit cell boundaries. Matformer effectively encodes periodic patterns, capturing the lattice size and orientation of the crystal. Additionally, Matformer employs an attention-based architecture, integrating edge attention and geometric information encoding, thereby enhancing its capability to process multi-atom crystal graphs. Experimental results indicate that Matformer outperforms baseline methods on the Materials Project and JARVIS datasets, offering advantages in both training and inference speed. By incorporating periodic orbital interaction features alongside fundamental atomic features, Matformer significantly enhances the accuracy of material property predictions, revealing promising potential for applications, particularly in the field of materials discovery.

Before introducing periodic invariance, we discuss unit cell E(3) invariance. Unit cell E(3) invariance can be observed as a function $f : (\boldsymbol{A}, \boldsymbol{X}, \boldsymbol{L}) \to \chi$, where the atom feature matrix $\boldsymbol{A}$ and position matrix $\boldsymbol{X}$ should describe unit cell itself, and $\boldsymbol{L}$ describes how a unit cell repeats itself in different directions. Thus, the definition clearly shows that regardless of whether the call is rotated, reflected, or translated, the structure of the cell itself remains unchanged. After considering the periodic invariance, the authors defined that unit cell E(3) function f is periodic invariant if $f(\boldsymbol{A}, \boldsymbol{X}, \boldsymbol{L}) = f(\phi(\hat{\boldsymbol{A}}, \hat{\boldsymbol{X}}, \alpha\boldsymbol{L}, p), \alpha\boldsymbol{L})$ holds for all $p \in \mathbb{R}^3$ and $\alpha \in \mathbb{N}_+^3$, where ϕ is a function such that $\phi : (\hat{\boldsymbol{A}}, \hat{\boldsymbol{X}}, \alpha\boldsymbol{L}, p) \to (\boldsymbol{A}, \boldsymbol{X})$. The authors also emphasized the importance of disrupting period invariance, namely, for the same crystal, this would result in different crystal graphs. Additionally, periodic pattern encoding is expressed by $\boldsymbol{L}$ to better represent infinite structures of crystals.

Some researchers use both multi-edge graph construction and fully-connected graph construction, which both satisfy periodic invariance, to build their Matformer.[73] Additionally, the radius-based method is used for better performance in experiments. Subsequently, self-connecting edges is incorporated to encode a periodic pattern, namely $\boldsymbol{L}$. For a direction vector l_i of $\boldsymbol{L} = [l_1, l_2, l_3]^T \in \mathbb{R}^{3\times3}$, it contains two parts, which are the length $\|l_i\|_2$ and orientation. Thus, the orientation should be encoded. The authors utilize additional distances to encode angles between two direction vectors. For example, the angle between l_1 and l_2 can be derived from $\|l_1\|_2$, $\|l_2\|_2$ and an additional distances $\|l_1 + l_2\|_2$.

In addition, the authors discussed the impact of introducing angular information. The utilization of angular information in practical tests does not appear to provide much hints about accuracy, but it triples the time cost. This result may be because periodic invariant graph construction and periodic patterns encoding in Matformer already provide sufficient information for the tests.

CT. Crystal twins (CT) is a self-supervised learning framework that can learn from large unlabeled datasets.[343] This framework represents one of the first applications of self-supervised learning methods to the prediction of crystalline properties, whereas before this, self-supervised learning was primarily applied to molecular systems. The authors conducted experiments on 14 datasets to evaluate the performance of the CT model and calculate various properties, such as exfoliation energy, band gap, and formation energy. The CT model demonstrated strong performance in most cases, although its results were not always be the best. Additionally, the authors assessed the effectiveness of augmentation methods and argue that the use of all three techniques enhances the overall effectiveness of the experiments.

The authors proposed a set of main processes. First, a CGCNN is used in pre-training to be an encoder to learn the effective representation of the crystal system; here, the authors proposed two different schemes based on Barlow Twins[344] and SimSiamese[345] loss functions. Thereafter, the weights are shared to initialize the encoder, and downstream tasks are fine-tuned with the aid of labeled data. In this study, the authors also introduced three augmentation methods, namely random perturbations, atom masking, and edge masking.

We focus on the description of two pre-training frameworks. In $\mathrm{CT}_{\mathrm{Barlow}}$, the CGCNN encoder would generate representations of augmented instances from the same crystal systems. The objective of pre-training here is to align the cross-correlation matrix of the two embeddings as closely as possible with the identity matrix. The Barlow Twins loss function can be defined as

$$\mathcal{L}_{BT} \triangleq \sum_i (1 - C_{ii})^2 + \lambda \sum_i \sum_{j \neq i} C_{ij}^2, \tag{32}$$

where $\boldsymbol{C}$ is the cross-correlation matrix, as

$$C_{ij} \triangleq \frac{\sum_b \boldsymbol{Z}_{b,i}^A \boldsymbol{Z}_{b,j}^B}{\sqrt{(\boldsymbol{Z}_{b,i}^A)^2}\sqrt{(\boldsymbol{Z}_{b,j}^B)^2}}. \tag{33}$$

In Eq. (33), b represents the index of the data within the batch, A and B both denote the augmented instances, and i and j represents the index of the vector dimensions of the projector output, namely $\boldsymbol{Z}^A$ and $\boldsymbol{Z}^B$. Another model is pre-trained using the SimSiamese loss function with the goal of maximizing the cosine similarity between the embeddings generated by the encoder for two augmented instances. Furthermore, in $\mathrm{CT}_{\mathrm{SimSiam}}$, one branch has a stop-gradient operation, whereas the other branch has a prediction header after the graph encoder. The loss function in this case can be defined as

$$\mathcal{L}_{\mathrm{SimSiam}} \triangleq \frac{1}{2}\sum_b (\mathcal{D}(\boldsymbol{P}_b^A, \mathrm{stopgrad}(\boldsymbol{Z}_b^B)) + \mathcal{D}(\boldsymbol{Z}_b^B, \mathrm{stopgrad}(\boldsymbol{Z}_b^A))), \tag{34}$$

where *stopgrad* represents disabling back propagation of gradients. The distance of two vectors can be defined as

$$\mathcal{D}(\boldsymbol{P}_b^A, \boldsymbol{P}_b^B) = -\frac{\boldsymbol{P}_b^A}{\|\boldsymbol{P}_b^A\|_2} \cdot \frac{\boldsymbol{Z}_b^B}{\|\boldsymbol{Z}_b^B\|_2}. \tag{35}$$

MMPT. Mutex masked pre-training (MMPT) is a self-supervised pre-training framework designed to address challenges that hinder the prediction of crystal properties, particularly the limited availability of labeled crystal data and the constraints of quantum chemistry.[346] The masking techniques employed in MMPT are inspired by the BERT framework.[347] The authors conducted their experiments using a subset of the Open Quantum Materials Database (OQMD).[348] Compared with other supervised and self-supervised methods, MMPT demonstrated strong performance. The experimental results indicated that MMPT alleviates, to some extent, the problem of limited labeled data. Furthermore, the authors assert that their results outperform those of the CT method, attributing this improvement to the effective utilization of E(3) invariance and the periodic invariance of crystals.

It is helpful to introduce the main framework of MMPT. A crystal is described using three vectors $\mathcal{M} = (\boldsymbol{A}, \boldsymbol{X}, \boldsymbol{L})$. First, two encoders are used here: one is a lattice encoder and the other is a structure encoder. Initially, the lattice encoder encodes the lattice matrix $\boldsymbol{L}$ into a lattice representation $\boldsymbol{h}_{\rm L}$, which contains the information of periodicity. The structure encoder first encodes $\mathcal{M}$ into a structure representation $\boldsymbol{h}_{\rm s}$ with the aid of a periodic invariance multi-graph (PIMG) module, and then two mutex representations $\boldsymbol{g}_{\rm s}$ and $\bar{\boldsymbol{g}}_{\rm s}$ are formed from $\boldsymbol{h}_{\rm S}$ by mutex masking. The next step is decoding. The lattice decoder decodes $\boldsymbol{h}_{\rm L}$ into $\boldsymbol{p}_{\rm L}$, and the coordinate and atom decoders decode $\boldsymbol{g}_{\rm s}$, $\bar{\boldsymbol{g}}_{\rm s}$ into $\boldsymbol{p}_{\rm C}$, $\bar{\boldsymbol{p}}_{\rm C}$, and $\boldsymbol{p}_{\rm A}$, $\bar{\boldsymbol{p}}_{\rm A}$, respectively. Finally, crystal reconstruction is conducted using $(\boldsymbol{h}_{\rm L}, \boldsymbol{p}_{\rm C}, \boldsymbol{p}_{\rm A})$ and $(\boldsymbol{h}_{\rm L}, \bar{\boldsymbol{p}}_{\rm C}, \bar{\boldsymbol{p}}_{\rm A})$. $\boldsymbol{p}_{\rm A}$ and $\bar{\boldsymbol{p}}_{\rm A}$ are used for atom-type contrastive learning, which emphasizes the role of the species of the atoms, and the periodic attribute learning (PAL), which can guarantee the introduction of the periodicity property.

Metux masking is a special point of this research. In a nutshell, $\boldsymbol{g}_{\rm s}$ can be defined as

$$\boldsymbol{g}_{\rm s}^{i} = \begin{cases} \boldsymbol{h}_{\rm s}^{i}, & i \notin \mathcal{M}, \\ [\text{MASK}], & i \in \mathcal{M}, \end{cases} \tag{36}$$

where $\mathcal{M}$ is a uniform distribution. $\bar{\boldsymbol{g}}_{\rm s}^{i}$ can be derived from the mutex mask of $\mathcal{M}$, namely $\bar{\mathcal{M}}$. This mask process enables the model to learn through structural relationships between two complementary sets of atoms. Based on the mutex masks, the authors designed crystal reconstruction and atom-type contrastive learning. They implemented crystal reconstruction by optimizing the loss function $\mathcal{L}_{\rm REC}$.

Because the crystal is described by three vectors, naturally $\mathcal{L}_{\rm REC}$ is also divided into three parts, namely $\mathcal{L}_A$, $\mathcal{L}_X$, and $\mathcal{L}_L$. $\mathcal{L}_A$ corresponds to $\boldsymbol{A}$, which is the cross entropy between real and predicted atom types. $\mathcal{L}_X$ corresponds to $\boldsymbol{X}$, which is based on the distance from the coordinate of each atom to the center coordinate. $\mathcal{L}_L$ corresponds to $\boldsymbol{L}$.

Owing to the influence of atom types for chemical properties, the learning of atom types was also referenced in this work. The authors utilized Barlow Twins loss to consider the significance of atom types. They aligned the cross-correlation matrix of $\boldsymbol{p}_A^i$ and $\bar{\boldsymbol{p}}_A^i$ as closely as possible with the identity matrix to perform the optimization.

The last point relates to periodicity-related arrangements. The authors introduced a PIMG and PAL to ensure the validity of periodicity. A crystal can be considered a multi-graph $\mathcal{G} := (\boldsymbol{A}, \boldsymbol{H})$, where $\boldsymbol{A}$ represents the set of atom nodes, and $\boldsymbol{H}$ represents the set of edges, which are relevant atom pairs. The authors ensured periodic invariance by constructing edges using Euclidean distance. Then, they designed a multi-graph attention mechanism to capture structural patterns. First, a linear transformation is applied to the initial feature vectors of the nodes, which is parameterized by the weight $\boldsymbol{W}$. Subsequently, the new atom node can be derived using

$$\begin{aligned} r_{ij} &= f_a(\boldsymbol{W}\boldsymbol{a}_i, \boldsymbol{W}\boldsymbol{a}_j), \\ \varepsilon_{ij} &= \frac{\exp(\text{LeakyReLU}(r_{ij}))}{\sum_{k\in\mathcal{N}_i}\exp(\text{LeakyReLU}(r_{ik}))}, \\ \hat{\boldsymbol{a}}_i &= \phi_{\rm FC}\left(\sum_{j\in\mathcal{N}_i}\varepsilon_{ij}\cdot\boldsymbol{a}_i\right), \end{aligned} \tag{37}$$

where f_a denotes a single-layer feed-forward neural network, and ε is a correlation coefficient. *LeakyReLU* is the activation function, and $\phi_{\rm FC}$ is a fully-connected layer. The final step is to send the multi-graph and new atom nodes into DimeNet++,[349] which is an E(3) invariance GNN, to learn the crystal structure representations. The PAL module focuses on learning about the three components associated with periodicity: discrete direction, unit cell position, and distance between nodes. They utilized three attribute learners to study these three sections and optimize the prediction by computing $\mathcal{L}_{\rm CAA}$, which contains three losses corresponding to three parts mentioned above.

3.4. Generative AI Accelerates Materials Discovery. In recent years, diffusion generative models have attracted significant interest for their realistic effects in image generation, such as stable diffusion.[350] Methods based on diffusion generative models, such as denoising diffusion probabilistic models (DDPMs)[351] and score-based diffusion,[352] have been widely applied in molecular docking (AlphaFold3,[353] DiffDock[354]), and molecular generation (torsional diffusion[355]). In the context of materials discovery, materials are in three categories: known knowns, known unknowns, and unknown unknowns. While the largest existing explorations of previously uncharted crystalline materials are on the order of 10^6 to 10^7 materials, the potential space of stable inorganic compounds, even within the realm of quaternary compounds and fixed stoichiometry, reaches an astounding 10^{10} possibilities. The third category, the "unknown unknowns", represents the most challenging yet vast frontier. Generative models present some of the most effective means of glimpsing into this largely uncharted space. In the field of material structure prediction, notable generative AI methods, including CDVAE,[23] CrystalGAN,[356] FlowMM,[357] DiffCSP,[24]

and DiffCSP++,[358] have emerged. This section will focus on these generative AI approaches.

CDVAE. The crystal diffusion variational autoencoder (CDVAE)[23] is a prominent early algorithm developed to generate stable periodic structures of materials. It employs a combination of joint equivariant diffusion and SE(3)-equivariant GNNs, explicitly encoding interactions across periodic boundaries while preserving permutation, translation, rotation, and periodic invariance. Furthermore, CDVAE introduces a noise conditional score network (NCSN)[352] as the VAE decoder to generate more realistic material structures and utilizes Langevin dynamics to refine the generation process. The algorithm also establishes three benchmark datasets specifically for material generation, along with a set of physically meaningful evaluation tasks and metrics. Extensive experiments validated the superior performance of CDVAE in tasks such as material reconstruction, generation, and property optimization, underscoring its significant potential in advancing the field of materials discovery. The workflow of CDVAE consists of several key steps. First, a periodic material encoder is employed to map the material $\boldsymbol{M}$ into a latent representation. Subsequently, three independent MLPs predict the composition $\boldsymbol{c}$, lattice $\boldsymbol{L}$, and number of atoms N, respectively. A conditional score matching decoder with equivariance is used to denoise the atomic coordinates and the probability distribution of atom types. A constraint is incorporated into the loss function to account for the periodicity of atomic coordinates. Finally, during each denoising step, atomic types and coordinates are updated using Langevin dynamics. Con-CDVAE[359] is a modified version of CDVAE designed to directly generate crystal structures based on crystal properties. Incorporating the conditional generation method of DALL-E2,[360] Con-CDVAE achieves this objective by introducing new modules specifically designed for crystal latent representations in CDVAE. In the first training phase, Con-CDVAE trains the core framework of CDVAE and applies MLPs to the crystal latent representations to predict crystal properties, aligning crystal structures with their corresponding properties. In the second training phase, Con-CDVAE introduces a prior module inspired by DALL-E2, which takes crystal properties as inputs to generate crystal latent representations. With these new modules, Con-CDVAE enables the direct generation of crystal structures from crystal properties. The model has been applied to conditional generation tasks based on formation energy and bandgap, revealing that the results for conditional generation of formation energy outperform those for bandgap. While achieving conditional generation, the model retains the crystal latent variables, potentially enabling manipulable structure generation such as latent variable interpolation. However, a key challenge lies in the design and training of the prior module to generate diverse and accurate crystal latent variables from the given crystal properties. The conditional CDVAE (Cond-CDVAE)[361] is a DL-based generative model, designed for crystal structure prediction (CSP). This model generates physically realistic crystal structures based on user-defined material compositions and external conditions, such as pressure. By leveraging Cond-CDVAE, the research team successfully generated high-fidelity crystal structures under various pressure conditions, achieving an accuracy of 59.3%, with an impressive 83.2% accuracy for structures containing fewer than 20 atoms–surpassing traditional global optimization-based CSP methods. Furthermore, a comprehensive dataset (MP60-CALYPSO) comprising over 670,000 local minimum structures, including both ambient and high-pressure crystal configurations, was established. The generated structures exhibited superior convergence rates and fewer ionic steps during DFT local optimization, indicating that they were closer to local energy minima. Cond-CDVAE integrates discrete chemical compositions and continuous pressure attributes, utilizing SE(3)-equivariant GNNs to encode crystal structures, thereby ensuring invariance under permutations, translations, rotations, and periodicity. Evaluation results underscored the model's high accuracy and reliability in CSP, illustrating the significant potential of DL generative models to accelerate the discovery and design of novel materials.

MatterGen. MatterGen[362] operates through a two-step process. In the first step, a base model is pre-trained to generate stable and diverse materials. The model was trained on data from the Materials Project and Alexandria databases, where stability is defined by DFT relaxation to a local energy minimum, with the energy per atom deviating no more than 0.1 eV from the reference database values. Novelty was ensured by verifying that the generated structures did not exist in the Alexandria dataset. In benchmark comparisons using the same Materials Project dataset, MatterGen outperformed CDVAE by achieving a higher proportion of stable, unique, and novel (S.U.N.) materials while also exhibiting lower root mean square deviation (RMSD) values, which indicates better alignment with DFT-relaxed structures. Furthermore, when trained on a larger dataset, MatterGen demonstrated even stronger performance. In the second step, MatterGen fine-tunes the base model using adapter modules, which allow for customization based on specific chemical compositions, symmetry requirements, and desired electronic, magnetic, and mechanical properties. This adaptability makes MatterGen a versatile and effective tool for targeted material discovery across a wide range of application domains. A similar generative algorithm is SyMat.[363]

DiffCSP. CSP using joint equivariant diffusion (DiffCSP)[24] is a specialized algorithm for CSP. It outperforms existing baseline methods, such as CDVAE, across multiple benchmark datasets while offering lower computational costs than DFT-based approaches. DiffCSP generates crystal structures that satisfy periodic E(3) invariance, ensuring stability in translation, rotation, and periodicity. Furthermore, DiffCSP demonstrates strong scalability, making it applicable not only to fixed-composition CSP but also to tasks involving atomic type generation

and property optimization. By employing a joint equivariant diffusion process, DiffCSP simultaneously operates on lattice vectors and atomic fractional coordinates to preserve periodic invariance, utilizing denoising models and message-passing mechanisms to improve prediction accuracy. The model demonstrated exceptional performance in crystal structure and property prediction experiments, underscoring its considerable potential to enhance both the accuracy and efficiency of CSP. In crystal structures, atoms are periodically arranged within the unit cell, denoted as $\mathcal{M} = (\boldsymbol{A}, \boldsymbol{X}, \boldsymbol{L})$, where $\boldsymbol{A} \in \mathbb{R}^{h\times N}$ indicates atom types, $\boldsymbol{X} \in \mathbb{R}^{3\times N}$ represents the Cartesian coordinates of each atom, and $\boldsymbol{L} \in \mathbb{R}^{3\times 3}$ is the lattice matrix defining crystal periodicity. Any atom's Cartesian coordinates and type within the crystal are expressed as $\{(\boldsymbol{a}_i', \boldsymbol{x}_i')|\boldsymbol{a}_i' = \boldsymbol{a}_i, \boldsymbol{x}_i' = \boldsymbol{x}_i + \boldsymbol{L}\boldsymbol{k}, \forall \boldsymbol{k} \in \mathbb{Z}^{3\times 1}\}$. A relationship between Cartesian and fractional coordinates is given by $\boldsymbol{x} = \sum_{i=1}^{3} f_i \boldsymbol{l}_i$. For the generation process, DiffCSP adopts a fractional coordinate system $\mathcal{M} = (\boldsymbol{A}, \boldsymbol{F}, \boldsymbol{L})$. With $\boldsymbol{L}$ as a continuous variable and the one-hot encoding of $\boldsymbol{A}$ treated similarly, a standard DDPM[69] can be used to generate $\boldsymbol{L}$ and $\boldsymbol{A}$, with the loss function

$$\mathcal{L}_{\boldsymbol{L}/\boldsymbol{A}} = \mathbb{E}_{\boldsymbol{\epsilon}\sim\mathcal{N}(0,\,\boldsymbol{I})}[\|\boldsymbol{\epsilon} - \hat{\boldsymbol{\epsilon}}_{\boldsymbol{L}/\boldsymbol{A}}(\mathcal{M}_t,\, t)\|_2^2]. \tag{38}$$

The equivariant denoising model ϕ predicts the denoising terms $\hat{\boldsymbol{\epsilon}}_{\boldsymbol{L}}(\mathcal{M}_t,\, t)$ and $\hat{\boldsymbol{\epsilon}}_{\boldsymbol{A}}(\mathcal{M}_t,\, t)$. For $\boldsymbol{F}$, periodicity is handled using a score-matching (SM) based framework.[352]

DiffCSP++. DiffCSP++[358] is an advanced crystal-structure generation algorithm specifically optimized to account for space group constraints. The algorithm demonstrates exceptional performance in generating crystal structures that adhere to specific space group symmetries. Compared with both learning-based and DFT-based methods, DiffCSP++ not only exhibits enhanced performance but also achieves notable success in ab initio crystal generation tasks, producing crystals with valid compositions and stable structures. Experimental results consistently show that DiffCSP++ surpasses existing baseline methods in both crystal structure generation and property statistics, underscoring its significant potential in materials design.

DiffCSP++ considers the constraints of space groups to generate crystal structures. Space groups are collections of symmetry operations of crystals, constrained by the o(3) invariance of the lattice matrix and the Wyckoff positions of fractional coordinates. According to the polar decomposition,[364] the lattice matrix $\boldsymbol{L} \in \mathbb{R}^{3\times 3}$ can be decomposed as $\boldsymbol{L} = \boldsymbol{Q}\exp(\boldsymbol{S})$, where $\boldsymbol{Q}$ is an orthogonal matrix, and $\boldsymbol{S}$ is a symmetric matrix. Any symmetric matrix can be expressed using six symmetric basis functions, with coefficients that are o(3) invariant:

$$\boldsymbol{S} = \sum_{i=1}^{6} k_i \boldsymbol{B}_i \tag{39}$$

$$\boldsymbol{B}_1 = \begin{pmatrix} 0 & 1 & 0 \\ 1 & 0 & 0 \\ 0 & 0 & 0 \end{pmatrix}, \quad \boldsymbol{B}_2 = \begin{pmatrix} 0 & 0 & 1 \\ 0 & 0 & 0 \\ 1 & 0 & 0 \end{pmatrix},$$

$$\boldsymbol{B}_3 = \begin{pmatrix} 0 & 0 & 0 \\ 0 & 0 & 1 \\ 0 & 1 & 0 \end{pmatrix}, \quad \boldsymbol{B}_4 = \begin{pmatrix} 1 & 0 & 0 \\ 0 & -1 & 0 \\ 0 & 0 & 0 \end{pmatrix},$$

$$\boldsymbol{B}_5 = \begin{pmatrix} 1 & 0 & 0 \\ 0 & 1 & 0 \\ 0 & 0 & -2 \end{pmatrix}, \quad \boldsymbol{B}_6 = \begin{pmatrix} 1 & 0 & 0 \\ 0 & 1 & 0 \\ 0 & 0 & 1 \end{pmatrix}.$$

By determining the coefficients $\boldsymbol{k}$ of six symmetric basis functions $\boldsymbol{B}$, DiffCSP++ ascertains the lattice matrix $\boldsymbol{L}$. During noise addition and denoising, these coefficients can be transformed. The 230 space groups are categorized into six crystal families G_{family} (triclinic, monoclinic, orthorhombic, tetragonal, hexagonal, and cubic), each imposing distinct constraints on k_i. These families define six projection spaces, ensuring consistent projections to the prior crystal family space throughout the crystal generation process. The Wyckoff positions ($W_{\text{positions}}$) represent the symmetry of equivalent atoms in the unit cell, with N fractional coordinates $\boldsymbol{F} \in \mathbb{R}^{3\times N}$ derived from N' basic fractional coordinates $\boldsymbol{F}' \in \mathbb{R}^{3\times N'}$. Noise addition and denoising can be performed on these basic coordinates $\boldsymbol{F}'$, enabling the determination of fractional coordinates for all atoms within the unit cell. The coefficients $\boldsymbol{k}$ are treated as continuous variables, and the one-hot encoded atomic types of Wyckoff positions are similarly considered, both generated using standard DDPM. Because the fractional coordinates of the Wyckoff positions are periodic, DiffCSP++ utilizes an SM framework for generation. CrystalFormer[365] also considers the constraints of space groups to generate crystals.

CrystalFormer. CrystalFormer[365] is a transformer-based autoregressive model specifically designed to generate crystal materials that respect space group symmetries. The model learns the discrete and sequential nature of Wyckoff positions to directly predict the type, position, and lattice parameters of symmetry-inequivalent atoms within the lattice, thereby generating crystal structures. Compared with traditional CSP methods, CrystalFormer has significant advantages in tasks such as symmetry structure initialization and element substitution. Additionally, CrystalFormer facilitates property-guided material design by integrating solid-state chemistry knowledge and heuristic rules, enabling systematic exploration of crystal materials and the discovery of novel superconductors with low Ehull values ($< 0.1\,\text{eV/atom}$). To achieve these capabilities, CrystalFormer incorporates algorithms such as Markov chain monte Carlo[366] sampling, Gaussian mixture models,[367] and von Mises distributions, effectively incorporating space symmetries and other physical constraints during the generation process. This research offers new insights into the discovery of high-temperature superconductors and advances the field of materials modeling and discovery.

GNoME. Graph networks for materials exploration (GNoME)[31] is a significant advancement in the generation and discovery of novel materials through an innovative active learning algorithm. Departing from conventional approaches that rely on sampling from existing datasets, GNoME challenges the prevailing assumption that newly generated materials must adhere to the same data distribution as the training set. By employing an active learning framework, it efficiently generates millions of novel crystal structures. This methodology uncovers 2.2 million potentially stable materials, many of which transcend traditional chemical intuition. Of these, 381,000 materials are integrated into the materials database, with 736 structures experimentally validated for stability, thereby enriching the field with valuable resources for further research and practical applications in materials science.

The GNoME framework operates through two key modules: symmetry-aware partial substitutions combined with random structure search, and GNN-based modeling of material properties. These components drive two independent material discovery pipelines. The structural pipeline focuses on evaluating the stability of crystal frameworks without considering specific atomic types, filtering randomly generated structures using GNoME to retain potentially stable frameworks. In contrast, the compositional pipeline uses chemical formulas as inputs for GNoME, identifying stable chemical combinations to explore novel material compositions. After structures are selected through these pipelines, DFT calculations are performed to further validate their structural stability. Stable materials are then added to the training set for subsequent iterations, creating an iterative active learning loop. This process facilitates the discovery of new materials that extend beyond existing data distributions.

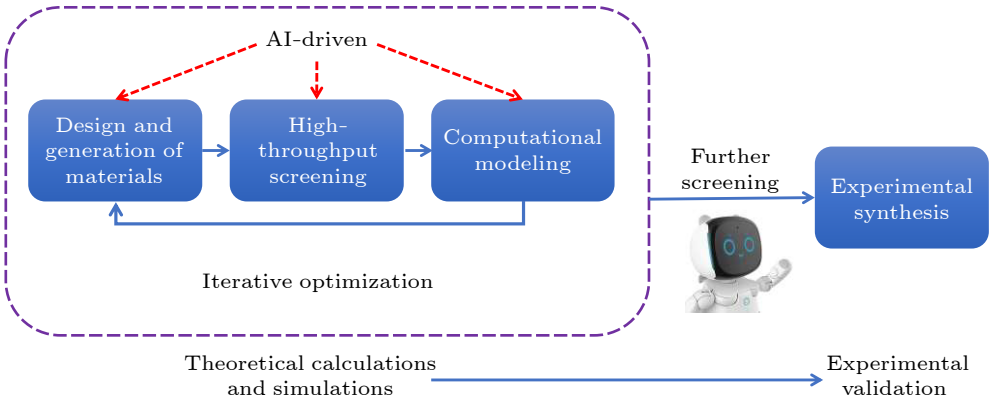

Fig. 5. General process of inverse design of materials, which is divided into two main parts: the AI-driven theoretical calculation and experimental validation parts. The theoretical calculation part is further subdivided into material design and generation, high-throughput screening, and computational modeling.

InvDesFlow. The InvDesFlow[72] develops an AI-driven workflow for discovering high-T_c superconductors that are not present in any existing database. In this survey, we summarize the general process of the inverse design of materials, as shown in Fig. 5. The process is divided into two main parts: theoretical calculations and experimental validation. The theoretical calculations are further subdivided into material design and generation, high-throughput screening, and computational models. Unlike traditional inverse design, the entire theoretical part is fully AI-driven, with AI implementing the entire theoretical simulation process.

OMat24. Meta has introduced Open Materials 2024 (OMat24),[32] a comprehensive dataset featuring over 110 million DFT-based calculations, emphasizing structural and compositional diversity. This dataset spans non-equilibrium atomic crystal structures and varied elemental compositions, offering a rich resource for materials discovery. Utilizing a pre-trained EquiformerV2 model, Meta achieved state-of-the-art results on the Matbench Discovery[‡] leaderboard. Through extensive experimentation, they explored the impact of different training strategies on model performance, providing valuable insights for future advancements. By openly sharing both the dataset and model, Meta empowers the research community to build upon and refine these foundational resources, fostering progress in AI-driven materials science.

FlowLLM. Meta has introduced FlowLLM,[368] an advanced crystal generation model that integrates LLMs with Riemannian flow matching (RFM) to enable the design of novel crystalline materials. FlowLLM first fine-tunes an LLM to capture an effective foundational distribution of metastable crystals within textual representations. After the conversion of text to graph representations, the RFM model further refines LLM-generated samples through iterative optimization of atomic coordinates and lattice parameters. FlowLLM surpasses existing state-of-the-art methods by over threefold in stable material generation rates. The structures produced by FlowLLM are notably closer to relaxed states, substantially reducing post-processing costs while improving both the efficiency and precision of material generation, thereby marking a

[‡]https://matbench-discovery.materialsproject.org/

significant advancement in the field of materials science.

3.5. Large Language Models. In recent years, LLMs, such as GPT-3.5 Turbo,[369] GPT-4[§], and BERT,[347] have been widely adopted across various scientific fields, becoming essential tools for natural language processing and knowledge generation. OpenAI's GPT-3.5 Turbo and GPT-4 are particularly popular owing to their ability to generate human-like text, answer complex questions, and facilitate knowledge synthesis. These models are powered by transformer-based architectures,[22] where self-attention mechanisms enable the efficient processing of large-scale textual data across diverse applications. Similarly, Google's BERT, distinguished by its bidirectional training approach, captures context from both directions in a text, making it particularly effective for tasks that require nuanced understanding, such as question-answering. In addition to these general-purpose models, domain-specific LLMs such as Coscientist,[370] SciBERT[371] and MatSciBERT[372] have been developed to improve performance in particular scientific domains. SciBERT, based on the BERT architecture, is fine-tuned on scientific literature, enabling more precise information retrieval and classification within scientific texts. Similarly, MatSciBERT, tailored for materials science, incorporates domain-specific language and terminology to enhance its effectiveness in analyzing material-related data and generating specialized tags. Building upon these foundational and domain-specific models, researchers are increasingly employing LLMs for inverse material design, using these models to effectively predict and optimize material properties, as discussed in the following sections.

In sustainable concrete design, a methodology using LLMs to develop alkali-activated concrete formulations to reduce the carbon footprint and environmental impact of concrete production was developed.[373] Researchers utilized GPT-3.5 Turbo and GPT-4 models to create a "knowledge-driven design" (KDD) system, which integrates domain-specific knowledge with experimental feedback to enhance the accuracy and efficiency of material design. Through the automated generation of low-calcium concrete formulations, property optimization, and performance prediction, this system demonstrated a marked improvement in predictive accuracy for complex composite mixtures. This innovative approach introduces a sustainable paradigm in concrete design, supporting the development of an environmentally friendly concrete industry. In the field of battery technology, particularly for rapid charging applications, the BatteryGPT system leverages LLMs to accelerate information extraction and innovation.[374] Utilizing retrieval-augmented generation technology, BatteryGPT aggregates data from over 2,200 publications and incorporates advanced technical methodologies to facilitate knowledge generation and optimization in fast-charging battery technology. BatteryGPT provides domain-specific literature reviews and recommends the latest solutions for fast-charging materials, such as Li_3P-enhanced solid electrolyte interfaces and laser patterning. This system significantly enhances the efficiency of information integration and processing in material innovation, supporting advancements in battery technology aimed at extending electric vehicle range and improving energy storage. In a study on microstructure evolution within materials, LLMs generated code and simulated complex multiphysics-coupled models.[375] The researchers employed ChatGPT to produce code based on phase-field models to simulate the evolution of material microstructures over time. Although the model-generated code required further validation and adjustments for complex equations, this research systematically explored the potential of LLMs in microstructure modeling. This novel approach highlights the utility of LLMs in materials education and research, offering new perspectives for integrated computational materials engineering (ICME)[¶]. From a broader perspective, Lei *et al.* investigated automation and knowledge integration benefits of LLMs within materials science.[376] The study showed that LLMs not only retrieve knowledge and generate code through natural language instructions but also conduct multi-level literature analysis and generate tags, such as for 3D microstructure analysis and micrograph labeling. By leveraging fine-tuned, domain-specific models such as SciBERT[371] and MatSciBERT,[377] this study demonstrated that LLMs effectively process complex materials science data and produce high-quality structured information. This advancement supports the automation of materials science workflows with significant applications in rapid charging and renewable energy integration.

In summary, LLMs have shown remarkable potential in inverse materials design, transforming traditional materials innovation processes. Leveraging advanced language processing and knowledge synthesis capabilities, LLMs have significantly enhanced the accuracy of property prediction and optimization while also providing sustainable solutions to pressing challenges in materials science. For instance, in sustainable concrete design, LLMs enable researchers to develop eco-friendly materials that lower carbon emissions. In battery technology, LLMs facilitate the integration of vast information, accelerating innovation in fast-charging batteries that support extended electric vehicle ranges and improved energy storage. Additionally, LLMs contribute to the simulation of material microstructures and multiphysics modeling, offering new possibilities for ICME and materials education. As applications of LLMs in inverse materials design continue to expand, these models are anticipated to become essential in property prediction, novel material discovery, and the automation of knowledge integration. Coupled with domain-specific models, LLMs promise breakthroughs in processing complex materials data and generating high-quality information, supporting the development of automated scientific workflows. Future research may further explore robust algorithm designs and the integration of real-time data anal-

[§] https://openai.com/gpt-4

[¶] https://link.springer.com/book/10.1007/978-3-030-40562-5

ysis with experimental feedback, thereby enhancing the breadth and depth of LLMs applications in materials science and providing technical support for sustainable and intelligent materials innovation.

3.6. Datasets. As the previous section shows, various datasets are typically used when testing the performance of a model. In Table 2, we briefly introduce a few common material datasets.

Table 2. Some typical databases. Listed in the table are their name, amount of data, description, and reference.

Datasets	Size	Description	Reference
QM7	$> 7,000$	DFT calculations	[378]
QM9	$> 134,000$	DFT calculations	[337]
MD17	$> 100,000$	MD simulation data	[379,380]
MP	$> 150,000$	Materials Project	[381]
OQMD	$> 1,226,000$	Quantum Materials	[348]
OC20	$> 133,940,000$	Open Catalyst 2020	[382]
JARVIS-DFT	$> 80,000$	DFT calculations	[383]
PubChemQC	$> 85,000,000$	DFT calculations	[384,385]

Different researchers have created different datasets for different types of materials. In the specific research, different datasets are selected according to the requirements, and the appropriate data from the dataset are selected to conduct experiments. Moreover, different researchers select different previous studies with some impact as benchmarks, such as CGCNN[73] and ALIGNN.[338] Some researchers use different frameworks as benchmarks for different parts in their studies.

4. Future Directions. The previous chapters have provided a comprehensive overview of the way that AI has accelerated advancements in the inverse design of functional materials, alongside a rapid evolution of AI technologies within the materials science domain. In this chapter, we will delve into potential future directions for AI across each critical stage of the reverse design workflow for functional materials. Key stages in this workflow encompass the design and generation of novel materials, high-throughput screening for target functional properties, theoretical validation of candidate materials through computational modeling, and the experimental synthesis and testing necessary to confirm material performance. By advancing and designing AI algorithms that deeply integrate with each of these stages, we aim to accelerate every step of the process, enabling AI to fully achieve its transformative potential in the inverse design of materials.

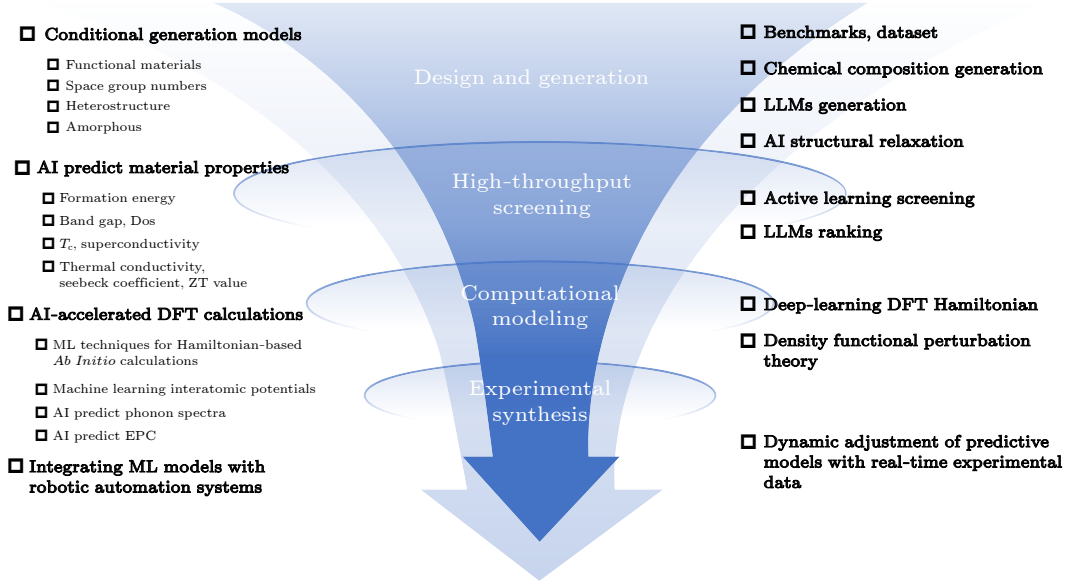

Fig. 6. Future of AI-driven inverse design of materials. This figure outlines the potential development directions of AI in the key stages of the functional material reverse design workflow, including the design and generation of new materials, high-throughput screening, computational modeling for candidate validation, and experimental synthesis and testing. By optimizing the integration of AI algorithms, these AI techniques can accelerate efficiency and innovation in materials discovery.

4.1. Design and Generation of New Materials. For the inverse design and generation of new functional materials, current generative models remain constrained in their capabilities and fail to satisfy the complex requirements of material design. The following challenges represent areas in which we anticipate AI advancements may provide impactful solutions in the future. The first one is that the AI-generated material structures are frequently not in a stable ground state, necessitating additional assessment and structural relaxation. Enhancing generative models to address this limitation remains a key objective for future development. The second one is the generative models based on chemical composition are currently scarce, despite being frequently required in experimental science. LLMs may provide such capabilities in the future. The third one is that we require conditional generation methods in which a partially known structure or chemical formula serves as input, producing a complete

structure or formula. For example, given part of a heterostructure, we aim to generate the remaining portion. The fourth one is that the space group family-based generation algorithms, such as DiffCSP++, have been achieved, but algorithms enabling direct control over space group numbers for new structure generation have yet to be developed. Moreover, the generative AI algorithms specifically designed for diverse functional materials have yet to be developed. A significant number of materials exist in amorphous rather than crystalline forms, highlighting the necessity for the future development of generative algorithms specifically for amorphous materials. Furthermore, the generative algorithms discussed above necessitate the development of more equitable benchmarks for assessing model performance. Consequently, the release of suitable datasets and corresponding benchmarks is a crucial task.

Creation and Updating of Datasets. With the assistance of AI, the development of materials science has progressed significantly, but some urgent problems remain to be solved. First, large databases already exist for some of the materials such as MP,[381] OQMD,[348] and OC20.[382] However, data for some complex materials such as HEAs are still lacking. Some methods are designed to deal with these materials.[262] However, the creation of a database of complex materials is also required. Second, with the assistance of AI, many new materials have been discovered that exist in theory, but these new materials may not actually be synthesized in actual experiments. Experimental validation is required to determine whether these materials should be added to the database. However, the progress of experiments is often insufficient. Thus, we could create a candidate database that records AI-generated materials. The third point is that many AI-generated materials do not have a standardized nomenclature. Many researchers use simple numbers to represent generated materials right in their own papers, which is not conducive to the documentation of new materials and the retrieval of new materials. All of the above are problems that must be solved or optimized with respect to the database. Additionally, some databases related to AI have been established, which can be considered as a future direction.

LLMs. The future prospects of LLMs in inverse material design are promising. As the technology matures, LLMs are expected to enable profound changes in autonomous material discovery and efficient data integration. First, a significant potential of LLMs in inverse material design lies in achieving autonomous material discovery and design systems. These systems can rapidly adjust design strategies while interpreting human instructions and dynamically adapt to different tasks and material properties, ultimately enabling an automated material research and development (R&D) process. For instance, the LLMatDesign[386] project demonstrated the potential of LLMs to achieve autonomous material design through instruction fine-tuning in low-sample environments. Its framework enables a model to perform material screening and optimization based on design instructions and chemical knowledge. With future enhancements in model optimization on datasets and improved multi-modal integration capabilities, LLMs are expected to be more flexible in complex material tasks, even forming "autonomous laboratories" to accelerate the material R&D process. The HoneyComb system[387] builds upon this by using its high-quality knowledge base, MatSciKB,[387] and computational tool center, ToolHub, to enable real-time data updates and cleaning support, providing a stronger data foundation and scientific computing capabilities for autonomous material design. This indicates that future LLMs will not only generate and evaluate material design schemes but also continuously learn and improve through knowledge bases, laying the foundation for fully automated material discovery. Second, future LLMs will make significant strides in the efficient integration and extraction of material data. The key to achieving this objective lies in building high-quality multi-modal datasets and enhancing a model's ability for complex reasoning. Several studies have emphasized the necessity of dataset expansion and multi-modal information integration. For example, Miret *et al.*[388] proposed a six-step interactive roadmap that progressively improves a model's reasoning performance in complex material tasks by integrating text, images, and experimental data. Similarly, Lei *et al.*[376] highlighted the importance of high-quality multi-modal data for enhancing the model's understanding of the complexity of the materials science field. The study indicated that by dynamically integrating experimental data, LLMs can significantly enhance their ability to parse information related to material properties and structures, thereby advancing the automation of the material discovery process. These studies indicate that through the construction and integration of multi-modal information, future LLMs will exhibit stronger reasoning capabilities in complex materials science tasks, particularly under conditions of limited data, providing reliable support for the design and validation of new materials.

In conclusion, the future development prospects of LLMs in inverse material design are extensive. As the capabilities of models in data processing, knowledge integration, and complex reasoning continue to improve, LLMs are anticipated to significantly accelerate the material R&D process, promoting autonomous and intelligent material design. By dynamically acquiring and parsing multi-modal data and continuously learning from the latest research developments in materials science, LLMs can effectively support all stages of material discovery, from screening to structural optimization and experimental plan generation, gradually achieving a more comprehensive and efficient material innovation process. This technological advancement will not only aid scientists in addressing current research challenges more rapidly but also create new research avenues in the field of materials science and laying a solid foundation for future technological innovation.

4.2. High-Throughput Screening of Functional Materials. In recent years, the high-throughput screening of target functional materials has predominantly utilized invariant GNNs to classify and predict material properties,

subsequently establishing specific thresholds for material selection. This approach has resulted in numerous significant contributions, enabling the accurate prediction of several physical properties, including formation energy, band gap, Debye temperature, and density of states. However, certain physical properties remain challenging to predict with high precision due to their inherent complexity. The following are potential challenges that require further investigation.

The rapid development of AI technology in recent years has provided new momentum for the inverse design of superconducting materials, resulting in the establishment of a comprehensive workflow for discovering new high-T_c superconductors. However, considerable potential for enhancement across various dimensions remains. For instance, the application of AI to accurately assess whether a material exhibits superconductivity, predict the T_c of any superconductor–whether characterized by conventional or unconventional properties and defined by its chemical formula or crystal structure–expedite the DFT verification process for EPC through AI integration, and provide more precise guidance for experimental directions using AI. Ultimately, we anticipate that advancements in AI will illuminate new physics related to superconducting mechanisms in the future.

For complex materials, such as high-entropy alloys, the primary challenge associated with AI-assisted computation is the limited size of available datasets. As previously stated, several workflows have been proposed in recent years to address this class of materials.[262,267,389] However, the corresponding methods require further promotion and application to assess their practicality and reasonableness. Concurrently, the necessity for high-quality datasets for complex materials persists. Moreover, some studies have used activating learning to discover new and efficient catalysts. This concept is very similar to the "exploration" and "exploitation" concepts in reinforcement learning. In the context of expanding the existing dataset, exploitation enables AI to generate more data of the same distribution, whereas exploration enables the step of activating learning. However, current activating learning still requires DFT or other methods for validation, and the verified samples must be manually added to the dataset for the next iteration. Therefore, if the steps of activating learning can be automated, future exploration of crystals through AI could significantly improve efficiency.

Note that in AI-driven high-throughput screening of functional materials, significant gaps remain in material classification and property prediction, particularly in terms of accuracy and handling complex properties. Future LLMs hold promise for advancing material recommendation, ranking, and structural design through frameworks such as natural language embeddings, which generate compositional and structural feature vectors of materials.[390] Such models aim to better represent materials, identify under-explored spaces, and streamline material optimization. Despite these advancements, current ML methods often struggle with reliably predicting key properties–such as thermal conductivity, Seebeck coefficient, and ZT value–owing to the challenges in modeling nonlinear relationships within complex material systems, including thermoelectric materials.[126] Additionally, the accurate prediction of dopant and structural effects on material performance remains limited, with models such as DopNet capturing only partial insights into these intricate dependencies.[129] Addressing these challenges requires AI models that can integrate multi-scale data and adapt to experimental feedback, ultimately improving robustness and reliability in predictions. Furthermore, systems such as the HoneyComb illustrate the need for interpretable AI models, which are essential for achieving precise material recommendation and structural optimization, particularly for high-stakes applications requiring practical and reliable adoption.

4.3. Computational Modeling for the Validation of Candidate Materials. Most conventional materials-calculation methods are based on the DFT. Nevertheless, DFT-based approaches are constrained in their ability to accommodate a comprehensive range of materials, largely owing to the influence of intricate terms such as the exchange-correlation functional. Therefore, it is unsurprising that most new calculation methods are developed to improve the quality of the calculations. Furthermore, the combination of *ab initio* calculation with AI is a popular and promising avenue of research.

Some related studies have focused on predicting complex terms with the assistance of AI. For example, some researchers have employed ML techniques to predict EPC[391–393] and others have employed AI to predict phonon spectra.[394,395] Furthermore, promising avenues for researchers to utilize AI in optimizing alternative versions of DFT beyond the prevalent Kohn–Sham DFT[396] exist. Attention should be given to recent research on DeepH,[397–406] which is a framework using ML techniques to study the Hamiltonian of materials to conduct *ab initio* calculation. This method is highly efficient and achieves high accuracy on many materials. Additionally, this approach is now being generalized to a wider range of systems, and many similar studies have been conducted, such as HamGNN.[196,407,408] More research and applications in these aspects are inevitable in the future.

To summarize, we can actually see the following points worth trying for the combination of AI and material calculation methods. The most important one is that the lack of a generalized network structure or a generalized approach to network selection, and the answer to how ML technology can be integrated into material computation methods is not conclusive, and many perspectives exist that are worth testing. Moreover, there is still a certain threshold for the various methods, which implies the necessity of writing relevant software packages or developing relevant software.

4.4. Experimental Synthesis and Testing for Validating Material Performance. As evidenced by recent research, a workflow that integrates computational prediction with experimental synthesis can be an invaluable tool for studying complex materials with limited datasets.[262,267,389] The

proposed workflow enables researchers to obtain actual materials directly, which is not always possible in other fields in which materials prediction involves a disconnect between computational prediction and experimental synthesis. Note that the time cost of this workflow is not insignificant and requires continuous improvement.

AI-guided experimentation holds significant promise for advancing functional material development, particularly in thermoelectric materials, where experimental synthesis and optimization remain complex and resource-intensive. In the field of thermoelectric materials, AI-driven approaches, such as error correction learning models, refine predictive accuracy through iterative experimental feedback, enabling faster identification of high-performance materials.[135] Future research in AI-guided experiments focuses on enhancing adaptability and scalability for large-scale synthesis processes, incorporating real-time data from experimental setups to dynamically adjust predictive models. Furthermore, AI-guided experimental planning proves invaluable for efficiently testing the effects of doping, strain, and nano-engineered structures, which are critical for improving ZT values in thermoelectric materials.[130] By integrating ML models with automation platforms, such as robotic experimental systems, researchers explore complex parameter spaces more efficiently, facilitating the development of sustainable and high-performance materials for applications such as waste heat recovery and thermal management in microelectronics.

5. Conclusion. In this paper, we discuss the history of the inverse design of materials to pinpoint the essence of AI-driven material design and to underscore the pivotal role of AI technology in the process of inverse design of materials. Furthermore, we comprehensively review of the latest endeavors aiming at enhancing AI-driven inverse design processes, encompassing recent AI-based discoveries on typical materials and the research progress and technological trajectories of AI in the field of materials science. These collective efforts have significantly contributed to the recent wave of advancements in AI-driven inverse design of materials. While existing AI-driven inverse design of materials has yielded promising results, particularly in the inverse design of functional materials for few-shot learning scenarios, the future development of AI technology in materials science and its application in key areas remain open questions. Particularly with the burgeoning growth of LLM technology, it is crucial to explore which aspects of materials science can benefit from improvements and optimizations offered by LLMs. We hope that our insights will inspire further efforts in this field and propel the development of AI-driven inverse design of materials forward.

Notes and Contributions.

Author Contributions. The contributions of all authors are listed as follows: Ze-Feng Gao and Zhong-Yi Lu led this survey program; Ze-Feng Gao and Xiao-Qi Han designed the structure of this paper; Ze-Feng Gao drafted the abstract and Section 1; Xiao-Qi Han, Xin-De Wang, Meng-Yuan Xu, Zhen Feng, and Bo-Wen Yao drafted Sections 2 and 3. All faculty authors drafted various topics in Section 4. Peng-Jie Guo provided comments to the manuscript, and Xiao-Qi Han and Ze-Feng Gao proofread the entire paper. The authors would like to thank Li-Jun Chen and Xi-Wen Liu for useful discussions.

Survey Writing. This survey was planned during a discussion meeting held by our research team, with the objective of summarizing the latest advancements in AI-driven inverse design of materials into a highly readable report. Subsequently, we extensively revised the writing and contents in several passes. Owing to space limitation, we could include only a fraction of existing AI methods in Fig. 4 by setting the selection criterion. We released the initial version on November 14, 2024, and this latest version on November 26, 2024.

Seeking for Advise. Despite our best efforts, this survey may still have many limitations, such as the potential omission of important references, models, methods, or topics, as well as the possibility of imprecise expressions and discussions. We will continue to update this survey and strive to enhance its quality as much as possible. For our research team, the process of writing this survey is also a journey of learning about research on AI-driven inverse design of materials. Readers who have constructive suggestions to improve this survey are welcome to send emails to our authors. We will revise future versions based on the comments and suggestions received and acknowledge those readers who have contributed constructive suggestions in our survey.

Update log. In this part, we regularly maintain an update log for the submissions of this survey to arXiv:

• First release on November 14, 2024: the initial version.

• Update on November 26, 2024: add several related studies in Sections 2 and 3, revise Fig. 4 and Table 2, add Fig. 5, improve the writing, and correct some minor errors.

Acknowledgements. The authors would like thank Lei Wang, Yong Xu, Xingao Gong, Wanjian Yin, Miao Liu, Hongjun Xiang, Hongming Weng, Jian Lv, Quansheng Wu for valuable discussions. The author would like to thank CPL editors for a huge amount of work in text editing of the manuscript. This work was financially supported by the National Natural Science Foundation of China (Grant Nos. 62476278, 12434009, and 12204533). Z.Y.L. was also supported by the National Key R&D Program of China (Grant No. 2024YFA1408601), and the Innovation Program for Quantum Science and Technology (Grant No. 2021ZD0302402).

References

[1] Zunger A 2018 *Nat. Rev. Chem.* **2** 0121
[2] Lee J, Park D, Lee M, Lee H, Park K, Lee I, and Ryu S 2023 *Mater. Horiz.* **10** 5436
[3] Wang J, Li X, Zhang T, Chen Y, Wang T, and Zhao Y 2022 *J. Phys. Chem. Lett.* **13** 622
[4] Long T, Zhang Y X, and Zhang H B 2024 arXiv:2409.19124 [cond-mat.mtrlsci]

[5] Wu Y 2024 *Physics-Informed Machine Learning Methods for Inverse Design of Multi-Phase Materials with Targeted Mechanical Properties* (PhD Dissertation)
[6] Chen L, Zhang W, Nie Z, Li S, and Pan F 2021 *J. Mater. Inform* **1** 4
[7] Abu-Mualla M and Huang J 2023 *Mater. Des.* **232** 112103
[8] Onnes H K 1991 *Through Measurement to Knowledge: The Selected Papers of Heike Kamerlingh Onnes 1853–1926* (Dordrecht: Springer Netherlands) p. 264
[9] Nagamatsu J, Nakagawa N, Muranaka T, Zenitani Y, and Akimitsu J 2001 *Nature* **410** 63
[10] Kim B, Lee S, and Kim J 2020 *Sci. Adv.* **6** eaax9324
[11] Vidmar D 2011 *PDF document provided on the internet by the Universidade Federal Rio Grande do Sul*
[12] Anderson C D 1932 *Science* **76** 238
[13] Bardeen J, Cooper L N, and Schrieffer J R 1957 *Phys. Rev.* **108** 1175
[14] Bardeen J 1955 *Phys. Rev.* **97** 1724
[15] Cooper L N 1956 *Phys. Rev.* **104** 1189
[16] Kresse G and Furthmüller J 1996 *Phys. Rev. B* **54** 11169
[17] Perdew J P, Burke K, and Ernzerhof M 1996 *Phys. Rev. Lett.* **77** 3865
[18] Blöchl P E 1994 *Phys. Rev. B* **50** 17953
[19] Novoselov K S, Geim A K, Morozov S V, Jiang D, Zhang Y, Dubonos S V, Grigorieva I V, and Firsov A A 2004 *Science* **306** 666
[20] Pople J A, Binkley J S, and Seeger R 1976 *Int. J. Quantum Chem.* **10** 1
[21] Park H, Li Z, and Walsh A 2024 *Matter* **7** 2355
[22] Vaswani A, Shazeer N, Parmar N *et al.* 2017 *Proceedings of the 31st International Conference on Neural Information Processing Systems* p. 6000
[23] Xie T, Fu X, Ganea O E, Barzilay R, and Jaakkola T 2022 *Proceedings of the 10th International Conference on Learning Representations*
[24] Jiao R, Huang W, Lin P, Han J, Chen P, Lu Y, and Liu Y 2023 *Advances in Neural Information Processing Systems*, December 10–16, New Orleans, USA, vol. 36, p. 17464
[25] Chen Y, Wang X, Deng X, Liu Y, Chen X, Zhang Y, Wang L, and Xiao H 2024 arXiv:2408.07608 [cond-mat.mtrl-sci]
[26] Choudhary K 2024 *J. Phys. Chem. Lett.* **15** 6909
[27] Fernandez-Zelaia P, Thapliyal S, Kannan R, Nandwana P, Yamamoto Y, Nycz A, Paquit V and Kirka M M 2024 *Additive Manufacturing* **94** 104478
[28] Lyu X and Ren X 2024 *Sci. Rep.* **14** 5041
[29] Gao Z F, Qu S, Zeng B C, Liu Y, Wen J R, Sun H, Guo P J, and Lu Z Y 2023 arXiv:2311.04418 [cond-mat.mtrl-sci]
[30] Ansari M, Watchorn J, Brown C E, and Brown J S 2024 *dZiner: Rational Inverse Design of Materials with AI Agents*
[31] Merchant A, Batzner S, Schoenholz S S, Aykol M, Cheon G, and Cubuk E D 2023 *Nature* **624** 80
[32] Barroso-Luque L, Shuaibi M, Fu X, Wood B M, Dzamba M, Gao M, Rizvi A, Zitnick C L, and Ulissi Z W 2024 arXiv:2410.12771 [condmat.mtrl-sci]
[33] Chen Y, Lan Z, Su Z, and Zhu J 2022 *Nanophotonics* **11** 4347
[34] Liu S and Yang C 2024 *Metals* **14** 235
[35] Han J, Cen J, Wu L, Li Z, Kong X, Jiao R, Yu Z, Xu T, Wu F, Wang Z, Xu H, Wei Z, Liu Y, Rong Y, and Huang W 2024 arXiv:2403.00485v1 [cs.LG]
[36] Reiser P, Neubert M, Eberhard A, Torresi L, Zhou C, Shao C, Metni H, van Hoesel C, Schopmans H, Sommer T, and Friederich P 2022 *Commun. Mater.* **3** 93
[37] Lvovsky Y, Stautner E W, and Zhang T 2013 *Supercond. Sci. Technol.* **26** 093001
[38] Bruzzone P, Fietz W H, Minervini J V, Novikov M, Yanagi N, Zhai Y, and Zheng J 2018 *Nucl. Fusion* **58** 103001
[39] Mirhosseini M, Sipahigil A, Kalaee M, and Painter O 2020 *Nature* **588** 599
[40] Gambetta J M, Chow J M, and Steffen M 2017 *NPJ Quantum Inf.* **3** 2
[41] Degen C L, Reinhard F, and Cappellaro P 2017 *Rev. Mod. Phys.* **89** 035002
[42] Onnes H K 1911 *Commun. Theor. Phys.* **120**
[43] Meissner W and Ochsenfeld R 1933 *Sci. Nat.* **21** 787
[44] Gavaler J R 1973 *Appl. Phys. Lett.* **23** 480
[45] Bednorz J G and Müller K A 1986 *Z. Phys. B* **64** 189
[46] Wu M K, Ashburn J R, Torng C J, Hor P H, Meng R L, Gao L, Huang Z J, Wang Y Q, and Chu C W 1987 *Phys. Rev. Lett.* **58** 908
[47] Ren Z A, Lu W, Yang J, Yi W, Shen X L, Che G C, Dong X L, Sun L L, Zhou F, and Zhao Z X 2008 *Chin. Phys. Lett.* **25** 2215
[48] Ying J, Liu S, Lu Q, Wen X, Gui Z, Zhang Y, Wang X, Sun J, and Chen X 2023 *Phys. Rev. Lett.* **130** 256002
[49] Sun H, Huo M, Hu X, Li J, Liu Z, Han Y, Tang L, Mao Z, Yang P, Wang B, Cheng J, Yao D X, Zhang G M, and Wang M 2023 *Nature* **621** 493
[50] Drozdov A P, Eremets M I, Troyan I A, Ksenofontov V, and Shylin S I 2015 *Nature* **525** 73
[51] Stanev V, Oses C, Kusne A G, Rodriguez E, Paglione J, Curtarolo S, and Takeuchi I 2018 *NPJ Comput. Mater.* **4** 29
[52] Ward L, Agrawal A, Choudhary A, and Wolverton C 2016 *NPJ Comput. Mater.* **2** 16028
[53] Li J, Fang W, Jin S, Zhang T, Wu Y, Xu X, Liu Y, and Yao D X 2024 arXiv:2409.07721 [cond-mat.supr-con]
[54] Zhang T D, Suo C Y, Wu Y L, Xu X D, Liu Y, Yao D X, and Li J 2024 arXiv:2409.09419 [cond-mat.supr-con]
[55] Scarselli F, Gori M, Tsoi A C, Hagenbuchner M, and Monfardini G 2008 *IEEE Trans. Neural Networks* **20** 61
[56] Wu Z, Pan S, Chen F, Long G, Zhang C, and Philip S Yu 2020 *IEEE Trans. Neural Networks Learn. Syst.* **32** 4
[57] Kipf T N and Welling M 2016 *5th International Conference on Learning Representations*, April 24–26, 2017, Toulon, France
[58] Hamilton W, Ying Z, and Leskovec J 2017 *Advances in Neural Information Processing Systems*, December 4–9, Long Beach, USA
[59] Veličković P, Cucurull G, Casanova A, Romero A, Lio P, and Bengio Y 2017 *6th International Conference on Learning Representations*, May 6–9, 2018, Vancouver, Canada
[60] Defferrard M, Bresson X, and Vandergheynst P 2016 *Advances in Neural Information Processing Systems*, December 5–10, Barcelona, Spain
[61] Choudhary K and Garrity K 2022 *NPJ Comput. Mater.* **8** 244
[62] Choudhary K and DeCost B 2021 *NPJ Comput. Mater.* **7** 185
[63] Wines D and Choudhary K 2024 *Materials futures* **3** 025602
[64] Zhao J, Wang J, He D, Li J, Sun Y, Chen X Q, and Liu P 2024 *Acta Metall. Sin.* **60** 1418
[65] Li J, Wei L, Shi X, Shi L, Si J, Liu P F, and Wang B T 2024 *Phys. Rev. B* **109** 174516
[66] Cerqueira T F T, Fang Y W, Errea I, Sanna A, and Marques M A L 2024 *Adv. Funct. Mater.* **34** 2404043

[67] Sommer T, Willa R, Schmalian J, and Friederich P 2023 *Sci. Data* **10** 816

[68] Rombach R, Blattmann A, Lorenz D, Esser P, and Ommer B 2022 *Proceedings of the IEEECVF Conference on Computer Vision and Pattern Recognition* p. 10674

[69] Ho J, Jain A, and Abbeel P 2020 *Advances in Neural Information Processing Systems* p. 6840

[70] Song Y and Ermon S 2019 *Advances in Neural Information Processing Systems* p. 11918

[71] Abramson J, Adler J, Dunger J, Evans R, Green T, Pritzel A, Ronneberger O, Willmore L, Ballard A J, Bambrick J *et al.* 2024 *Nature* **630** 493

[72] Han X Q, Ouyang Z, Guo P J, Sun H, Gao Z F, and Lu Z Y 2024 arXiv:2409.08065 [cond-mat.supr-con]

[73] Xie T and Grossman J C 2018 *Phys. Rev. Lett.* **120** 145301

[74] Gao Z F, Qu S, Zeng B C, Liu Y, Wen J R, Sun H, Guo P J, and Lu Z Y 2024 arXiv:2311.04418 [cond-mat.mtrl-sci]

[75] Chen C, Ye W, Zuo Y, Zheng C, and Ong S P 2019 *Chem. Mater.* **31** 3564

[76] Zhang C, Tang H, Pan C, Jiang H, Sun H J, Ho K M, and Wang C Z 2023 *Phys. Rev. B* **108** 024512

[77] Zhang D, Liu X, Zhang X, Zhang C, Cai C, Bi H, Du Y, Qin X, Peng A, Huang J *et al.* 2024 *NPJ Comput. Mater.* **10** 293

[78] Wines D, Xie T, and Choudhary K 2023 *J. Phys. Chem. Lett.* **14** 6630

[79] Okabe R, Chotrattanapituk A, Boonkird A, Andrejevic N, Fu X, Jaakkola T S, Song Q, Nguyen T, Drucker N, Mu S, Wang Y, Liao B, Cheng Y, and Li M 2024 *Nat. Comput. Sci.* **4** 522

[80] Zhong Y, Liu S, Zhang B, Tao Z, Sun Y, Chu W, Gong X G, Yang J H, and Xiang H 2024 *Nat. Comput. Sci.* **4** 615

[81] Chmaissem O, Jorgensen J D, Short S, Knizhnik A, Eckstein Y, and Shaked H 1999 *Nature* **397** 45

[82] Lee C H, Kihou K, Iyo A, Kito H, Shirage P M, and Eisaki H 2012 *Solid State Commun.* **152** 644

[83] Mizuguchi Y, Hara Y, Deguchi K, Tsuda S, Yamaguchi T, Takeda K, Kotegawa H, Tou H, and Takano Y 2010 *Supercond. Sci. Tech.* **23** 054013

[84] Peng Y Y, Dellea G, Minola M, Conni M, Amorese A, Di Castro D, De Luca G M, Kummer K, Salluzzo M, Sun X *et al.* 2017 *Nature Phys.* **13** 1201

[85] Gu L, Liu Y, Chen P, Huang H, Chen N, Li Y, Lookman T, Lu Y, and Su Y 2024 *Mater. Genome Eng. Adv.* e48

[86] Pogue E A, New A, McElroy K, Le N Q, Pekala M J, McCue I, Gienger E, Domenico J, Hedrick E, McQueen T M, Wilfong B, Piatko C D, Ratto C R, Lennon A, Chung C, Montalbano T, Bassen G, and Stiles C D 2023 *NPJ Comput. Mater.* **9** 181

[87] Cullity B D and Graham C D 2011 *Introduction to Magnetic Materials* (Hoboken, NJ: John Wiley & Sons)

[88] Goldman A 2012 *Handbook of Modern Ferromagnetic Materials* (New York, NY: Springer Science & Business Media)

[89] Jungwirth T, Marti X, Wadley P and Wunderlich J 2016 *Nat. Nanotech.* **11** 231

[90] Šmejkal L, Sinova J and Jungwirth T 2022 *Phys. Rev. X* **12** 040501

[91] Šmejkal L, Sinova J and Jungwirth T 2022 *Phys. Rev. X* **12** 031042

[92] Mazin I 2022 *Phys. Rev. X* **12** 040002

[93] Hayami S, Yanagi Y, and Kusunose H 2019 *J. Phys. Soc. Japan* **88** 123702

[94] Šmejkal L, González-Hernández R, Jungwirth T, and Sinova J 2020 *Sci. Adv.* **6** eaaz8809

[95] Yuan L D, Wang Z, Luo J W, Rashba E I, and Zunger A 2020 *Phys. Rev. B* **102** 014422

[96] Mazin I I, Koepernik K, Johannes M D, González-Hernández R, and Šmejkal L 2021 *Proc. Natl. Acad. Sci. U.S.A.* **118** e2108924118

[97] Jungwirth T, Fernandes R M, Sinova J, and Smejkal L 2024 arXiv:2409.10034 [cond-mat.mtrl-sci]

[98] Bouhon A, Lange G F, and Slager R J 2021 *Phys. Rev. B* **103** 245127

[99] Hubert A and Schafer R 1998 *Magnetic Domains: The Analysis of Magnetic Microstructures* (Berlin, Heidelberg: Springer) p. XXIII, 696

[100] Šmejkal L, Hellenes A B, González-Hernández R, Sinova J, and Jungwirth T 2022 *Phys. Rev. X* **12** 011028

[101] Zhu D, Zhuang Z Y, Wu Z, and Yan Z 2023 *Phys. Rev. B* **108** 184505

[102] Li Y X and Liu C C 2023 *Phys. Rev. B* **108** 205410

[103] Ma H Y, Hu M, Li N, Liu J, Yao W, Jia J F, and Liu J 2021 *Nat. Commun.* **12** 2846

[104] González-Hernández R, Šmejkal L, Výborný K, Yahagi Y, Sinova J, Jungwirth T, and Železný J 2021 *Phys. Rev. Lett.* **126** 127701

[105] Bai H, Han L, Feng X Y, Zhou Y J, Su R X, Wang Q, Liao L Y, Zhu W X, Chen X Z, Pan F, Fan X L, and Song C 2022 *Phys. Rev. Lett.* **128** 197202

[106] Karube S, Tanaka T, Sugawara D, Kadoguchi N, Kohda M, and Nitta J 2022 *Phys. Rev. Lett.* **129** 137201

[107] Šmejkal L, MacDonald A H, Sinova J, Nakatsuji S, and Jungwirth T 2022 *Nat. Rev. Mater.* **7** 482

[108] Feng Z, Zhou X, Šmejkal L, Wu L, Zhu Z, Guo H, González-Hernández R, Wang X, Yan H, Qin P, Zhang X, Wu H, Chen H, Meng Z, Liu L, Xia Z, Sinova J, Jungwirth T, and Liu Z 2022 *Nat. Electron.* **5** 735

[109] Gonzalez Betancourt R D, Zubáč J, Gonzalez-Hernández R, Geishendorf K, Šobáň Z, Springholz G, Olejník K, Šmejkal L, Sinova J, Jungwirth T, Goennenwein S T B, Thomas A, Reichlová H, Železný J and Kriegner D 2023 *Phys. Rev. Lett.* **130** 036702

[110] Hou X Y, Yang H C, Liu Z X, Guo P J, and Lu Z Y 2023 *Phys. Rev. B* **107** L161109

[111] Zhou X, Feng W, Yang X, Guo G Y, and Yao Y 2021 *Phys. Rev. B* **104** 024401

[112] Zhou X, Feng W, Zhang R W, Šmejkal L, Sinova J, Mokrousov Y, and Yao Y 2024 *Phys. Rev. Lett.* **132** 056701

[113] Guo P J, Liu Z X, and Lu Z Y 2023 *NPJ Comput. Mater.* **9** 70

[114] Li Y X, Liu Y, and Liu C C 2024 *Phys. Rev. B* **109** L201109

[115] Guo P J, Gu Y H, Gao Z F, and Lu Z Y 2023 arXiv:2312.13911 [condmat.mtrl-sci]

[116] Qu S, Gao Z F, Sun H, Liu K, Guo P J, and Lu Z Y 2024 arXiv:2401.11065 [cond-mat.mtrl-sci]

[117] Tan C Y, Gao Z F, Yang H C, Liu K, Guo P J, and Lu Z Y 2024 arXiv:2406.16603 [cond-mat.mtrl-sci]

[118] Itani S, Zhang Y, and Zang J 2024 arXiv:2409.15675 [cond-mat.mtrl-sci]

[119] Zhang Y, Itani S, Khanal K, Okyere E, Smith G, Takahashi K, and Zang J 2024 *J. Magn. Magn. Mater.* **597** 172001

[120] Jain A, Montoya J, Dwaraknath S, Zimmermann N E R, Dagdelen J, Horton M, Huck P, Winston D, Cholia S, Ong S P *et al.* 2020 *Handbook of Materials : Methods: Theory and Modeling* (Berlin: Springer) p. 1751

[121] Rowe D M 2018 *Thermoelectrics Handbook: Macro to Nano* (Boca Raton: CRC Press)

[122] Tan G, Zhao L D, and Kanatzidis M G 2016 *Chem. Rev.* **116** 12123

[123] Mamur H, Dilmaç Ö F, Begum J, and Bhuiyan M R A 2021 *Cleaner Mater.* **2** 100030

[124] Vedernikov M V and Iordanishvili E K 1998 *Seventeenth International Conference on Thermoelectrics. Proceedings ICT98* (IEEE) p. 37
[125] Zevalkink A, Smiadak D M, Blackburn J L, Ferguson A J, Chabinyc M L, Delaire O, Wang J, Kovnir K, Martin J, Schelhas L T *et al.* 2018 *Appl. Phys. Rev.* **5** 021303
[126] Gorai P, Stevanović V, and Toberer E S 2017 *Nature Rev. Mater.* **2** 17053
[127] Chen D, Jiang F, Fang L, Zhu Y B, Ye C C, and Liu W S 2022 *Rare Metals* **41** 1543
[128] Jia X, Deng Y, Bao X, Yao H, Li S, Li Z, Chen C, Wang X, Mao J, Cao F *et al.* 2022 *NPJ Comput. Mater.* **8** 34
[129] Na G S, Jang S, and Chang H 2021 *NPJ Comput. Mater.* **7** 106
[130] Sasaki M, Ju S, Xu Y, Shiomi J, and Goto M 2020 *ACS Comb. Sci.* **22** 782
[131] Li R, Li X, Xi L, Yang J, Singh D J, and Zhang W 2019 *ACS Appl. Mater. Interfaces* **11** 24859
[132] Gan Y, Wang G, Zhou J, and Sun Z 2021 *NPJ Comput. Mater.* **7** 176
[133] Islamov M, Babaei H, Anderson R, Sezginel K B, Long J R, McGaughey A J H, Gomez-Gualdron D A, and Wilmer C E 2023 *NPJ Comput. Mater.* **9** 11
[134] Luo H, Li X, Wang Y, Jin Y, Yao M, and Yang J 2022 *NPJ Comput. Mater.* **8** 199
[135] Choubisa H, Haque M A, Zhu T, Zeng L, Vafaie M, Baran D, and Sargent E H 2023 *Adv. Mater.* **35** 2302575
[136] Iijima S 1991 *Nature* **354** 56
[137] Geim A K and Novoselov K S 2007 *Nat. Mater.* **6** 183
[138] Mendoza-Cachú D, López-Miranda J L, Mercado-Zúñiga C, and Rosas G 2018 *Diam Relat Mater* **84** 26
[139] Javey A, Guo J, Wang Q, Lundstrom M, and Dai H 2003 *Nature* **424** 654
[140] Yu M F, Lourie O, Dyer M J, Moloni K, Kelly T F, and Ruoff R S 2000 *Science* **287** 637
[141] An K H, Kim W S, Park Y S, Choi Y C, Lee S M, Chung D C, Bae D J, Lim S C, and Lee Y H 2001 *Adv. Mater.* **13** 497
[142] Zhang D, Yi P, Lai X, Peng L, and Li H 2024 *Nat. Commun.* **15** 344
[143] Hedman D, McLean B, Bichara C, Maruyama S, Larsson J A, and Ding F 2024 *Nat. Commun.* **15** 4076
[144] Li Y, Wang S, Lv Z, Wang Z, Zhao Y, Xie Y, Xu Y, Qian L, Yang Y, Zhao Z *et al.* 2024 arXiv:2404.01006v1 [physics.app-ph]
[145] Liu B, Vu-Bac N, Zhuang X, Fu X and Rabczuk T 2022 *Compos. Struct.* **289** 115393
[146] Elaskalany M and Behdinan K 2024 *Adv. Eng. Mater.* **43** 2401233
[147] Matos M A S, Pinho S T, and Tagarielli V L 2019 *Scr. Mater.* **166** 117
[148] Safavigerdini K, Nouduri K, Surya R, Reinhard A, Quinlan Z, Bunyak F, Maschmann MR and Palaniappan K 2023 *Predicting mechanical properties of carbon nanotube (cnt) images using multi-layer synthetic finite element model simulations IEEE International Conference on Image Processing* (ICIP) p. 3264
[149] Papadopoulos V, Soimiris G, Giovanis D G, and Papadrakakis M 2018 *Comput. Methods. Appl. Mech. Eng.* **328** 411
[150] Fernandez M, Shi H, and Barnard A S 2016 *Carbon* **103** 142
[151] Alred J M, Bets K V, Xie Y, and Yakobson B I 2018 *Compos. Sci. Technol.* **166** 3
[152] Singh A V, Rosenkranz D, Ansari M H D, Singh R, Kanase A, Singh S P, Johnston B, Tentschert J, Laux P, and Luch A 2020 *Adv. Intell. Syst.* **2** 2000084
[153] Novoselov K S, Mishchenko A, Carvalho A, and Castro Neto A H 2016 *Science* **353** aac9439
[154] Slager R J, Mesaros A, Juričić V, and Zaanen J 2013 *Nat. Phys.* **9** 98
[155] Kruthoff J, de Boer J, van Wezel J, Kane C L, and Slager R J 2017 *Phys. Rev. X* **7** 041069
[156] Po H C, Vishwanath A, and Watanabe H 2017 *Nat. Commun.* **8** 50
[157] Bradlyn B, Elcoro L, Cano J, Vergniory M G, Wang Z, Felser C, Aroyo M I, and Bernevig B A 2017 *Nature* **547** 298
[158] Vergniory M G, Elcoro L, Felser C, Regnault N, Bernevig B A, and Wang Z 2019 *Nature* **566** 480
[159] Zhang T, Jiang Y, Song Z, Huang H, He Y, Fang Z, Weng H, and Fang C 2019 *Nature* **566** 475
[160] Chen W, George J, Varley J B, Rignanese G M, and Hautier G 2019 *NPJ Comput. Mater.* **5** 72
[161] Horton M K, Montoya J H, Liu M, and Persson K A 2019 *NPJ Comput. Mater.* **5** 64
[162] Geim A K 2009 *Science* **324** 1530
[163] Manzeli S, Ovchinnikov D, Pasquier D, Yazyev O V, and Kis A 2017 *Nat. Rev. Mater.* **2** 17033
[164] Pei S, Wang Z, and Xia J 2022 *ACS Nano* **16** 11498
[165] Das S K, Yan B, van den Brink J, and Fulga I C 2019 *Phys. Rev. B* **99** 165418
[166] Yi M and Shen Z 2015 *Mater. Chem. A* **3** 11700
[167] Zhang Y, Zhang L, and Zhou C 2013 *Acc. Chem. Res.* **46** 2329
[168] Lu M, Ji H, Zhao Y, Chen Y, Tao J, Ou Y, Wang Y, Huang Y, Wang J, and Hao G 2022 *ACS Appl. Mater. Interfaces* **15** 1871
[169] Ryu B, Wang L, Pu H, Chan M, and Chen J 2022 *Chem. Soc. Rev.* **51** 1899
[170] Hasan M Z and Kane C L 2010 *Rev. Mod. Phys* **82** 3045
[171] Ando Y 2013 *J. Phys. Soc. Jpn.* **82** 102001
[172] Schleder G R, Focassio B, and Fazzio A 2021 *Appl. Phys. Rev.* **8** 031409
[173] Choudhary K, Kalish I, Beams R, and Tavazza F 2017 *Sci. Rep.* **7** 5179
[174] Mounet N, Gibertini M, Schwaller P, Campi D, Merkys A, Marrazzo A, Sohier T, Castelli I E, Cepellotti A, Pizzi G *et al.* 2018 *Nat. Nanotechnol.* **13** 246
[175] Choudhary K, Garrity K F, Hartman S T, Pilania G, and Tavazza F 2004 *Phys. Rev. Mater.* **1** 014009
[176] Harris S B, Biswas A, Yun S J, Roccapriore K M, Rouleau C M, Puretzky A A, Vasudevan R K, Geohegan D B, and Xiao K 2024 *Small Methods* **8** 2301763
[177] Wang Z, Cai J, Wang Q, Wu S, and Li J 2021 *NPJ Comput. Mater.* **7** 128
[178] Frey N C, Wang J, Vega Bellido G I, Anasori B, Gogotsi Y, and Shenoy V B 2019 *ACS nano* **13** 3031
[179] Li Z, Yao F, and Sun H 2024 *IISE Trans.* **56** 811
[180] Rajak P, Krishnamoorthy A, Kalia R, Nakano A, and Vashishta P 2020 *Quantum material synthesis by reinforcement learning* p. 170
[181] Xu M, Tang B, Lu Y, Zhu C, Lu Q, Zhu C, Zheng L, Zhang J, Han N, Fang W *et al.* 2021 *J. Am. Chem. Soc.* **143** 18103
[182] Tang B, Lu Y, Zhou J, Chouhan T, Wang H, Golani P, Xu M, Xu Q, Guan C, and Liu Z 2020 *Mater. Today* **41** 72
[183] Haastrup S, Strange M, Pandey M, Deilmann T, Schmidt P, Hinsche N, Gjerding M, Torelli D, Larsen P, Riis-Jensen A *et al.* 2018 *2D Mater.* **5** 042002
[184] Gjerding M N, Taghizadeh A, Rasmussen A, Ali S, Bertoldo F, Deilmann T, Knøsgaard N R, Kruse M, Larsen A H, Manti S *et al.* 2021 *2D Mater.* **8** 044002

[185] Zhou J, Shen L, Costa M, Persson K, Ong S, Huck P, Lu Y, Ma X, Chen Y, Tang H *et al.* 2019 *Sci. data* **6** 86
[186] Talirz L, Kumbhar S, Passaro E, Yakutovich A, Granata V, Gargiulo F, Borelli M, Uhrin M, Huber S, Zoupanos S *et al.* 2020 *Sci. Data* **7** 299
[187] Campi D, Mounet N, Gibertini M, Pizzi G, and Marzari N 2023 *ACS nano* **17** 11268
[188] Marchenko E I, Fateev S A, Petrov A A, Korolev V V, Mitrofanov A, Petrov A V, Goodilin E A, and Tarasov A B 2020 *Chem. Mater.* **32** 7383
[189] Frey N C, Akinwande D, Jariwala D, and Shenoy V B 2020 *ACS nano* **14** 13406
[190] Xu P, Ji X, Li M, and Lu W 2023 *NPJ Comput. Mater.* **9** 42
[191] Brito A C M, Oliveira M C F, Oliveira O N, Silva F N, and Amancio D R 2023 *ACS Appl. Mater. Interfaces* **15** 27437
[192] Green M A, Dunlop E D, Yoshita M, Kopidakis N, Bothe K, Siefer G, Hinken D, Rauer M, Hohl-Ebinger J, and Hao X 2024 *Prog. Photovolt.* **32** 425
[193] Polman A, Knight M, Garnett E C, Ehrler B, and Sinke W C 2016 *Science* **352** aad4424
[194] Nelson J 2003 *The physics of solar cells* (London: Imperial College Press)
[195] Wang R, Yu H, Zhong Y, and Xiang H 2024 *J. Phys. Chem. C* **128** 12677
[196] Zhong Y, Yu H, Su M, Gong X, and Xiang H 2023 *NPJ Comput. Mater.* **9** 182
[197] Philipps S and Warmuth W 2019 *ISE with Support of PSE GmbH November 14th; Fraunhofer ISE: Freiburg, Germany*
[198] Streetman B, Banerjee S *et al.* 2000 *Solid State Electronic Devices* (New Jersey: Prentice hall)
[199] Nakamura S and Fasol G 2013 *The blue laser diode: GaN based light emitters and lasers* (New York: Springer Science & Business Media)
[200] Levinshtein M E, Rumyantsev S L and Shur M S 2001 *Properties of Advanced Semiconductor Materials: GaN, AlN, InN, BN, SiC, SiGe* (New Jersey: John Wiley & Sons)
[201] Li J, Aierken A, Liu Y, Zhuang Y, Yang X, Mo J H, Fan R K, Chen Q Y, Zhang S Y, Huang Y M, and Zhang Q 2021 *Front. Phys.* **8** 631925
[202] Dimroth F and Kurtz S 2007 *MRS Bull.* **32** 230
[203] Kojima A, Teshima K, Shirai Y, and Miyasaka T 2009 *J. Am. Chem. Soc.* **131** 6050
[204] Snaith H J 2013 *J. Phys. Chem. Lett.* **4** 3623
[205] Tilley R J D 2016 *Perovskites: structure-property relationships* (New Jersey: John Wiley & Sons)
[206] Tao Q, Xu P, Li M, and Lu W 2021 *NPJ Comput. Mater.* **7** 23
[207] Roy P, Ghosh A, Barclay F, Khare A, and Cuce E 2022 *Coatings* **12** 1089
[208] Liu Y, Tan X, Xiang P, Tu Y, Shao T, Zang Y, Li X, and Yan W 2024 *Mater. Today Phys.* **42** 101359
[209] Mohanty D and Palai A K 2023 *Adv. Theory Simul.* **6** 2300309
[210] Akbar B, Tayara H, and Chong K T 2024 *iScience* **27** 109200
[211] Karimitari N, Baldwin W J, Muller E W, Bare Z J L, Kennedy W J, Csányi G, and Sutton C 2024 *J. Am. Chem. Soc.* **146** 27392
[212] Ran J, Wang B, Wu Y, Liu D, Mora Perez C, Vasenko A S, and Prezhdo O V 2023 *J. Phys. Chem. Lett.* **14** 6028
[213] Bi H, Wang M, Liu L, Yan J, Zeng R, Xu Z, and Wang J 2024 *J. Mater. Chem. A* **12** 12744
[214] Wu Y, Wang C F, Ju M G, Jia Q, Zhou Q, Lu S, Gao X, Zhang Y, and Wang J 2024 *Nat. Commun.* **15** 138
[215] Mai H, Wen X, Li X, Dissanayake N S L, Sun X, Lu Y, Le T C, Russo S P, Chen D, and Winkler D A 2024 *Mater. Today* **74** 12
[216] Li X, Mai H, Lu J, Wen X, Le T C, Russo S P, Winkler D A, Chen D, and Caruso R A 2023 *Angew. Chem. Int. Ed.* **62** e202315002
[217] Choubisa H, Todorović P, Pina J M, Parmar D H, Li Z L, Voznyy O, Tamblyn I, and Sargent E H 2023 *NPJ Comput. Mater.* **9** 117
[218] Selvaratnam B, Oliynyk A O, and Mar A 2023 *Inorg. Chem.* **62** 10865
[219] Solak E K and Irmak E 2023 *RSC Adv.* **13** 12244
[220] Brabec C J, Gowrisanker S, Halls J J M, Laird D, Jia S, and Williams S P 2010 *Adv. Mater.* **22** 3839
[221] Sariciftci N S, Smilowitz L, Heeger A J, and Wudl F 1992 *Science* **258** 1474
[222] Li G, Zhu R, and Yang Y 2012 *Nat. Photonics.* **6** 153
[223] Yuan J, Zhang Y Q, Zhou L Y *et al.* 2019 *Joule* **3** 1140
[224] Solak E K and Irmak E 2023 *RSC Adv.* **13** 12244
[225] Zhang Q, Zheng Y J, Sun W, Ou Z, Odunmbaku O, Li M, Chen S, Zhou Y, Li J, Qin B, and Sun K 2022 *Adv. Sci.* **9** 2104742
[226] Morishita Y, Yarimizu M, Kaneko M, and Muraoka A 2024 *Chem. Phys. Lett.* **857** 141719
[227] Liu X, Shao Y, Lu T, Chang D, Li M, and Lu W 2022 *Mater. Des.* **216** 110561
[228] Suthar R, Abhijith T, Sharma P, and Karak S 2023 *Sol Energy* **250** 119
[229] Li M, Zhang C R, Zhang M L, Gong J J, Liu X M, Chen Y H, Liu Z J, Wu Y Z, and Chen H S 2024 *Phys. Status. Solidi. A* **221** 2400008
[230] Shetty P, Adeboye A, Gupta S, Zhang C, and Ramprasad R 2024 *Chem. Mater.* **36** 7676
[231] Suthar R, T A, Karak S 2023 *J. Mater. Chem. A* **11** 22248
[232] Miyake Y, Kranthiraja K, Ishiwari F, and Saeki A 2022 *Chem. Mater.* **34** 6912
[233] Wang H, Feng J, Dong Z, Jin L, Li M, Yuan J, and Li Y 2023 *NPJ Comput. Mater.* **9** 200
[234] Mou L H, Han T T, Smith P E S, Sharman E, and Jiang J 2023 *Adv. Sci.* **10** 2301020
[235] Guo Y, He X, Su Y, Dai Y, Xie M, Yang S, Chen J, Wang K, Zhou D, and Wang C 2021 *J. Am. Chem. Soc.* **143** 5755
[236] Ishioka S, Fujiwara A, Nakanowatari S, Takahashi L, Taniike T, and Takahashi K 2022 *ACS Catal* **12** 11541
[237] Andersen M, Levchenko S V, Scheffler M, and Reuter K 2019 *ACS Catal.* **9** 2752
[238] Ouyang R, Curtarolo S, Ahmetcik E, Scheffler M, and Ghiringhelli L M 2018 *Phys. Rev. Mater.* **2** 083802
[239] Bartel C J, Sutton C, Goldsmith B R, Ouyang R, Musgrave C B, Ghiringhelli L M, and Scheffler M 2019 *Sci. Adv.* **5** eaav0693
[240] Xu W, Andersen M, and Reuter K 2020 *ACS Catal.* **11** 734
[241] Mou T, Pillai H S, Wang S, Wan M, Han X, Schweitzer N M, Che F, and Xin H 2023 *Nat. Catal.* **6** 122
[242] Ren C, Lu S, Wu Y, Ouyang Y, Zhang Y, Li Q, Ling C, and Wang J 2022 *J. Am. Chem. Soc.* **144** 12874
[243] Li Z, Wang S, Chin W S, Achenie L E, and Xin H 2017 *J. Mater. Chem. A.* **5** 24131
[244] Li Z, Achenie L E K, and Xin H 2020 *ACS Catal.* **10** 4377
[245] Lu Z, Chen Z W, and Singh C V 2020 *Matter* **3** 1318
[246] Wang X, Ye S, Hu W, Sharman E, Liu R, Liu Y, Luo Y, and Jiang J 2020 *J. Am. Chem. Soc.* **142** 7737
[247] Zhong W, Qiu Y, Shen H, Wang X, Yuan J, Jia C, Bi S, and Jiang J 2021 *J. Am. Chem. Soc.* **143** 4405
[248] Gu Y, Zhu Q, Liu Z, Fu C, Wu J, Zhu Q, Jia Q, and Ma J 2022 *J. Mater. Chem. A* **10** 14976

[249] Williams T, McCullough K, and Lauterbach J A 2019 *Chem. Mater.* **32** 157
[250] Karim M R, Ferrandon M, Medina S, Sture E, Kariuki N, Myers D J, Holby E F, Zelenay P, and Ahmed T 2020 *ACS Appl. Energy Mater.* **3** 9083
[251] Artrith N, Lin Z, and Chen J G 2020 *ACS Catal.* **10** 9438
[252] Zhu Q, Zhang F, Huang Y, Xiao H, Zhao L Y, Zhang X C, Song T, Tang X S, Li X, He G *et al.* 2022 *Natl. Sci. Rev.* **9** nwac190
[253] Zhong M, Tran K, Min Y, Wang C, Wang Z, Dinh C T, De Luna P, Yu Z, Rasouli A S, Brodersen P *et al.* 2020 *Nature* **581** 178
[254] Han Z K, Sarker D, Ouyang R, Mazheika A, Gao Y, and Levchenko S V 2021 *Nat. Commun.* **12** 1833
[255] Yin P, Niu X, Li S B, Chen K, Zhang X, Zuo M, Zhang L, and Liang H W 2024 *Nat. Commun.* **15** 415
[256] Chen L, Tian Y, Hu X, Yao S, Lu Z, Chen S, Zhang X, and Zhou Z 2022 *Adv. Funct. Mater.* **32** 2208418
[257] Mok D H and Back S 2024 *J. Am. Chem. Soc.* **146** 33712
[258] Yeh J W, Chen S K, Lin S J, Gan J Y, Chin T S, Shun T T, Tsau C H, and Chang S Y 2004 *Adv. Eng. Mater.* **6** 299
[259] Cantor B, Chang I T H, Knight P, and Vincent A J B 2004 *Mater. Sci. Eng. A* **375** 213
[260] George E P, Raabe D, and Ritchie R O 2019 *Nat. Rev. Mater.* **4** 515
[261] Otto F, Yang Y, Bei H, and George E P 2013 *Acta Mater.* **61** 2628
[262] Rao Z, Tung P Y, Xie R, Wei Y, Zhang H, Ferrari A, Klaver TPC, Körmann F, Sukumar P T, Kwiatkowski da Silva A *et al.* 2022 *Science* **3** 78
[263] Wang J, Kwon H, Kim H S, and Lee B J 2023 *NPJ Comput. Mater* **9** 60
[264] Chau N H, Kubo M, Hai L V, and Yamamoto T 2023 *Vietnam J. Comput. Sci.* **10** 101
[265] Huang W, Martin P, and Zhuang H L 2019 *Acta Mater.* **169** 225
[266] Krishna Y V, Jaiswal U K, and Rahul M 2021 *Scr. Mater.* **197** 113804
[267] Li H C, Yuan R H, Liang H, Wang W Y, Li J S, and Wang J 2022 *Mater. Des.* **223** 111186
[268] Zhu W, Huo W, Wang S, Wang X, Ren K, Tan S, Fang F, Xie Z, and Jiang J 2022 *J. Mater. Res. Technol.* **18** 800
[269] Wang X M, Tran N D, Zeng S M, Hou C, Chen Y, and Ni J 2022 *NPJ Comput. Mater.* **8** 253
[270] Pei Z R, Rozman K A, Doğan Ö N, Wen Y H, Gao N, Holm E A, Hawk J A, Alman D E, and Gao M C 2021 *Adv. Sci.* **8** 2101207
[271] Slater A G and Cooper A I 2015 *Science* **348** aaa8075
[272] Thomas A 2020 *Nat. Commun.* **11** 4985
[273] Park J, Gill A P S, Moosavi S M, and Kim J 2024 *J. Mater. Chem. A* **12** 6507
[274] Yao Z, Sánchez-Lengeling B, Bobbitt N S, Bucior B J, Kumar S G H, Collins S P, Burns T, Woo T K, Farha O K, Snurr R Q *et al.* 2021 *Nature Mach. Intell.* **3** 76
[275] Park H, Yan X, Zhu R, Huerta E A, Chaudhuri S, Cooper D, Foster I, and Tajkhorshid E 2024 *Commun. Chem.* **7** 21
[276] Igashov I, Stärk H, Vignac C, Schneuing A, Satorras V G, Frossard P, Welling M, Bronstein M, and Correia B 2024 *Nat. Mach. Intell.* **6** 417
[277] Fu X, Xie T, Rosen A S, Jaakkola T S, and Smith J A 2024 *12th International Conference on Learning Representations*, May 7–11, 2024, Vienna, Austria
[278] Park J, Lee Y and Kim J 2024 *ChemRxiv*
[279] Wang T, Pan R, Martins M L, Cui J, Huang Z, Thapaliya B, Do-Thanh C, Zhou M, Fan J, Yang Z *et al.* 2023 *Nat. Commun.* **14** 4607
[280] Kumar S, Ignacz G, and Szekely G 2021 *Green Chem.* **23** 8932
[281] Delpisheh M, Ebrahimpour B, Fattahi A, Siavashi M, Mir H, Mashhadimoslem H, Abdol M A, Ghorbani M, Shokri J, Niblett D, Khosravi K, Rahimi S, Alirahmi S M, Yu H, Elkamel A, Niasar V, and Mamlouk M 2024 *J. Mater. Chem. A* **12** 20717
[282] D'Elia M, Deng H, Fraces C, Garikipati K, Graham-Brady L, Howard A, Karniadakis G, Keshavarzzadeh V, Kirby R M, Kutz N, Li C, Liu X, Lu H, Newell P, O'Malley D, Prodanovic M, Srinivasan G, Tartakovsky A, Tartakovsky D M, Tchelepi H, Vazic B, Viswanathan H, Yoon H, and Zarzycki P 2022 arXiv:2202.04137 [cs.LG]
[283] Breiman L 2001 *Mach. Learn.* **4** 5
[284] Quinlan J R 1986 *Mach. Learn.* **1** 81
[285] Cortes C and Vapnik V 1995 *Mach. Learn.* **20** 273
[286] Rumelhart D E, Hinton G E, and Williams R J 1986 *Nature* **323** 533
[287] Goodfellow I, Bengio Y, and Courville A 2016 *Deep Learning* Cambridge, Massachusetts : The MIT Press
[288] Deng B, Zareei A, Ding X, Weaver J C, Rycroft C H, and Bertoldi K 2022 *Adv. Mater.* **34** 2206238
[289] Geng X, Cheng Z, Wang S, Peng C, Ullah A, Wang H, and Wu G 2022 *J. Mater. Sci.* **57** 10755
[290] Ijaz S, Noureen S, Rehman B, Aldaghri O, Cabrera H, Ibnaouf K H, Madkhali N, and Mehmood M Q 2023 *Mater. Today Commun.* **37** 106951
[291] McDonald S M, Augustine E K, Lanners Q, Rudin C, Brinson C L, and Becker M L 2023 *Nat. Commun.* **14** 4838
[292] Lei X, Liu C, Du Z, Zhang W, and Guo X 2019 *J. Appl. Mech.* **86** 011004
[293] LeCun Y, Bengio Y, and Hinton G 2015 *Nature* **521** 436
[294] He K, Zhang X, Ren S, and Sun J 2016 *Proceedings of the IEEE conference on computer vision and pattern recognition* p. 770
[295] Abueidda D W, Koric S, and Sobh N A 2020 *Comput. Struct.* **237** 106283
[296] Wei X, van der Zwaag S, Jia Z, Wang C, and Xu W 2022 *Acta Mater.* **235** 118103
[297] Gu G X, Chen C T, and Buehler M J 2018 *Extreme Mech. Lett.* **18** 19
[298] Gilmer J, Schoenholz S S, Riley P F, Vinyals O, and Dahl G E 2017 *Proceedings of the 34th International Conference on Machine Learning* p. 1263
[299] Schütt K T, Sauceda H E, Kindermans P J, Tkatchenko A, and Müller K R 2018 *J. Chem. Phys.* **148** 241722
[300] Schütt K T, Arbabzadah F, Chmiela S, Müller K R, and Tkatchenko A 2017 *Nat. Commun.* **8** 13890
[301] Hu W, Shuaibi M, Das A, Goyal S, Sriram A, Leskovec J, Parikh D, and Zitnick C L 2021 arXiv:2103.01436 [cs.LG]
[302] Xie T and Grossman J C 2018 *Phys. Rev. Lett.* **120** 145301
[303] Unke O T and Meuwly M 2019 *J. Chem. Theory Comput.* **15** 3678
[304] Gasteiger J, Groß J, and Günnemann S 2020 arXiv:2003.03123 [cs.LG]
[305] Liu Y, Wang L, Liu M, Lin Y, Zhang X, Oztekin B, and Ji S 2022 Spherical Message Passing for 3D Molecular Graphs International Conference on Learning Representations
[306] Yue A, Luo D, and Xu H 2024 *Proc. AAAI Conf. Artif. Intell.* **38** 16633
[307] Gasteiger J, Becker F, and Günnemann S 2024 arXiv:2106.08903v1 [physics.comp-ph]

[308] Wang L, Liu Y, Lin Y, Liu H, and Ji S 2022 *ComENet: Towards Complete and Efficient Message Passing for 3D Molecular Graphs Advances in Neural Information Processing Systems*, 2022, New Orleans, Louisiana, USA, p. 650

[309] Garcia Satorras V, Hoogeboom E, and Welling M E 2021 *Proceedings of the 38th International Conference on Machine Learning* **139** 9323

[310] Schütt K, Kindermans P, Sauceda FEH, Chmiela S, Tkatchenko A, and Müller K R 2017 *SchNet: A continuous-filter convolutional neural network for modeling quantum interactions* p. 992

[311] Köhler J, Klein L, and Noé F 2019 arXiv:1910.00753v1 [stat.ML]

[312] Huang W, Han J, Rong Y, Xu T, Sun F, and Huang J 2022 *International Conference on Learning Representations*

[313] Du W, Zhang H, Du Y, Meng Q, Chen W, Zheng N, Shao B, and Liu T Y 2022 *Proceedings of the 39th International Conference on Machine Learning* **162** 5583

[314] Kofinas M, Nagaraja N S, and Gavves E 2022 *Advances in Neural Information Processing Systems* **34** 6417

[315] Kofinas M, Bekkers E J, Nagaraja N S, and Gavves E 2023 *Advances in Neural Information Processing Systems* **36** 31780

[316] Jing B, Eismann S, Suriana P, Townshend R J L, and Dror R 2021 *ICLR*

[317] Du Y, Wang L, Feng D, Wang G, Ji S, Gomes C P, and Ma Z M 2024 *Advances in Neural Information Processing Systems* **36**

[318] Puny O, Atzmon M, Smith E J, Misra I, Grover A, Ben-Hamu H, and Lipman Y 2021 *International Conference on Learning Representations*

[319] Han J, Huang W, Xu T, and Rong Y 2022 *NeurIPS*

[320] Thomas N, Smidt T, Kearnes S, Yang L, Li L, Kohlhoff K, and Riley P 2018 arXiv:1802.08219 [cs.LG]

[321] Geiger M and Smidt T 2022 arXiv:2207.09453 [cs.LG]

[322] Brandstetter J, Hesselink R, van der Pol E, Bekkers E J, and Welling M 2022 arXiv:2110.02905 [cs.LG]

[323] Batzner S, Musaelian A, Sun L, Geiger M, Mailoa J P, Kornbluth M, Molinari N, Smidt T E, and Kozinsky B 2022 *Nat. Commun.* **13** 2453

[324] Wang R, Yu H, Zhong Y, and Xiang H 2024 *JMI* **4** 32

[325] Gasteiger J, GroßJ, and Günnemann S 2022 arXiv:2003.03123 [cs.LG]

[326] Zitnick C L, Das A, Kolluru A, Lan J, Shuaibi M, Sriram A, Ulissi Z, and Wood B 2022 arXiv:2206.14331 [physics.chem-ph]

[327] Passaro S and Zitnick C L 2023 arXiv:2302.03655 [cs.LG]

[328] Batatia I, Kovács D P, Simm G N C, Ortner C, and Csányi G 2023 arXiv:2206.07697 [stat.ML]

[329] Schütt K T, Unke O T, and Gastegger M 2021 arXiv:2102.03150 [cs.LG]

[330] Musaelian A, Batzner S, Johansson A, Sun L, Owen C J, Kornbluth M, and Kozinsky B 2023 *Nat. Commun.* **14** 579

[331] Liao Y and Smidt T 2023 arXiv:2206.11990 [cs.LG]

[332] Liao Y L, Wood B, Das A, and Smidt T 2024 arXiv:2306.12059 [cs.LG]

[333] Ying C, Cai T, Luo S, Zheng S, Ke G, He D, Shen Y, and Liu T 2021 arXiv:2106.05234 [cs.LG]

[334] Fuchs F, Worrall D, Fischer V, and Welling M 2020 *Adv. Neural Inf. Process. Syst.* **33** 1970

[335] Thölke P and De Fabritiis G 2022 arXiv:2202.02541 [cs.LG]

[336] Hutchinson M, Lan C, Zaidi S, Dupont E, Teh Y, and Kim H 2021 *Proc. 38th Int. Conf. Mach. Learn.* **139** 4533

[337] Ramakrishnan R, Dral P O, Rupp M and Von Lilienfeld O A 2014 *Sci. Data* **1** 1

[338] Choudhary K and DeCost B 2021 *NPJ Comput. Mater.* **7** 185

[339] Karamad M, Magar R, Shi Y, Siahrostami S, Gates I D, and Barati Farimani A 2020 *Phys. Rev. Mater.* **4** 093801

[340] Lam P T, Kino H, Terakura K, Miyake T, Tsuda K, Takigawa I, and Chi D H 2017 *Sci. Technol. Adv. Mater.* **18** 756

[341] Kaba O and Ravanbakhsh S 2022 *Advances in Neural Information Processing Systems* **35** 4150

[342] Yan K, Liu Y, Lin Y and Ji S 2022 *Advances in Neural Information Processing Systems* **35** 15066

[343] Magar R, Wang Y, and Barati Farimani A 2022 *NPJ Comput. Mater* **8** 231

[344] Zbontar J, Jing L, Misra I, LeCun Y, and Deny S 2021 *Proceedings of the 38th International Conference on Machine Learning* **139** 12310

[345] Chen T, Kornblith S, Norouzi M, and Hinton G A 2020 *Proceedings of the 37th International Conference on Machine Learning* **119** 1597

[346] Yu H, Song Y, Hu J, Guo C, and Yang B 2023 arXiv:2306.05344v2 [cs.LG]

[347] Devlin J, Chang MW, Lee K, and Toutanova K 2018 arXiv:1810.04805v2 [cs.CL]

[348] Kirklin S, Saal J E, Meredig B, Thompson A, Doak J W, Aykol M, Rühl S, and Wolverton C 2015 *NPJ Comput. Mater.* **1** 15010

[349] Gasteiger J, Giri S, Margraf J T, and Günnemann S 2020 arXiv:2011.14115v3 [cs.LG]

[350] Rombach R, Blattmann A, Lorenz D, Esser P, and Ommer B 2022 *IEEE/CVF Conference on Computer Vision and Pattern Recognition (CVPR) p. 10684*

[351] Ho J, Jain A, and Abbeel P 2020 *Denoising diffusion probabilistic models, Advances in Neural Information Processing System* **33** 6840

[352] Song Y, Sohl-Dickstein J, Kingma D P, Kumar A, Ermon S, and Poole B 2021 *International Conference on Learning Representations*

[353] Abramson J, Adler J, Dunger J, and Evans R 2024 *Nature* **630** 493

[354] Corso G, Stärk H, Jing B, Barzilay R, and Jaakkola T S 2023 *The Eleventh International Conference on Learning Representations*

[355] Jing B, Corso G, Chang J, Barzilay R, and Jaakkola T S 2022 *Advances in Neural Information Processing Systems 35: Annual Conference on Neural Information Processing Systems* p. 24240

[356] Nouira A, Sokolovska N, and Crivello J C 2019 arXiv:1810.11203v3 [cs.LG]

[357] Miller B K, Chen R T Q, Sriram A, and Wood B M 2024 arXiv:2406.04713 [cs.LG]

[358] Jiao R, Huang W, Liu Y, Zhao D, and Liu Y 2024 arXiv:2402.03992v2 [cs.LG]

[359] Ye C Y, Weng H M, and Wu Q S 2024 *Comput. Mater. Today* **1** 100003

[360] Ramesh A, Dhariwal P, Nichol A, Chu C, and Chen M 2022 arXiv:2204.06125 [cs.CV]

[361] Luo X, Wang Z, Gao P, Lv J, Wang Y, Chen C, and Ma Y 2024 *NPJ Comput. Mater.* **10** 254

[362] Zeni C, Pinsler R, Zügner D, Fowler A, Horton M, Fu X, Wang Z, Shysheya A, Crabbé J, Ueda S, Sordillo R, Sun L, Smith J, Nguyen B, Schulz H, Lewis S, Huang C W, Lu Z, Zhou Y, Yang H, Hao H, Li J, Yang C, Li W, Tomioka R, and Xie T 2025 *Nature*

[363] Joshi C, Bodnar C, Mathis S, Cohen T, and Lio P 2023 *Proceedings of the 40th International Conference on Machine Learning* **202** 15330

[364] Hall B C 2013 *Quantum Theory for Mathematicians* (Springer)

[365] Cao Z, Luo X, Lv J, and Wang L 2024 arXiv:2403.15734 [condmat.mtrl-sci]
[366] Brooks S 1998 *J. R. Stat. Soc. Ser. D* **47** 69
[367] Reynolds D 2009 *Encycl. Biometrics* **741** 659
[368] Sriram A, Miller B K, Chen R T Q, and Wood B M 2024 arXiv:2410.23405 [cs.LG]
[369] Brown T B, Mann B, Ryder N *et al.* 2020 *Advances in Neural Information Processing Systems* **33** 1877
[370] Boiko D A, MacKnight R, Kline B, and Gomes G 2023 *Nature* **624** 570
[371] Beltagy I, Lo K and Cohan A 2019 *Proceedings of the 2019 Conference on Empirical Methods in Natural Language Processing and the 9th International Joint Conference on Natural Language Processing* (EMNLP-IJCNLP) p. 3615
[372] Gupta T, Zaki M, Krishnan N M *et al.* 2021 *NPJ Comput. Mater.* **8** 102
[373] Völker C, Rug T, Jablonka K and Kruschwitz S 2024 *LLMs can Design Sustainable Concrete -a Systematic Benchmark* (re-submitted version)
[374] Zhao S, Chen S, Zhou J, Li C, Tang T, Harris S J, Liu Y, Wan J, and Li X 2024 *Cell Rep. Phys. Sci.* **5** 101844
[375] Satpute P, Tiwari S, Gupta M, and Ghosh S 2024 *Mater. Today Commun.* **40** 109583
[376] Lei G, Docherty R, and Cooper S J 2024 *Digital Discovery* **3** 1257
[377] Gupta T, Zaki M, Krishnan N M A, and Mausam 2022 *NPJ Comput. Mater.* **8** 102
[378] Blum L C and Reymond J L 2009 *J. Am. Chem. Soc.* **131** 8732
[379] Chmiela S, Tkatchenko A, Sauceda H E, Poltavsky I, Schütt K T, and Müller K R 2017 *Science Adv.* **3** e1603015
[380] Chmiela S, Sauceda H E, Müller K R, and Tkatchenko A 2018 *Nat. Commun.* **9** 3887
[381] Jain A, Ong S P, Hautier G, Chen W, Richards WD, Dacek S, Cholia S, Gunter D, Skinner D, Ceder G *et al.* 2013 *APL. Mater.* **1** 011002
[382] Chanussot L, Das A, Goyal S, Lavril T, Shuaibi M, Riviere M, Tran K, Heras-Domingo J, Ho C, Hu W *et al.* 2021 *ACS Catal.* **11** 6059
[383] Choudhary K, Garrity K F, Reid A C E, DeCost B, Biacchi A J, Hight Walker A R, Trautt Z, Hattrick-Simpers J, Kusne A G, and Centrone A *et al.* 2020 *NPJ Comput. Mater.* **6** 173
[384] Nakata M and Maeda T 2023 *J Chem. Inf. Model.* **63** 5734
[385] Ullah A, Chen Y, and Dral P O 2024 *Mach. Learn.: Sci. Technol.* **5** 041001
[386] Jia S, Zhang C, and Fung V 2024 arXiv:2406.13163 [cond-mat.mtrl-sci]
[387] Zhang H, Song Y, Hou Z, Miret S, and Liu B 2024 arXiv:2409.00135 [cs.CL]
[388] Miret S and Krishnan N M A 2024 arXiv:2402.05200 [cond-mat.mtrl-sci]
[389] Nie S, Xiang Y, Wu L, Lin G, Liu Q, Chu S, and Wang X 2024 *J. Am. Chem. Soc.* **146** 29325
[390] Qu J, Xie Y, Ciesielski K, Porter C, Toberer E, and Ertekin E 2023 arXiv:2305.01101 [cond-mat.mtrl-sci]
[391] Zhong Y, Tao Z G, Chu W B, Gong X G, and Xiang H J 2023 arXiv:2302.00439 [physics.comp-ph]
[392] Gibson J B, Hire A C, Dee P M, Barrera O, Geisler B, Hirschfeld P J, and Hennig R G 2025 *NPJ Comput. Mater.* **11** 7
[393] Haldar A, Clark Q, Zacharias M, Giustino F, and Sharifzadeh S 2024 *Phys. Rev. Mater.* **8** L101001
[394] Okabe R, Chotrattanapituk A, Boonkird A, Andrejevic N, Fu X, Jaakkola T S, Song Q, Nguyen T, Drucker N, Mu S *et al.* 2024 *Nat. Comput. Sci.* **4** 522
[395] Fang S, Geiger M, Checkelsky J G, and Smidt T 2024 arXiv:2403.11347 [cond-mat.dis-nn]
[396] Zhang H, Liu S, You J, Liu C, Zheng S, Lu Z, Wang T, Zheng N, and Shao B 2024 *Nat. Comput. Sci.* **4** 210
[397] Li H, Wang Z, Zou N, Ye M, Xu R, Gong X, Duan W, and Xu Y 2022 *Nat. Comput. Sci.* **2** 367
[398] Gong X, Li H, Zou N, Xu R, Duan W, and Xu Y 2023 *Nat. Commun.* **14** 2848
[399] Li H, Tang Z, Fu J, Dong W H, Zou N, Gong X, Duan W, and Xu Y 2024 *Phys. Rev. Lett.* **132** 096401
[400] Li H, Tang Z, Gong X, Zou N, Duan W, and Xu Y 2023 *Nat. Comput. Sci.* **3** 321
[401] Tang Z, Li H, Lin P, Gong X, Jin G, He L, Jiang H, Ren X, Duan W, and Xu Y 2024 *Nat. Commun.* **15** 8815
[402] Gong X, Louie S G, Duan W, and Xu Y 2024 *Nat. Comput. Sci.* **4** 752
[403] Tang Z, Zou N, Li H, Wang Y, Yuan Z, Tao H, Li Y, Chen Z, Zhao B, Sun M *et al.* 2024 arXiv:2406.17561 [physics.comp-ph]
[404] Wang Y, Li H, Tang Z, Tao H, Wang Y, Yuan Z, Chen Z, Duan W, and Xu Y 2024 arXiv:2401.17015 [physics.comp-ph]
[405] Li Y, Tang Z, Chen Z, Sun M, Zhao B, Li H, Tao H, Yuan Z, Duan W, and Xu Y 2024 *Phys. Rev. Lett.* **133** 076401
[406] Wang Y, Li Y, Tang Z, Li H, Yuan Z, Tao H, Zou N, Bao T, Liang X, Chen Z *et al.* 2024 *Science Bulletin* **69** 2514
[407] Zhong Y, Yu H, Yang J, Guo X, Xiang H, and Gong X 2024 *Chin. Phys. Lett.* **41** 077103
[408] Su M, Yang J H, Xiang H J, and Gong X G 2023 *Mach. Learn.: Sci. Technol.* **4** 035010